U.S. Department of Interior
U.S. Geological Survey

In Cooperation with the Town of Rye, New Hampshire

# Borehole-Geophysical Characterization of a Fractured-Bedrock Aquifer, Rye, New Hampshire

By Carole D. Johnson, Alicia H. Dunstan, Thomas J. Mack, and John W. Lane, Jr.

**Open-File Report 98-558**

**Pembroke, New Hampshire**
**1999**

U.S. DEPARTMENT OF THE INTERIOR
BRUCE BABBITT, Secretary

U.S. GEOLOGICAL SURVEY
Charles G. Groat, Director



---

For additional information write to:

District Chief
U.S. Geological Survey
New Hampshire/Vermont District
361 Commerce Way
Pembroke, NH 03275-3718

Copies of this report can be purchased from:

U.S. Geological Survey
Branch of Information Services
Box 25286, Federal Center
Denver, CO 80225

# CONTENTS



## FIGURES

## TABLES



## CONVERSION FACTORS, VERTICAL DATUM, AND ABBREVIATIONS

| Multiply | By | To obtain |
|---|---|---|
| inch (in.) | 25.4 | millimeter |
| foot (ft) | 0.3048 | meter |
| meter (m) | 3.281 | foot |
| gallon per minute (gal/min) | 0.00006309 | cubic meter per second |

Temperature in degrees Fahrenheit ($^{o}F$) can be converted to degrees Celsius ($^{o}C$) as follows:
$^{o}C = 5/9\ (^{o}F - 32)$.

**Sea Level:** In this report "sea level" refers to the National Geodetic Vertical Datum of 1929 (NGVD of 1929)—a geodetic datum derived from a general adjustment of the first-order level nets of both the United States and Canada, formerly called Sea Level Datum of 1929.

OTHER ABBREVIATIONS USED IN THIS REPORT:

| | |
|---|---|
| dB/m | decibels per meter |
| MHz | megahertz |
| m/μs | meters per microsecond |
| OHM-m | ohms-meter |
| μS/cm | microsiemens per centimeter |

# Borehole-Geophysical Characterization of a Fractured-Bedrock Aquifer, Rye, New Hampshire

*By* Carole D. Johnson, Alicia H. Dunstan, Thomas J. Mack, *and* John W. Lane, Jr.

## Abstract

Borehole geophysical logs collected from six wells were analyzed to characterize a high-yield bedrock aquifer in the Town of Rye, New Hampshire. Video camera, caliper, fluid temperature and conductivity, natural gamma, and deviation logs were used to identify and characterize the fractured bedrock. More advanced geophysical tools included acoustic televiewer and borehole radar, which were used to determine the orientation of fractures and fracture zones that intersect and surround each of the six wells. Borehole-radar surveys included single-hole directional-reflection surveys. The borehole-radar logs indicate that the bedrock aquifer is highly fractured. Zones of low velocity and high attenuation in the radar logs correlated with the fractures and fracture zones observed in the standard geophysical logs of the six wells. The strikes of the fracture sets, as determined by the acoustic televiewer, coincide with photolineaments identified on high-altitude and low-altitude aerial photography and side-looking airborne radar (SLAR). The coincident fracture sets and lineaments trend N100°E, N140°E, N170°E, and N40°E.

## INTRODUCTION

Many towns and communities in New Hampshire have limited amounts or an absence of sand and gravel aquifers, which are favorable for constructing high-yield wells. These towns must look for additional water resources in crystalline bedrock, which generally yields very small quantities (a few gallons per minute) of water to wells. A number of bedrock wells constructed in the Grove Road area in Rye, N.H., yield more than 100 gal/min. Information on the hydraulic characteristics of the fractured bedrock aquifer in this area, including the primary flow pathways to the wells, is needed to protect this water resource and to identify those characteristics that may be useful in locating other high-yield wells in fractured bedrock aquifers. The U.S. Geological Survey (USGS), in cooperation with the Town of Rye, in southeastern N.H. (fig. 1), used geophysical methods to characterize hydraulic properties in six wells and to determine the nature of fractures in the high-yield bedrock aquifer.

### Purpose and Scope

The purpose of this report is to demonstrate how advanced borehole geophysical techniques, in combination with remotely sensed lineament analysis, are applied and used to characterize a fractured bedrock aquifer underlying Rye, N.H. The results of the study are the interpretation of the location, nature, and extent of fractures in a bedrock aquifer. Geophysical logs collected from six boreholes are presented and interpreted in order to characterize the bedrock aquifer.

### Description of the Study Area

The study area consists of a bedrock aquifer off Garland Road in the southeastern corner of the Town of Rye, N.H. (fig. 1). Test wells in this bedrock aquifer are 323 to 550 ft deep, and are 6- and 8-in. in diameter. There are two well fields in the study area—the Bailey Brook well field and the Cedar Run well field. Three bedrock wells (W-3, W-4, W-5) are

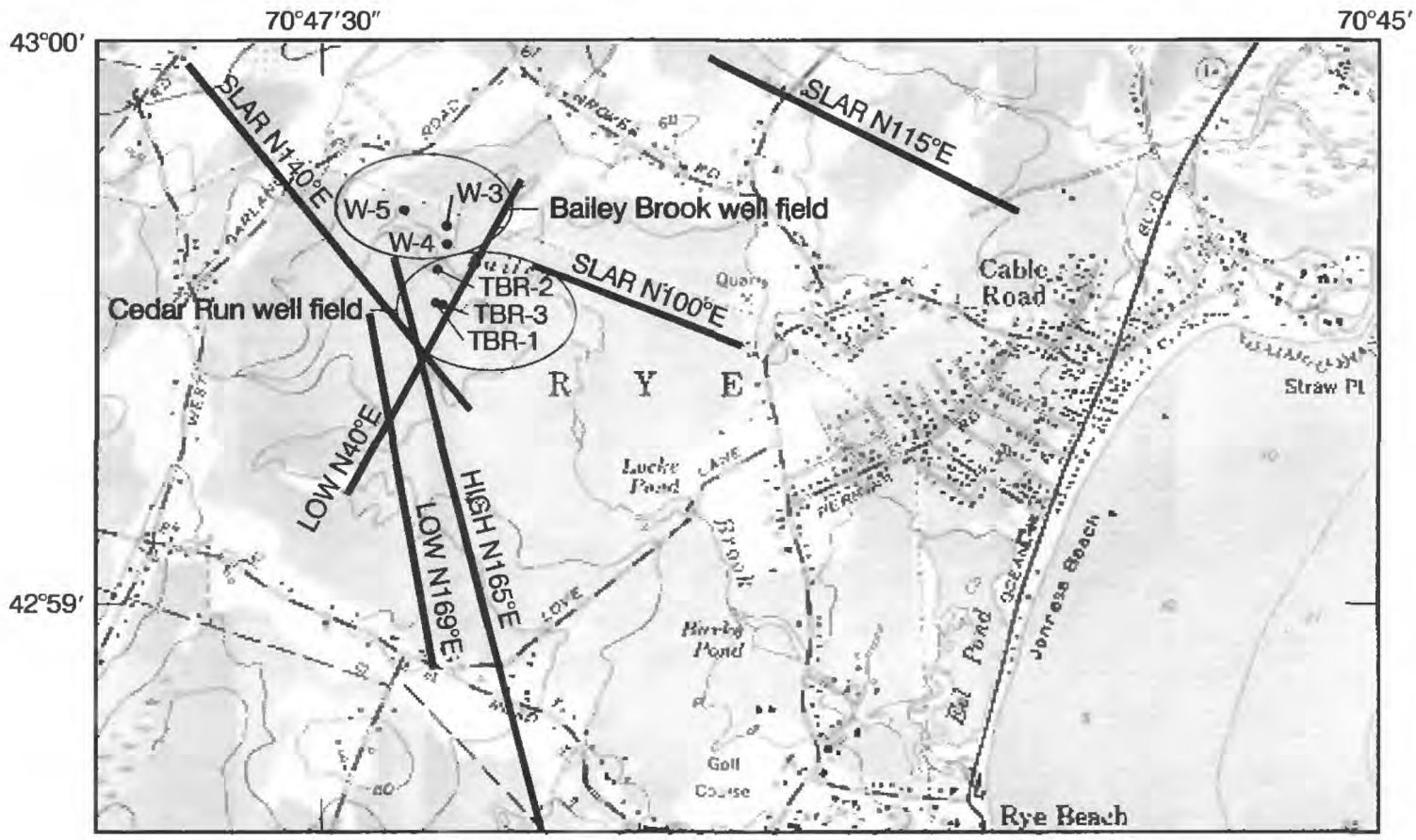


**Figure 1.** Locations of study area and photolinear data in Rye, New Hampshire.

adjacent to Bailey Brook and the Bailey Brook municipal-supply well (fig. 1). Three other wells are located about 900 ft south of the Bailey Brook well, in the Cedar Run well field, an area suspected to be at the junction of numerous lineaments (D.L. Maher, 1982) and, therefore, the focus of this investigation. Bedrock wells in the Cedar Run well field include TBR-2, adjacent to Bailey Brook, TBR-1, and TBR-3, which is about 12 ft east of TBR-1 (D.L. Maher, 1982). The Cedar Run field is overlain by glacial till, which ranges in thickness from 0-25 ft. The till consists of compact unsorted sand, silt, clay, and rocks. The Cedar Run municipal well, drilled after the field effort of this study, was completed to a depth of 437 ft and yields greater than 350 gal/min. (Reidar Bomengen, D.L. Maher, written commun., 1998).


## Acknowledgments

Appreciation is expressed to officials and employees of the Rye Water District who provided assistance and access to their wells. Special thanks are extended to Gary Smith, of D.L. Maher, Inc., for providing assistance and insight throughout the investigation regarding wells, fracture-trace analysis, and the bedrock aquifer in Rye.


## STUDY METHODS

Borehole geophysical logs were used to characterize the geohydrology of the fractured bedrock aquifer. The borehole logs collected in wells TBR-1, TBR-2, TBR-3, W-3, W-4, and W-5 included a standard suite of geophysical logs such as video camera, caliper, fluid temperature and resistivity, and natural gamma. More advanced geophysical logs that were collected include acoustic televiewer (ATV) and deviation. Heat-pulse flowmeter data were collected in TBR-3. Single-hole-directional radar-reflection surveys were collected in TBR-2, TBR-3, W-3, W-4, and W-5. In all geophysical logs, depth measurements are referenced to the top of the steel well casing.

### Standard Logs

A submersible color video camera was used to examine the wells to discern rock types, fractures, possible faults, and the condition or integrity of the well. The camera had a digital depth counter, which was incremented in tenths of feet and was superimposed onto the analog picture. Continuous images were recorded on video cassettes. The locations of fractures and rock types were identified directly from the images and were tabulated and plotted. The fractures were described with a code that indicates if it appears to be (1) a "major fracture," (2) a "fracture," or (3) a "possible fracture." The term "major fracture" was used to describe an open fracture that exhibits a wide aperture and (or) oxidation or alteration of the adjacent rock. A fracture without a wide aperture or oxidation was coded simply as "fracture." The term "possible fracture" was assigned to features that appeared as dark-lines in the borehole images and could potentially be fractures. However, it is not always possible to verify the presence of a fracture by visual inspection. Techniques and equipment for borehole imaging used for the well surveys are described by Johnson (1996) and Johnson and Dunstan (1998). Video logs were collected in all of the wells. However, only the upper 291 ft were logged in TBR-1 because below that depth, the water was murky and the view of the borehole was obscured. TBR-3 was logged to a depth of 208 ft, where there was an obstruction.

The caliper log was used to generate a continuous profile of the borehole diameter. This log shows the mechanical measurement as a spring-loaded, three-arm caliper tool is pulled up the well. The arms open as they pass borehole enlargements. Enlargements in the borehole diameter generally are related to fractures, but can also be caused by changes in lithology or well construction. The profile indicates the roughness of the borehole wall. Some enlargements may be larger than the caliper diameter, which is 18 in.

The fluid temperature log displays a continuous measurement of the temperature of fluid in the borehole. In the absence of ground-water flow, the temperature gradually increases with the geothermal gradient, which is 0.6°C per 100 ft of depth (Keyes, 1988). A continuous plot of the fluid temperature with depth is used to identify zones that deviate from the expected geothermal gradient. Deviations from the gradient indicate locations where ground water enters or exits the borehole.

The fluid-resistivity log records the electrical resistance of the fluid in the borehole. Changes in the electrical resistance of the water in the borehole

indicate differences in the concentration of the total dissolved solids in the water in the borehole. These differences typically indicate sources of water that have contrasting chemistry and have come from alternate water-bearing zones. Fluid conductivity is computed as the reciprocal of the fluid resistivity.

The gamma log measures the natural-gamma radioactivity of the formation surrounding the borehole. Gamma radiation is a natural product of the radioactive decay of potassium-40, and a daughter product of uranium and thorium decay. The gamma log used in this investigation does not differentiate between the sources of the gamma radiation. It counts the total gamma-radiation emissions, which can often be correlated with the rock type or with fracture infillings. Potassium-40 is abundant in potassium feldspar (microcline and orthoclase), which alters to sericite and clay. In the alteration process, potassium-40 is concentrated in the clay by processes of adsorption and ion exchange. Deviations in the gamma log trace indicate changes in the rock type or the presence of mineralized fractures. Clay minerals, which sometimes comprise the infilling of fractures, generally have an elevated concentration of potassium-40 minerals and cause an increase in the gamma log. Mafic dikes are devoid of gamma emitters and have a low gamma signature.

## Advanced Logs

A flowmeter measures the velocity of vertical flow in the borehole. Used in conjunction with the other geophysical logs, individual fractures or zones of fractures can be identified as the locations where water enters or exits the borehole. Under ambient conditions, differences in hydraulic heads between two water-bearing zones produce vertical flow in the well. The water enters the borehole from the water-bearing zone with the higher head and flows towards and out of the zone with lower head. The flowmeter used in this investigation makes use of a heat-pulse tracer rather than the more conventional impeller method described by Paillet and Williams (1992). The heat-pulse flowmeter uses a thermal tracer to measure flows as small as 0.01 gal/min (Hess and Paillet, 1990). The measurements are collected at discrete locations, usually above and below fractures.

Boreholes drilled into crystalline rock frequently deviate from vertical due to variations in rock properties, the fabric of the bedrock, or the presence of fracturing. In addition, the deviation of the borehole may be enhanced by drilling techniques. The deviation log records the azimuthal direction (0-360°) and the inclination (0-90°) of the borehole over the depth of the borehole. This log is used to correct the orientation of fractures determined from the acoustic televiewer (ATV) logs.

The ATV was used to map the location and orientation of fractures that intersect a well. The ATV tool emits a narrow acoustic beam that rotates 360° and is focused at the solid borehole wall. The acoustic wave moves through the fluid in the borehole and is reflected off the borehole wall. The log records the amplitude and travel time of the reflected signal (fig. 2) The product is a high-resolution, digital image, oriented to magnetic north, that can be used to determine the location and orientation (strike and dip) of fractures and some lithologic contacts. The travel time can be displayed in the form of an acoustic caliper log that shows the oriented cross-sectional dimensions of the borehole. A fracture that intersects the borehole causes the impedance and scattering of the acoustic wave and a low amplitude response of the signal. The amplitude of the reflected acoustic signal of a smooth and intact borehole wall is higher than the signal response of a rough or fractured borehole wall. A segment of the ATV data collected in well TBR-2 is shown in figure 2. A fracture appears on the image as a high contrast, low amplitude line (dark bands in fig. 2). On the acoustic caliper log, a fracture is indicated by an increase in the one-way travel time of the wave, which is converted to a borehole diameter (fig. 2). Borehole diameter is shown in two directions, north to south and east to west. The trace of the north-south caliper log has been reversed and decreases from 18 to 2 in., whereas the east-to-west caliper trace extends from 2 to 18 in. In this form, the two adjacent plots give the appearance of a cross section of the well diameter.

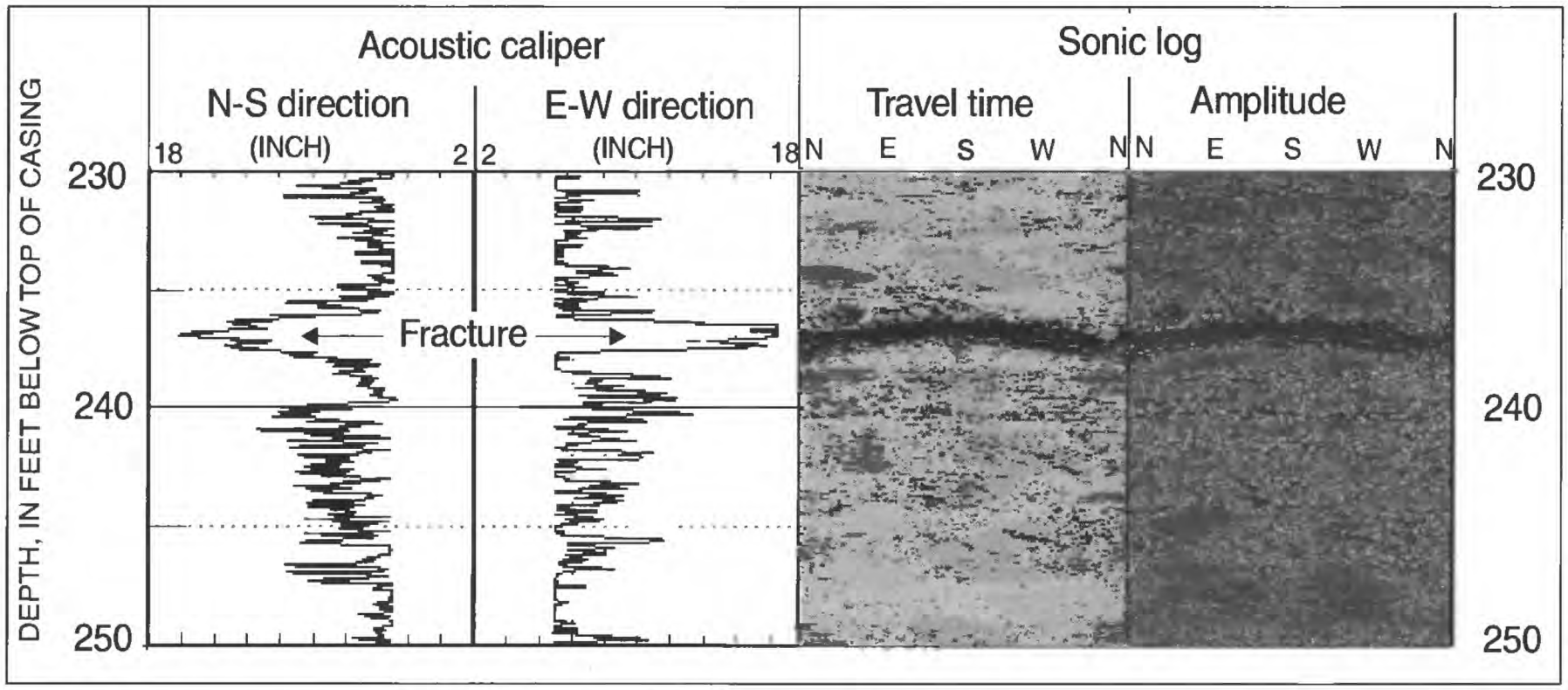


**Figure 2.** Acoustic televiewer (ATV) log of well TBR-2 in Rye, New Hampshire.

## Radar-Reflection Surveys

Borehole-radar surveys were conducted to determine the orientation and location of discrete fractures or fracture zones surrounding the borehole. Following the methods of Lane and others (1994), single-hole directional surveys were conducted in wells TBR-2, TBR-3, W-3, W-4, and W-5. The directional antenna is used to determine the strike and dip of the reflectors surrounding the borehole. The two antennas used in this investigation were a broad-based electric-dipole transmitting antenna with a center frequency of 22 MHz and a 60-MHz directional-receiving antenna. The transmitting and receiving antennas were separated by a distance of 21 ft.

Borehole-radar logs were used to determine the location and lateral extent of fractures in the bedrock surrounding the borehole. A transmitting antenna radiates pulses of electromagnetic energy that propagate from the borehole into the surrounding rock. Point or planar reflectors at interfaces between two electromagnetically different materials can be identified in the log. Reflections are caused by water-filled fractures, faults, bedding, changes in rock type, or water quality (Lane and others, 1994). The electromagnetic waves continue to propagate and be reflected until all of the energy is dissipated. The total distance of penetration away from the borehole depends on the frequency, arrangement of the transmitting and receiving antennas, and the electromagnetic properties of the rock. Under ideal conditions, the radar can "see" into the surrounding rock up to radial distances of 100 or more feet.

# GEOHYDROLOGY OF THE BEDROCK

## Lithology

The rocks that underlie the Rye well fields are folded, fractured, metasedimentary rocks of the Ordovician (?) age to Late Proterozoic (?) Rye Complex (Lyons and others, 1997). Tectonic compressional events in the Paleozoic age caused deformation of the crystalline rock. Major faults (including the Portsmouth Fault and Great Common Fault) and small scale faulting are mapped to the west and north of the study area (Novotny, 1969; Brooks, 1986; Brooks and Rickerich, 1996; Hussey and Bothner, 1993). Brooks (1986) summarized the prominent structural fabrics of the seacoast region. Joints and faults in the Rye Complex were reported to trend 0°, 40-45°, 60-70°, 90°, 305°, and 340° east of north, and strike-slip faults in the Rye Complex trend N40°E and N60-80°E.

The lower member of the Rye Complex consists of light-colored to gray schists, quartzites, and gneisses (Novotny, 1969) and is distinguished from the upper member by a predominance of light-colored minerals such as plagioclase, feldspar, and quartz. The upper and lower members are coarse grained and distinctly banded. The Rye Complex has been intruded by many younger intrusive granitic and diabase structures (Novotny, 1969).

Most of the rocks encountered in the wells were metasedimentary rocks, including schist and gneiss with lesser amounts of quartzite and basalt. Drill cuttings from a production well (Cedar Run well) drilled in 1997 are described (Kevin Trainer, University of New Hampshire, written commun. to Town of Rye, 1997) as five rock types including (1) gray quartz-feldspar-muscovite schist; (2) gray quartz-feldspar-biotite-muscovite-garnet schist; (3) dark gray basalt; (4) dark gray quartz; and (5) light gray quartz-feldspar-muscovite-biotite gneiss granite.

## Fracture-Trace Analysis

A fracture-trace analysis of bedrock in the study area was performed by the USGS as part of a statewide bedrock aquifer-mapping assessment (Moore and Clark, 1995; Ferguson and other, 1997). Fracture-trace analysis identifies straight-line features on the land surface, as viewed on multiple platforms of remotely-sensed images, that are most likely related to the surface expression of steeply dipping fractures or fracture zones. These linear features, or lineaments, are noted by the detection of narrow troughs in the topography, truncated geomorphic features, gaps in ridges, straight-line stream segments, and (or) variations in the vegetation or soil. This method provides trend of the linear feature, but does not provide a measurement of dip angle. If the land surface is flat, then dipping beds can appear as linear features on remotely-sensed images. Any relief on the land surface causes non-vertical features to appear as curvilinear features on remotely-sensed images.

The methods and criteria of the statewide fracture-trace analysis are described by Clark and others (1996). The technique used by the statewide analysis requires the identification of lineaments by two independent observers on multiple scales and types of imagery including black and white aerial photography (at a scale of 1:20,000 and 1:80,000), side-looking airborne radar (SLAR) (at a scale of 1:250,000) and Landsat (at a scale of 1:1,000,000).

Lineaments identified at or near the study area by Ferguson and others (1997) are shown in figure 1. A low-altitude (1:20,000) lineament (N 40°E) intersects the study area, near TBR-3, and was also noted by a previous investigation (D.L. Maher, 1982). Upstream of the well field, Bailey Brook follows a trend that parallels the low-altitude lineament with a trend of N40°E, which correlates to one of the dominant joint trends (Brooks, 1986). The brook bends abruptly near W-5 and follows the trend of a SLAR lineament bearing N100°E. This trend (N100°E) is close to dominant joint sets of N90°E and N290°, reported by Brooks (1986). In addition, there is a SLAR lineament, northeast of the well field, that trends N115°E. The lineaments trending N169°E and N165°E that are mapped in the study area have a similar trend (N340°E) to a dominant joint set mapped in the Rye Formation (Brooks, 1986).

Although Clark and others (1996) used a standardized process and criteria for lineament mapping, the technique can be somewhat subjective. Depending on the platform scale observed, and the methods and criteria used, additional or different patterns of lineaments could be mapped for the study area. For example, some of the same lineaments were identified in a previous study by D.L. Maher, Inc. (1982, fig. 3). The earlier study, however, also identified numerous lineaments with orientations other than those shown on figure 1. A site-specific study, such as that done by D.L. Maher, Inc., is likely to be concerned with finding all possible lineaments, rather than more selectively identifying lineaments following the consistent criteria used by Clark and others (1996).

## INTERPRETATION OF GEOPHYSICAL LOGS

Borehole-radar logs were completed in February 1997. Other logs were collected in February and March of 1997. The geophysical logs were examined to identify anomalies or changes in the measured properties that relate to locations of fractures or lithologic contacts. Borehole video, ATV, and radar data are either not shown, or only a segment is shown, in this report. (Original data are maintained on file in the New Hampshire/Vermont District office.)

## Standard Logs

Plots of standard logs are shown in figures 3-8 (wells TBR-1, TBR-2, TBR-3, W-3, W-4, and W-5). Graphic plots of log data are used to identify the locations of fractures, changes in water chemistry, changes in lithology, and vertical flow in the well. In the caliper log, a fracture appears as an increase in the borehole diameter. In figures 3-8, the large spikes or enlargements in the caliper log correlate with the fractures that were described as "major" or "wide" in interpretation of the video images. In general, the minor deflections in the caliper correlate with moderately wide fractures.

Numerous deflections in the individual logs of TBR-1 and TBR-3 (fig. 3 and 5) are apparent with depth. The wells at the center of the Cedar Run well field appear to have at least two significant fracture zones, where water movement affects fluid conductance and (or) fluid temperature. These deflections in the log traces are most noticeable in the fluid conductance logs at depths of approximately 60 and 200 ft. In well TBR-3, fluid conductance increases from about 270 to 330 µS/cm at 60 ft and decreases from 330 to 300 µS/cm at 200 ft. The fluid-temperature log shows an abrupt change at 200 ft, which indicates inflow or outflow of water at this point. The caliper and video logs were used to confirm the presence of fractures at the two locations. An extensive fracture zone is apparent from the caliper, ATV, and video logs at 200 to 210 ft. There is also a minor deflection in the fluid conductivity log of TBR-3 at approximately 80 ft. Between 80 and 200 ft, the fluid conductivity is constant, indicating vertical flow in the well. In addition, the log indicates vertical flow between 200 and 373 ft. The direction of vertical flow, however, cannot be determined in the standard logs. A flowmeter must be used to determine the direction and magnitude of flow.

The interpretations of the zones of fluid inflow and outflow were confirmed by the flowmeter. Two suites of heat-pulse flowmeter measurements were collected in well TBR-3 in February 1997. The results were influenced by pumping at the municipal well or by tidal fluctuations over the approximately 3 hours needed per well to collect flow data. These data indicate that under ambient conditions (no pumpage in well TBR-3) water enters the well near the base of the boring (below the blockage at 370 ft) at 0.37 gal/min. Under natural conditions, the water flowed upwards, and about one half of the water exited the well at about 200 ft. The remainder of the water exited the well at the fractures at 60 and 80 ft in the first test and at 60 ft in the second test. Although the hydraulic conditions were changing during the collection of the data, the interpretation of where the majority of the water entered and exited the well is consistent.

The overall pattern of the gamma logs for TBR-1 and TBR-3 are similar, indicating similarity in the rock types in the two wells. Between 30 and 280 ft, the pattern, which is most evident from 105 to 135 ft, is slightly deeper in TBR-1 than in TBR-3, indicating that the bedding is dipping in a westerly direction.

The logs of well TBR-2 (fig. 4), which is 300 ft north of TBR-1 and TBR-3 and adjacent to Bailey Brook, indicate that significant fractures correspond to the changes in the caliper, fluid conductance and fluid temperature logs at 40, 50, 120, 163, and 298 ft. The temperature log shows major breaks in slope at 50, 122, 163, and 298 ft. In addition, the fractures at 120 and 298 ft show abrupt changes in the fluid conductivity adjacent to major fractures and constant conductivity and minor changes in the fluid between the fractures. These deflections are interpreted as points of inflow to and outflow from the well with vertical flow between the fractures. The fracture locations are confirmed by video, ATV, and caliper data. The video log indicates that the well intersects quartzo-feldspathic-biotite-muscovite gneiss and schist with basalt dikes. The locations of the basalt dikes, which were viewed in the video images, are prominent negative spikes in the gamma log at 200, 215, and 380 ft.

Major deflections in the logs for wells in the Bailey Brook well field (fig. 6, 7, and 8) are also apparent. These deflections in the log traces are generally most noticeable in the fluid conductance logs. Standard logs of W-3 (fig. 6) indicate numerous fractures. Abrupt changes in the fluid conductivity log at 152, 178, 402, and 440 ft indicate hydraulically active fractures. These zones coincide with enlargements indicated by the caliper log and zones that were described as fractured from direct inspection with the ATV and video camera. The fluid conductivity log is constant (400 µS/cm) between the "major fracture" at 178 ft and the "major fracture" at 402 ft. The low-resistivity gradient between the abrupt changes in fluid resistivity at the fractures is interpreted as a zone with vertical flow between inflowing and outflowing fractures.

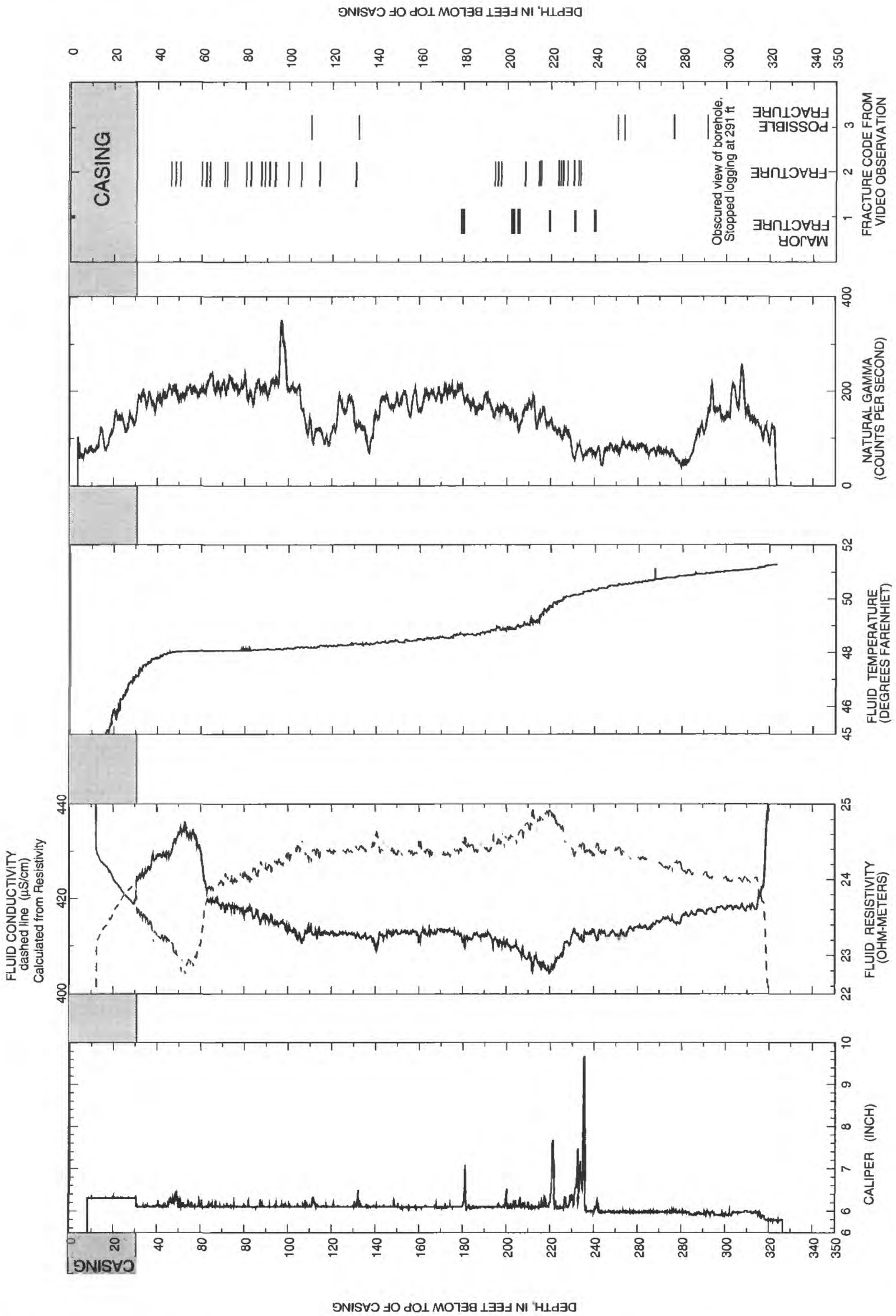


**Figure 3.** Geophysical logs of well TBR-1 in Rye, New Hampshire.

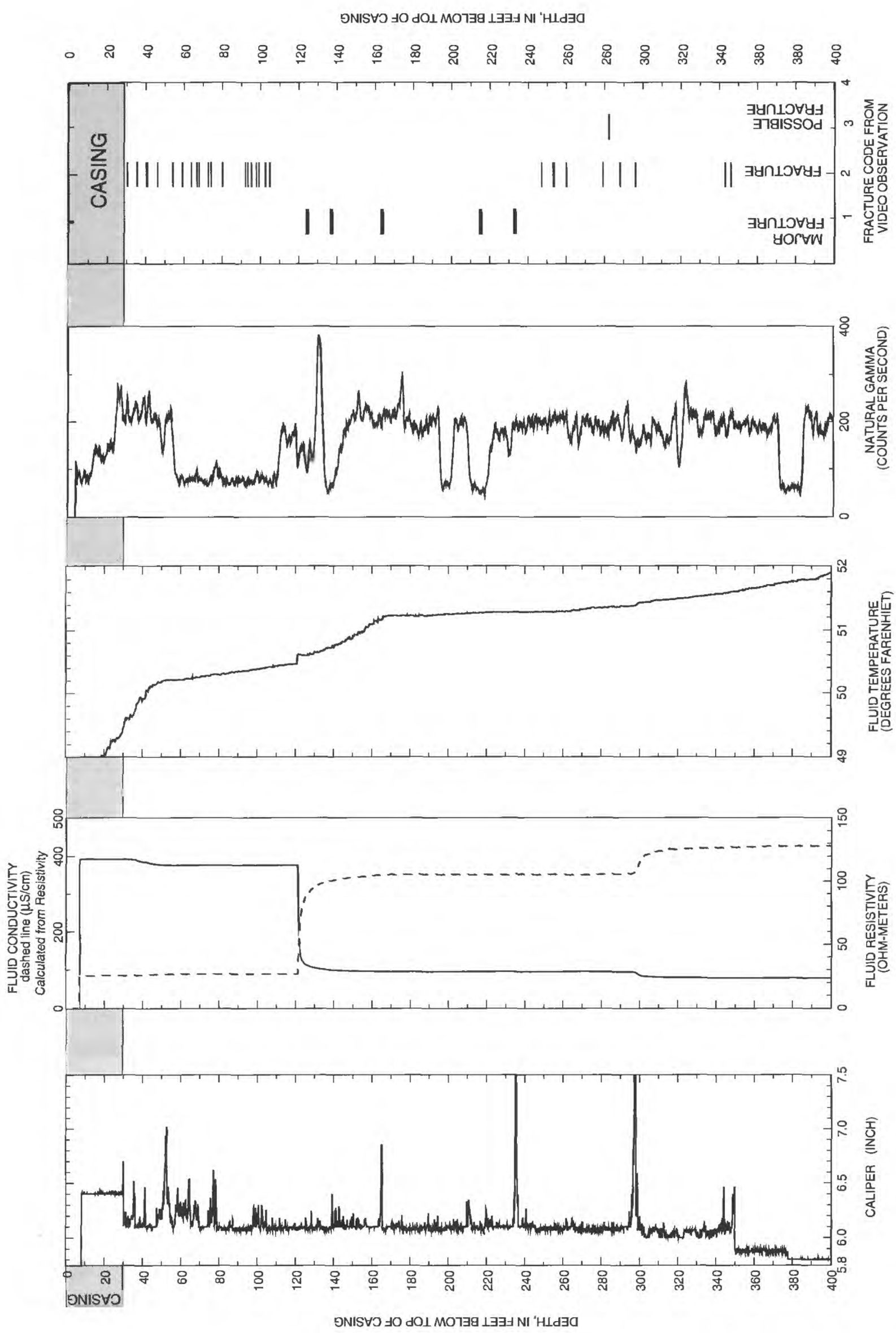


**Figure 4.** Geophysical logs of well TBR-2 in Rye, New Hampshire.

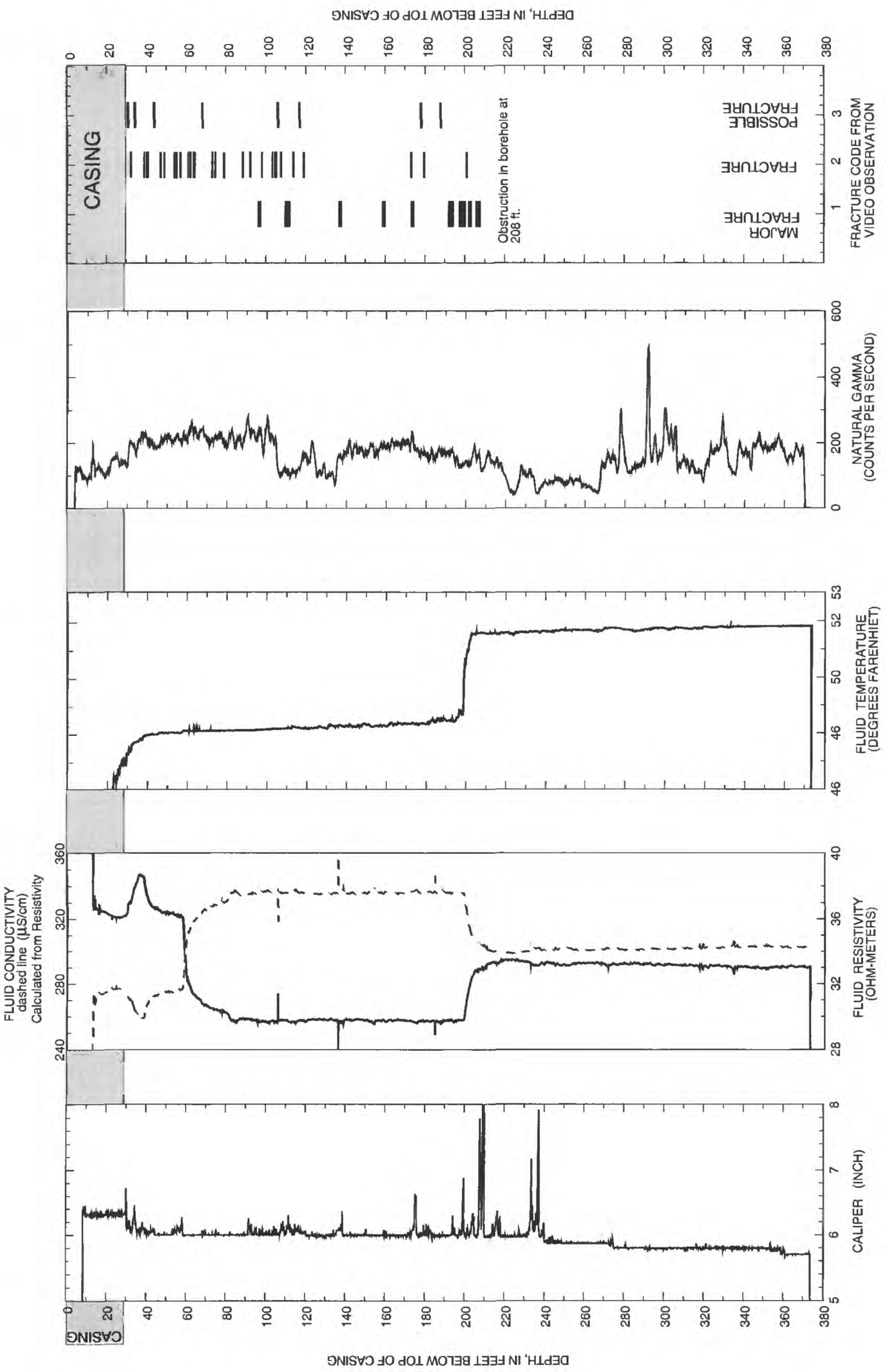


**Figure 5.** Geophysical logs of well TBR-3 in Rye, New Hampshire.

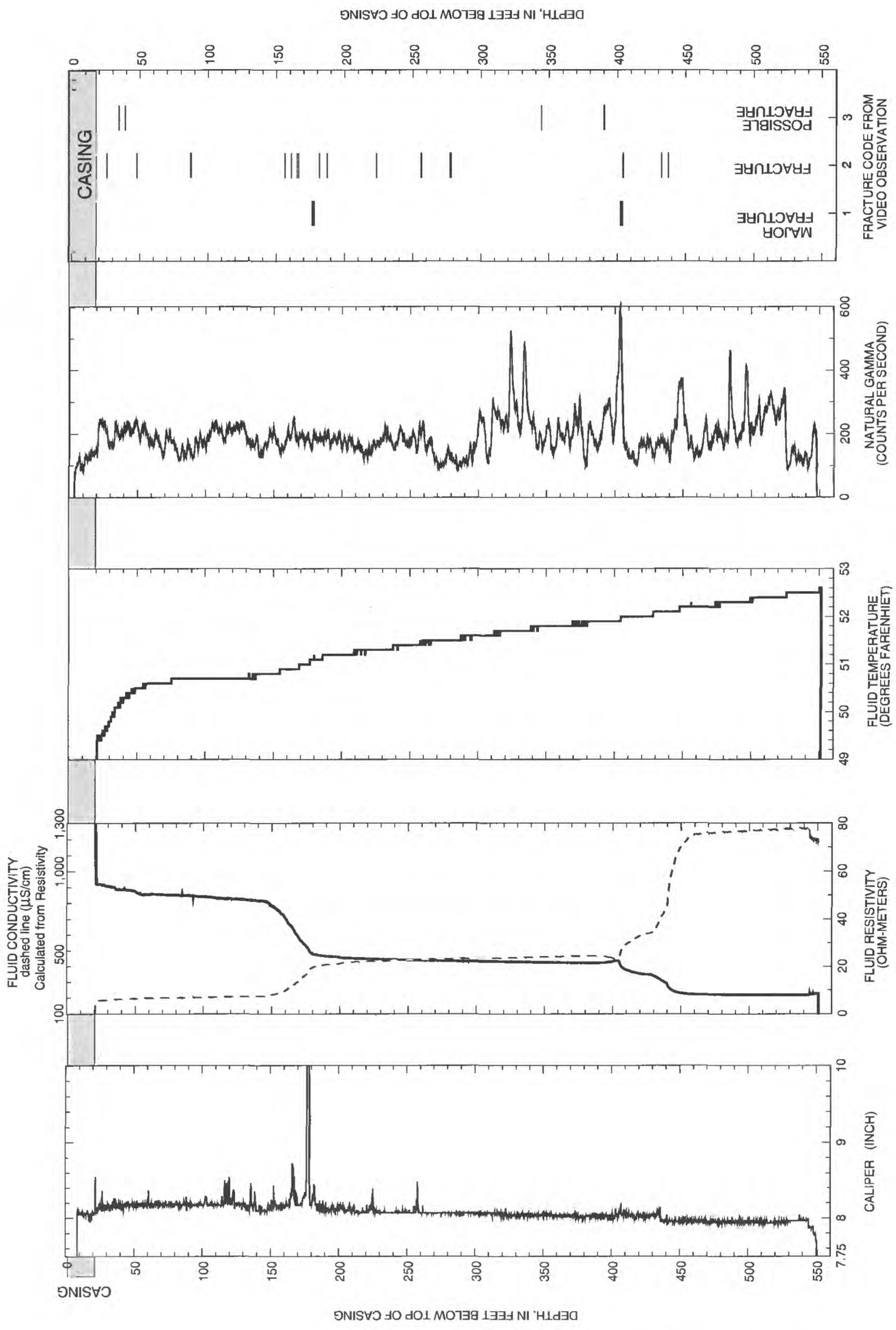


**Figure 6.** Geophysical logs of well W-3 in Rye, New Hampshire.

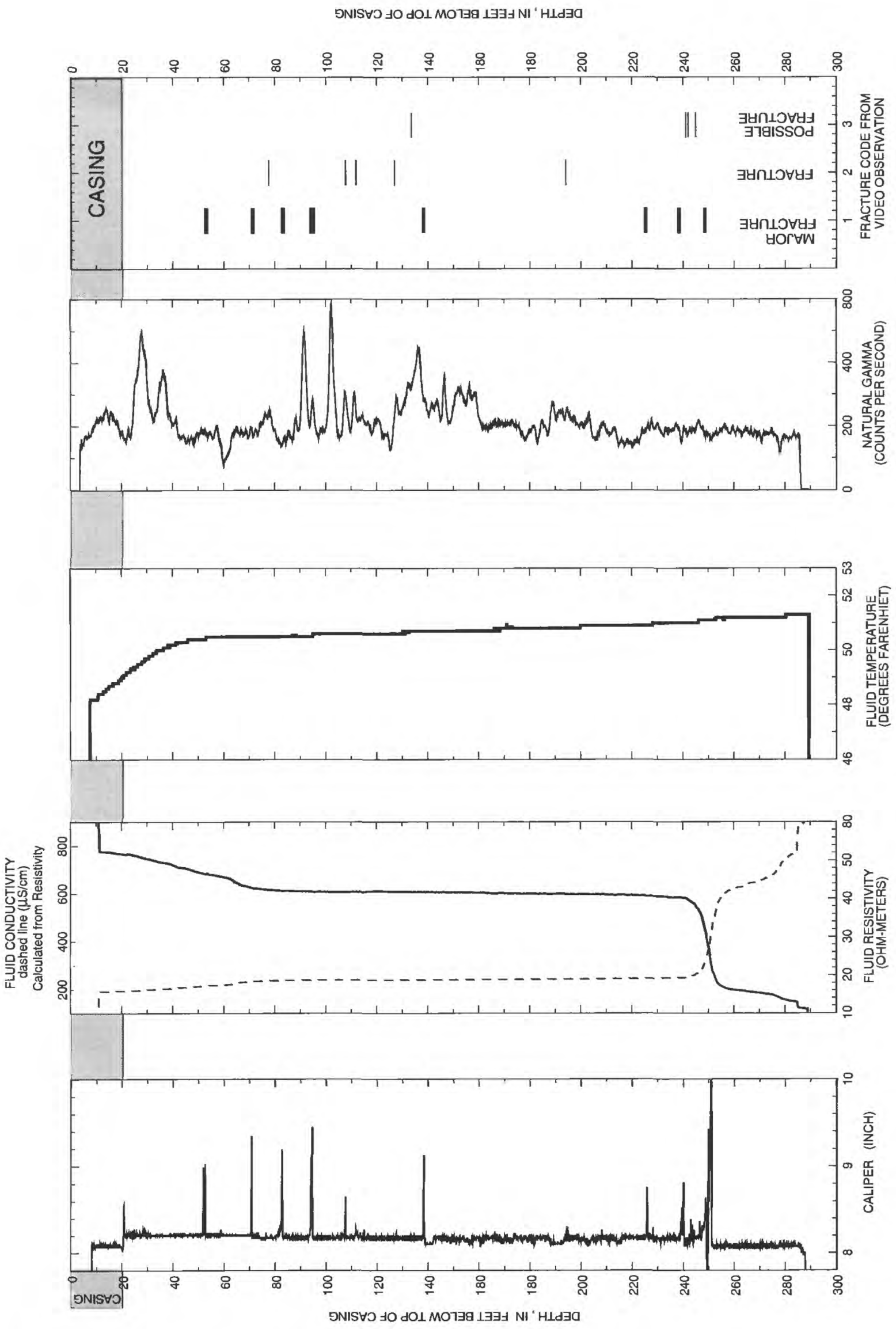


**Figure 7.** Geophysical logs of well W-4 in Rye, New Hampshire.

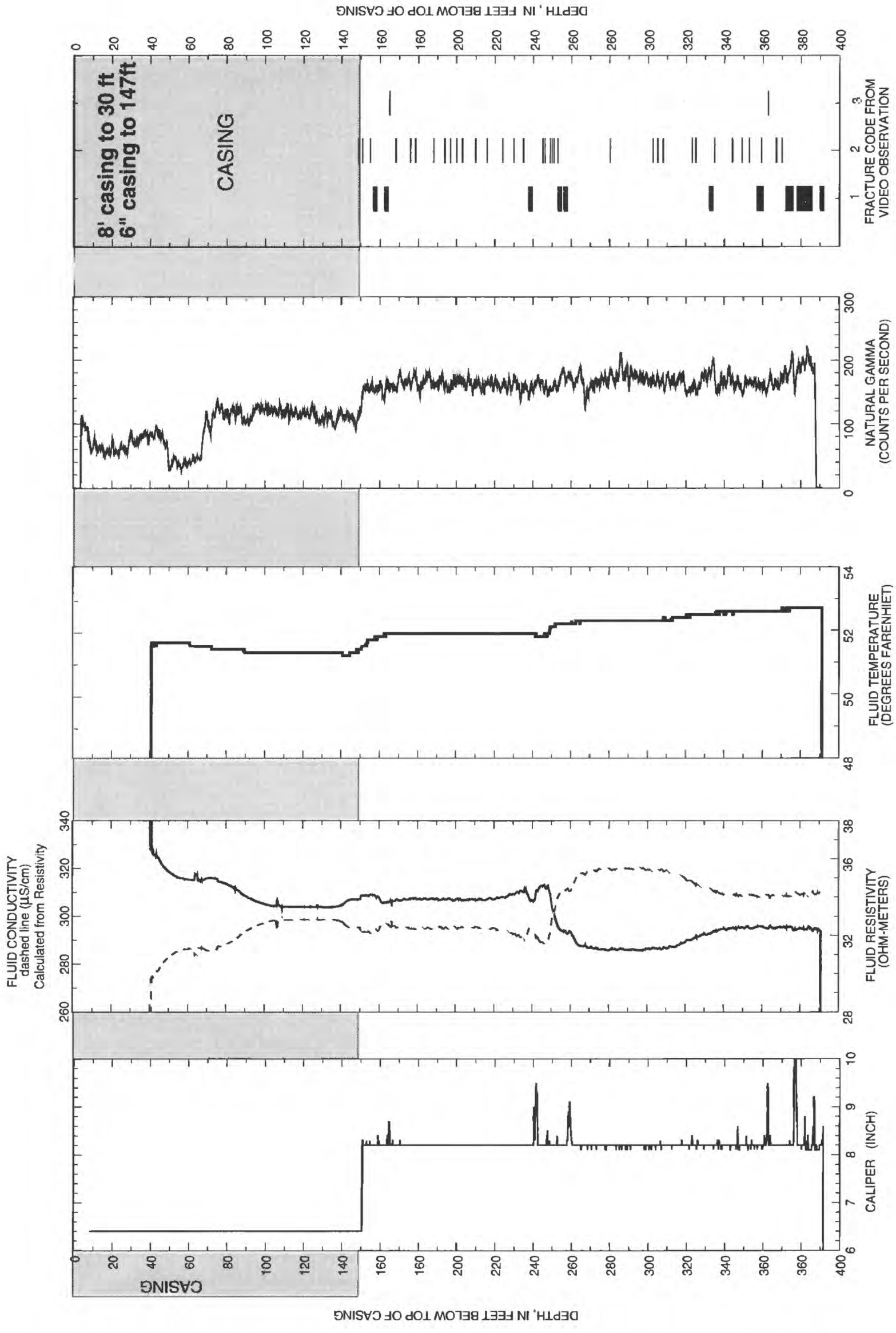


**Figure 8.** Geophysical logs of well W-5 in Rye, New Hampshire.

Although the caliper log in well W-4 (fig. 7) indicates numerous borehole enlargements, only three fractures affect the fluid conductivity in the borehole. These fractures, which are at 70, 240, and 250 ft, were described as major fractures in the video and ATV logs. The fluid resistivity log also shows the potential for vertical flow between the fracture at 70 ft and the fracture zone at 240 ft.

Well W-5 (fig. 8), adjacent to the Bailey Brook municipal well, is an 8-in-diameter hole that was originally drilled to 500 ft. It collapsed and is blocked at 393 ft in a fracture zone that appears to be open and enlarged above the blockage. In addition, a 6-in-diameter casing was installed into bedrock to a depth of 139 ft, as seen in the caliper and gamma logs. The fluid conductivity log in well W-5 indicates major hydraulically active fracture zones at 240 and 260 ft and minor zones at 160 and 320 ft. A downhole view from video images of the major fracture zones in well W-5 at 239, 256, 323, and 393 ft are shown in figure 9. The fractures at 239 and 323 ft (fig. 9a and 9c) appear to be nearly horizontal, whereas the fracture intersecting the well at 256 ft (fig. 9b) is nearly vertical. Angular rocks and the enlarged borehole where the well collapsed just below an open, enlarged zone, are shown in figure 9d.


(a) Shows an open and enlarged fracture at 239.6 ft the fracture is nearly horizontal.


(b) Shows a vertical fracture that intersects the well at approximately 256 ft.

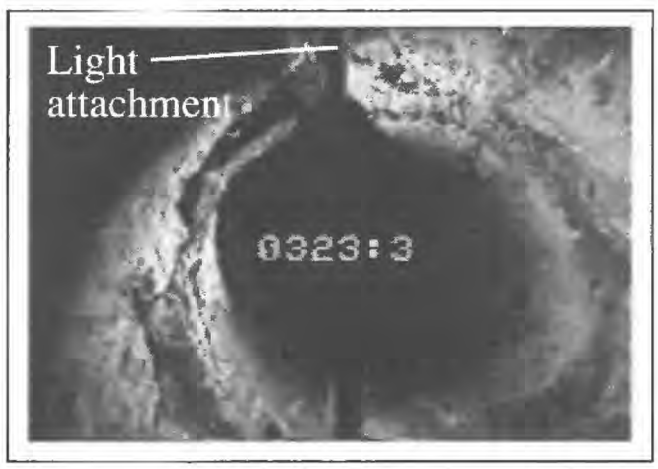


(c) Shows a nearly horizontal set of fractures that are open and oxidized.


(d) Shows the zone at 393 ft where the well collapsed at a wide, open and enlarged fracture.

**Figure 9.** Selected borehole video images from well W-5 in Rye, New Hampshire. The dark circle in the center of the screen is the light source to the camera, which is pointed down the well.

## Advanced Logs

The deviations of the wells are shown in radial plots (figs. 10 a-f), in which the center of the plot for each well represents the well location at land surface. The well location is plotted as a function of depth with respect to True North. The deviation data were used in the interpretation of the ATV fracture orientations to account for the inclination of the well. Well TBR-3 deviates nearly due east (N97°E). Although TBR-3 was drilled a total of 390 ft, its true depth is 366.6 ft, and the bottom of the well is 42.6 ft east of where it originated at the land surface. Because wells in metasedimentary rocks tend to deviate into the foliation, an easterly deviating well may indicate that the foliation and fabric are dipping west. The foliation measured in the ATV log of TBR-3 had a dip direction that ranges from N270° to N305°E, and an average dip of 50°. Other nearby wells, including W-3, W-4, and TBR-2, deviate in about the same direction (N100°E, N90°E, and N134°E, respectively). Well W-5, which intersects fewer foliated rocks than all the other wells, deviated only 4 ft.

Interpretations of the ATV logs and acoustic caliper logs provide the location and orientation of fractures in each well. Images of the ATV logs are provided in appendix 1. The original digital data are stored at the USGS. The fracture planes that could be determined were assigned a code similar to the codes used in video interpretation to describe the fracture. A code of 1 indicates a feature that is unmistakably a wide aperture fracture in the ATV log. The strike and dip could not be determined at some of the enlarged fracture zones. A code of 2 indicates fractures for which there may be a descriptor listed under comments, such as "faint," or "minor" used to further describe the fracture. A code of 3 is used when the interpretation is uncertain. Sometimes it is unclear if a planar feature is related to the rock (such as foliation or igneous dikes) or if it is a fracture. The midpoint depth and strike and dip of fracture planes that could be discerned from the ATV log are listed in table 1. The strike is reported in "right-hand-rule" in azimuthal degrees east of True North. By this nomenclature, a fracture's dip is to the right of the strike direction. For example, a North-South striking fracture, with a dip to the west, would have an orientation of N180°E, as opposed to N0°E.

A lower-hemisphere, equal-area projection, also called a stereogram, was used to plot the orientation of fractures. A stereogram reduces each fracture plane to a point that represents the intersection of a pole, perpendicular to a fracture plane, with a lower hemisphere (fig. 11). For example, a horizontal fracture would be indicated by a point in the center of the stereogram, whereas a fracture striking N215°E with a dip of 80°W would be indicated by a point towards the right (Eastern) edge of the outer circle. The orientation of the fracture plane in figure 11 is reported as N215°E, 80°, which in the right-hand-rule format implies that the fracture dips west (80° to the right of the 215° bearing).

Two stereograms were generated for each well. A series of figures that graphically depict fracture orientations from the ATV data for each of the six wells are shown in figures 12-17. Each figure includes a plot that shows the location of the fracture plotted as the fracture type (code = 1, 2 or 3) with respect to depth below the top of casing (fig. 12a). These plots can be compared directly with the standard logs (fig. 3-6). In addition, one stereogram, in each of the six figures, shows all of the fractures that were identified in the well (fig. 12b). In this stereogram, the symbol type indicates the type (code = 1, 2, or 3) of fracture. The second stereogram (fig. 12c) shows a subset of poles to fracture planes for the fractures that were interpreted as hydraulically active in the interpretation of the standard logs. The poles in these plots are labeled with the depth of intersection, which can be referenced to the standard logs and to the table (table 1) describing the ATV features. [Standard logs were collected under natural conditions, thus, under pumping conditions there could be different hydraulically active fractures.]

The poles of several of the stereograms show a wide range of orientations with no obvious pattern. The scatter in these plots is probably caused by the presence of multiple fracture sets. Because the poles to planes are not unimodal (from a single fracture population), the mean vector is not a reliable estimator of the distribution. Eigenvector analysis provides a method for evaluating the degree of clustering of poles around planes that fit through fracture sets in the distribution (Woodcock, 1977). Eigenvector analysis produces three vectors, which are fit to the distribution of poles. An eigenvalue is computed for each vector. The sum of the eigenvalues is one, and the magnitude of each eigenvalue represents the concentration of the poles associated with the respective eigenvector.

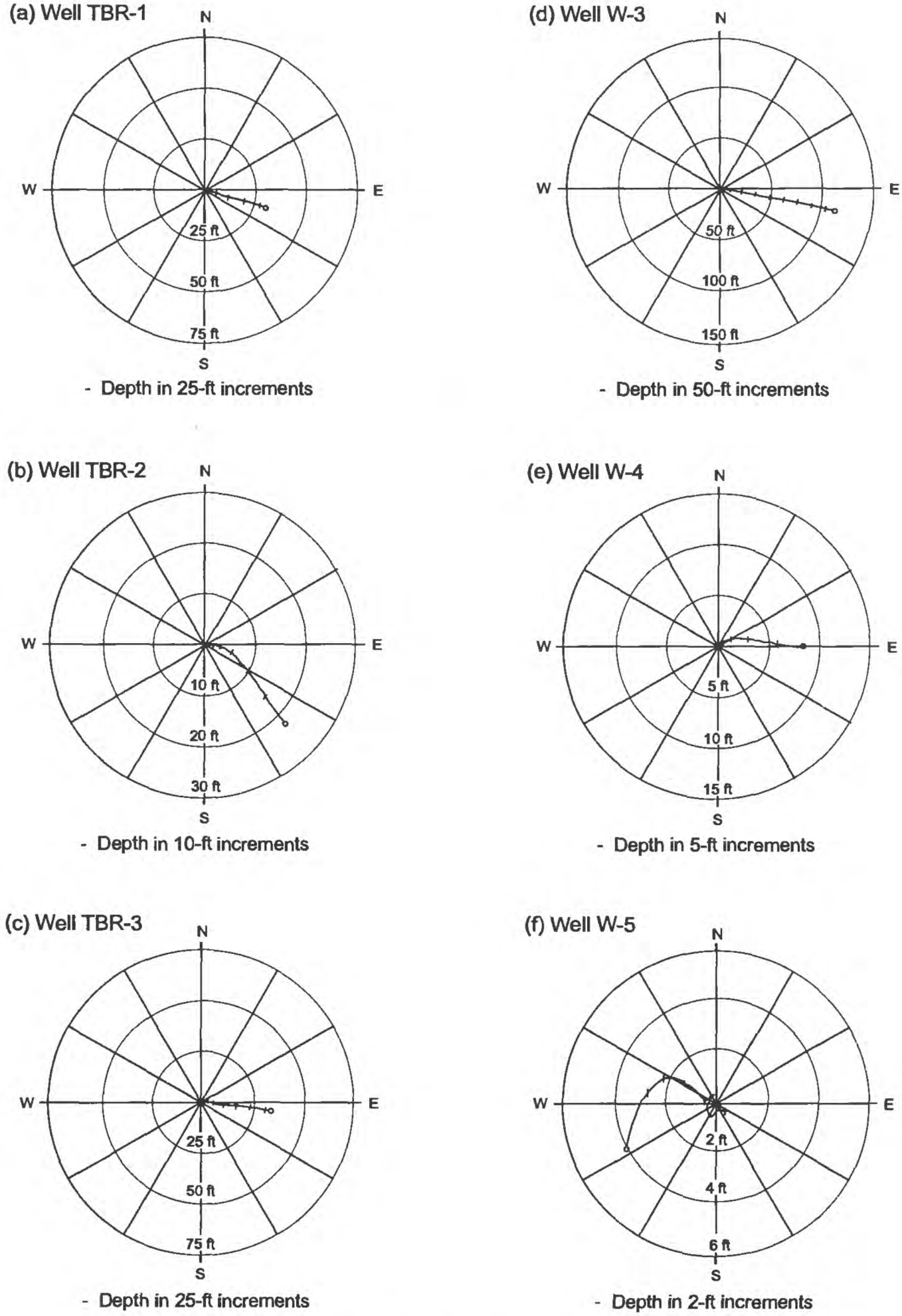


**Figure 10.** Deviation logs of wells TBR-1, TBR-2, TBR-3, W-3, W-4, and W-5 in Rye, New Hampshire. Radial distances are shown in feet (ft).

**Table 1.** Midpoint depth, strike, and dip of fractures identified in wells TBR-1, TBR-2, TBR-3, W-3, W-4, and W-5, by acoustic televiewer in Rye, New Hampshire

[Strike is reported in azmuthal degrees, east of True North in "right-hand rule" where the direction of the dip is to the right of the strike; --, no data available]

| Well TBR-1 | | | |
|---|---|---|---|
| Midpoint depth, (in feet) | Strike (degrees) | Dip (degrees) | Comments |
| | | **Major fractures (code 1)** | |
| 49.9 | 224 | 55 | Wide fracture |
| 62.8 | 330 | 5 | Wide fracture |
| 63.7 | 142 | 3 | Wide fracture |
| 78.7 | 188 | 29 | Wide fracture |
| 82.8 | 182 | 52 | Wide fracture |
| 103.0 | 325 | 58 | Fracture |
| 182.1 | 154 | 48 | Top of wide fracture |
| 182.5 | 152 | 47 | Bottom of wide fracture |
| 197.3 | 164 | 44 | Wide fracture |
| 221.0 | 54 | 30 | Top of wide fracture |
| 223.6 | 154 | 14 | Bottom of wide fracture |
| 228.9 | 258 | 38 | Top of big wide fracture zone |
| 236.3 | 28 | 38 | Bottom of wide fracture |
| 241.5 | 266 | 55 | Top of wide fracture |
| 242.6 | 208 | 21 | Bottom of wide fracture |
| 252.7 | 345 | 65 | Wide fracture |
| | | **Fractures (code 2)** | |
| 51.9 | 195 | 74 | Fracture |
| 52.6 | 184 | 69 | Fracture |
| 54.6 | 211 | 62 | Fracture |
| 61.2 | 190 | 71 | Faint fracture |
| 65.9 | 183 | 73 | Fracture |
| 66.3 | 171 | 71 | Fracture |
| 72.6 | 138 | 64 | Fracture |
| 74.4 | 194 | 51 | Fracture |
| 75.3 | 177 | 59 | Fracture |
| 114.0 | 263 | 59 | Fracture - low confidence strike and dip |
| 123.1 | 183 | 41 | Fracture |
| 134.7 | 193 | 66 | Fracture |
| 137.6 | 196 | 62 | Fracture |
| 143.8 | 160 | 24 | Faint fracture |
| 145.6 | 168 | 33 | Fracture |
| 151.9 | 179 | 50 | Fracture |
| 155.7 | 325 | 37 | Faint fracture |
| 159.0 | 157 | 38 | Faint fracture |
| 164.7 | 250 | 55 | Faint fracture |
| 169.1 | 242 | 52 | Fracture |
| 197.7 | 165 | 27 | Fracture |
| 199.8 | 353 | 58 | Fracture |
| 201.4 | 47 | 68 | Fracture |
| 203.1 | 175 | 28 | Fracture |
| 204.4 | 10 | 57 | Fracture |
| 205.0 | 12 | 75 | Fracture |

| Well TBR-1—Continued | | | |
|---|---|---|---|
| Midpoint depth, (in feet) | Strike (degrees) | Dip (degrees) | Comments |
| | | **Fractures (code 2)--Continued** | |
| 209.6 | 146 | 31 | Fracture |
| 210.6 | 6 | 49 | Fracture |
| 211.3 | 15 | 56 | Fracture |
| 216.1 | 154 | 35 | Fracture |
| 217.1 | 11 | 33 | Fracture |
| 217.4 | 191 | 77 | Fracture |
| 219.2 | 195 | 80 | Fracture |
| 246.8 | 322 | 70 | Faint fracture· |
| 248.1 | 158 | 7 | Fracture |
| 277.9 | 133 | 74 | Fracture |
| 278.7 | 131 | 79 | Fracture |
| | | **Possible fractures (code 3)** | |
| 67.9 | 206 | 79 | Possible fracture |
| 86.8 | 158 | 63 | Possible fracture |
| 97.3 | 203 | 41 | Possible fracture |
| 101.3 | 277 | 45 | Possible fracture |
| 110.6 | 228 | 66 | Possible fracture |
| 181.4 | 338 | 5 | Possible fracture |
| 207.4 | 35 | 77 | Bottom of a partial fracture |
| 240.5 | 342 | 49 | Possible fracture |
| 255.3 | 353 | 51 | Possible fracture |
| 326.6 | | | Bottom of well |

| Well TBR-2 | | | |
|---|---|---|---|
| Midpoint depth, (in feet) | Strike (degrees) | Dip (degrees) | Comments |
| | | **Major fractures (code 1)** | |
| 39.7 | 107 | 10 | Top of wide fracture |
| 40.4 | 126 | 16 | Bottom of wide fracture |
| 45.2 | 108 | 4 | Top of wide fracture |
| 45.7 | 91 | 18 | Bottom of wide fracture |
| 80.4 | 134 | 32 | Fracture |
| 81.9 | 207 | 73 | Bottom of wide fracture |
| 128.6 | 165 | 23 | Wide fracture |
| 142.8 | 243 | 74 | Wide fracture |
| 167.6 | 358 | 24 | Wide fracture |
| 212.0 | 32 | 69 | Wide fracture |
| 236.6 | 230 | 49 | Bottom of wide fracture zone |
| 237.5 | 239 | 61 | Bottom of wide fracture zone |
| 297.8 | 203 | 58 | Top of wide fracture |
| 298.6 | 193 | 47 | Bottom of wide fracture |
| 349.3 | 213 | 58 | Top of wide fracture |
| 350.0 | 213 | 62 | Bottom of wide fracture |

**Table 1.** Midpoint depth, strike, and dip of fractures identified in wells TBR-1, TBR-2, TBR-3, W-3, W-4, and W-5, by acoustic televiewer in Rye, New Hampshire--Continued

| Well TBR-2—Continued | | | |
|---|---|---|---|
| Midpoint depth, (in feet) | Strike (degrees) | Dip (degrees) | Comments |
| **Fractures (code 2)** | | | |
| 51.6 | 248 | 16 | Fracture |
| 55.4 | 242 | 67 | Fracture |
| 59.6 | 342 | 21 | Fracture |
| 61.7 | 260 | 83 | Fracture with irregular shape |
| 68.3 | 276 | 63 | Fracture |
| 68.3 | 287 | 69 | Fracture |
| 72.7 | 235 | 73 | Fracture |
| 78.4 | 24 | 75 | Fracture |
| 83.3 | 97 | 10 | Fracture |
| 84.6 | 251 | 31 | Faint fracture |
| 84.7 | 241 | 32 | Faint fracture |
| 86.3 | 356 | 7 | Faint fracture |
| 87.2 | 218 | 73 | Faint fracture |
| 89.7 | 226 | 70 | Fracture |
| 92.3 | 354 | 11 | Fracture |
| 94.7 | 33 | 17 | Fracture |
| 95.8 | 21 | 14 | Faint fracture |
| 97.3 | 345 | 7 | Fracture |
| 98.1 | 3 | 7 | Faint fracture |
| 98.2 | 20 | 5 | Faint fracture |
| 100.0 | 105 | 55 | Fracture |
| 103.8 | 90 | 27 | Fracture |
| 106.3 | 230 | 79 | Fracture with irregular shape |
| 106.7 | 194 | 80 | Fracture with irregular shape |
| 106.9 | 88 | 26 | Fracture |
| 109.5 | 356 | 17 | Fracture |
| 110.3 | 210 | 71 | Fracture with irregular shape |
| 111.0 | 316 | 43 | Fracture |
| 112.0 | 89 | 45 | Fracture |
| 113.1 | 329 | 30 | Fracture |
| 116.4 | 251 | 56 | Fracture |
| 120.6 | 138 | 44 | Faint fracture |
| 123.2 | 109 | 50 | Fracture |
| 128.3 | 80 | 24 | Fracture |
| 167.1 | 349 | 8 | Fracture |
| 211.6 | 15 | 58 | Fracture |
| 218.6 | 263 | 54 | Fracture |
| 218.8 | 248 | 40 | Fracture |
| 221.8 | 25 | 64 | Fracture |
| 254.3 | 168 | 54 | Fracture |
| 257.1 | 146 | 35 | Fracture |
| 262.3 | 130 | 63 | Fracture |
| 271.3 | 331 | 27 | Fracture |
| 308.7 | 201 | 73 | Fracture |

| Well TBR-2—Continued | | | |
|---|---|---|---|
| Midpoint depth, (in feet) | Strike (degrees) | Dip (degrees) | Comments |
| **Fractures (code 2)--Continued** | | | |
| 335.0 | 196 | 58 | Fracture |
| 336.5 | 215 | 54 | Faint fracture |
| 344.6 | 198 | 40 | Fracture wide |
| 347.5 | 193 | 32 | Fracture |
| **Possible fractures (code 3)** | | | |
| 57.2 | 236 | 75 | Possible fracture |
| 68.7 | 266 | 78 | Possible fracture |
| 101.3 | 353 | 64 | Fracture or contact |
| 113.5 | 258 | 80 | Fracture or contact |
| 122.5 | 113 | 43 | Fracture or lithologic contact |
| 196.7 | 62 | 53 | Possible fracture |
| 266.2 | 83 | 69 | Possible fracture |
| 267.3 | 277 | 17 | Possible fracture |
| 282.3 | 168 | 63 | Possible fracture |
| 296.7 | 184 | 51 | Possible fracture |
| 299.7 | 323 | 17 | Possible fracture |
| 302.0 | 313 | 19 | Fracture or lithologic contact |
| 313.5 | 223 | 61 | Possible fracture |
| 329.5 | 199 | 58 | Possible fracture |
| 402.0 | -- | -- | Major fracture |

| Well TBR-3 | | | |
|---|---|---|---|
| Midpoint depth, (in feet) | Strike (degrees) | Dip (degrees) | Comments |
| **Major fractures (code 1)** | | | |
| 43.9 | 169 | 30 | Wide fracture |
| 47.1 | 190 | 19 | Wide fracture |
| 61.0 | 184 | 37 | Top of wide fracture |
| 61.2 | 192 | 33 | Bottom of wide fracture |
| 140.7 | 269 | 26 | Top of wide fracture |
| 141.0 | 268 | 22 | Bottom of wide fracture |
| 161.7 | 189 | 28 | Wide fracture |
| 162.5 | 252 | 51 | Wide fracture |
| 177.0 | 145 | 40 | Top of wide fracture |
| 177.9 | 175 | 29 | Bottom of wide fracture |
| 182.9 | 152 | 31 | Wide fracture |
| 191.0 | 158 | 38 | Wide fracture |
| 195.6 | 81 | 6 | Top of wide fracture |
| 196.9 | 156 | 29 | Bottom of wide fracture |
| 200.7 | 12 | 33 | Top of wide fracture |
| 203.0 | 18 | 54 | Wide fracture |
| 205.5 | 183 | 36 | Wide fracture |
| 205.9 | 21 | 68 | Wide fracture |
| 209.1 | 42 | 36 | Top of wide fracture |

**Table 1.** Midpoint depth, strike, and dip of fractures identified in wells TBR-1, TBR-2, TBR-3, W-3, W-4, and W-5, by acoustic televiewer in Rye, New Hampshire--Continued

| Well TBR-3—Continued | | | |
|---|---|---|---|
| Midpoint depth, (in feet) | Strike (degrees) | Dip (degrees) | Comments |
| **Major fractures (code 1)--Continued** | | | |
| 209.9 | 352 | 28 | Bottom of wide fracture |
| 210.4 | 69 | 33 | Top of wide fracture |
| 211.4 | 153 | 38 | Bottom of wide fracture |
| 217.3 | 154 | 27 | Top of wide fracture |
| 218.2 | 149 | 16 | Bottom of wide fracture |
| 219.3 | 170 | 34 | Top of wide fracture |
| 219.6 | 185 | 31 | Bottom of wide fracture |
| 228.9 | 273 | 39 | Wide fracture |
| 234.0 | 263 | 41 | Top of wide fracture |
| 235.6 | 268 | 34 | Bottom of wide fracture |
| 237.8 | 126 | 28 | Top of wide fracture |
| 238.7 | 121 | 25 | Bottom of wide fracture |
| 240.3 | 153 | 6 | Top of wide fracture |
| 241.0 | 99 | 21 | Bottom of wide fracture |
| **Fractures (code 2)** | | | |
| 43.2 | 113 | 64 | Fracture |
| 50.3 | 276 | 70 | Fracture |
| 52.1 | 281 | 58 | Fracture |
| 59.4 | 211 | 65 | Fracture |
| 62.9 | 279 | 78 | Faint fracture |
| 71.5 | 286 | 57 | Fracture |
| 78.0 | 201 | 31 | Fracture |
| 87.8 | 163 | 82 | Faint fracture |
| 95.4 | 229 | 36 | Fracture |
| 100.4 | 294 | 72 | Fracture |
| 104.1 | 185 | 52 | Fracture |
| 104.4 | 148 | 60 | Fracture |
| 106.9 | 280 | 39 | Fracture |
| 108.2 | 88 | 41 | Fracture |
| 109.6 | 142 | 22 | Fracture |
| 113.8 | 296 | 60 | Fracture |
| 114.3 | 214 | 63 | Fracture |
| 120.9 | 51 | 82 | Faint fracture |
| 121.1 | 212 | 47 | Fracture |
| 122.3 | 177 | 32 | Fracture |
| 140.6 | 167 | 34 | Fracture |
| 142.7 | 167 | 52 | Fracture |
| 179.9 | 211 | 72 | Faint fracture |
| 180.6 | 153 | 30 | Fracture |
| 192.7 | 190 | 36 | Fracture |
| 198.3 | 129 | 79 | Fracture |
| 201.5 | 173 | 68 | Fracture |
| 201.7 | 105 | 25 | Fracture |
| 216.5 | 190 | 72 | Fracture |

| Well TBR-3—Continued | | | |
|---|---|---|---|
| Midpoint depth, (in feet) | Strike (degrees) | Dip (degrees) | Comments |
| **Fractures (code 2)--Continued** | | | |
| 220.5 | 110 | 70 | Faint fracture |
| 222.1 | 202 | 68 | Faint fracture |
| 224.5 | 289 | 59 | Fracture |
| 228.8 | 118 | 80 | Fracture |
| 237.0 | 335 | 59 | Fracture |
| 240.7 | 44 | 78 | Faint fracture |
| 246.4 | 29 | 52 | Fracture |
| 246.7 | 234 | 81 | Fracture |
| 246.7 | 350 | 61 | Fracture |
| 248.8 | 232 | 77 | Fracture |
| 249.0 | 311 | 72 | Fracture |
| 249.7 | 319 | 77 | Faint fracture |
| 251.9 | 19 | 53 | Fracture |
| 256.6 | 15 | 45 | Faint fracture |
| 259.6 | 104 | 56 | Faint fracture |
| 263.6 | 120 | 72 | Fracture |
| 265.5 | 124 | 58 | Fracture |
| 276.1 | 111 | 82 | Fracture |
| 286.4 | 189 | 34 | Fracture |
| 288.7 | 278 | 76 | Fracture |
| 290.2 | 182 | 28 | Fracture |
| 292.8 | 205 | 25 | Fracture |
| 294.8 | 95 | 85 | Faint fracture |
| 310.5 | 237 | 37 | Fracture |
| 310.9 | 243 | 69 | Faint fracture |
| 316.8 | 225 | 25 | Fracture |
| 350.4 | 256 | 33 | Fracture |
| 351.2 | 278 | 68 | Fracture |
| 353.7 | 211 | 41 | Fracture |
| 358.8 | 156 | 71 | Fracture |
| 360.1 | 143 | 80 | Fracture |
| 362.2 | 265 | 63 | Faint fracture |
| **Possible fractures (code 3)** | | | |
| 59.9 | 305 | 64 | Possible fracture |
| 70.8 | 217 | 59 | Possible fracture |
| 76.2 | 152 | 15 | Possible fracture |
| 86.4 | 185 | 59 | Possible fracture |
| 103.7 | 210 | 60 | Possible fracture |
| 117.2 | 191 | 52 | Fracture or contact |
| 117.5 | 187 | 50 | Fracture or contact |
| 118.3 | 160 | 18 | Fracture or contact |
| 130.6 | 175 | 21 | Fracture or contact |
| 142.8 | 303 | 73 | Possible fracture |
| 152.9 | 212 | 50 | Possible fracture |

**Table 1.** Midpoint depth, strike, and dip of fractures identified in wells TBR-1, TBR-2, TBR-3, W-3, W-4, and W-5, by acoustic televiewer in Rye, New Hampshire--Continued

**Well TBR-3—Continued**

| Midpoint depth, (in feet) | Strike (degrees) | Dip (degrees) | Comments |
|---|---|---|---|
| | **Possible fractures (code 3)--Continued** | | |
| 157.8 | 170 | 35 | Fracture or contact |
| 180.0 | 72 | 13 | Possible fracture |
| 181.3 | 5 | 17 | Possible fracture |
| 183.4 | 168 | 30 | Possible fracture |
| 183.9 | 151 | 26 | Possible fracture |
| 184.2 | 140 | 21 | Possible fracture |
| 185.1 | 160 | 24 | Possible fracture |
| 230.8 | 252 | 38 | Fracture or contact |
| 259.8 | 66 | 34 | Possible fracture |
| 270.8 | 275 | 77 | Possible fracture |
| 284.8 | 274 | 74 | Possible fracture |
| 311.4 | 188 | 36 | Possible fracture |
| 351.9 | 137 | 57 | Possible fracture |
| 354.3 | 256 | 38 | Possible fracture |
| 355.2 | 248 | 41 | Possible fracture |
| 358.4 | 215 | 37 | Possible fracture |
| 358.7 | 215 | 42 | Possible fracture |
| 362.2 | 120 | 82 | Possible fracture |
| 364.7 | 211 | 41 | Possible fracture |
| 364.7 | 211 | 41 | Possible fracture |

**W-3**

| Midpoint depth, (in feet) | Strike (degrees) | Dip (degrees) | Comments |
|---|---|---|---|
| | **Major fractures (code 1)** | | |
| 36.6 | 338 | 60 | Wide fracture |
| 168.2 | 338 | 55 | Top of wide fracture zone |
| 168.9 | 337 | 54 | Bottom of wide fracture zone |
| 178.7 | 332 | 49 | Top of wide fracture zone |
| 180.3 | 310 | 29 | Bottom of wide fracture zone |
| 184.4 | 340 | 55 | Wide fracture |
| 259.0 | 342 | 54 | Wide fracture |
| 537.7 | 340 | 50 | Wide fracture |
| 550.4 | 292 | 17 | Wide fracture |
| | **Fractures (code 2)** | | |
| 28.3 | 276 | 3 | Fracture |
| 29.2 | 278 | 3 | Fracture |
| 51.3 | 320 | 45 | Fracture |
| 69.1 | 326 | 51 | Fracture |
| 83.2 | 330 | 56 | Fracture |
| 90.6 | 317 | 40 | Fracture |
| 122.7 | 343 | 70 | Fracture |

**W-3—Continued**

| Midpoint depth, (in feet) | Strike (degrees) | Dip (degrees) | Comments |
|---|---|---|---|
| | **Fractures (code 2)--Continued** | | |
| 150.9 | 340 | 56 | Fracture |
| 159.3 | 327 | 51 | Fracture |
| 170.0 | 332 | 47 | Fracture |
| 189.2 | 333 | 65 | Fracture |
| 191.2 | 343 | 58 | Fracture |
| 210.3 | 339 | 53 | Fracture |
| 226.1 | 351 | 66 | Fracture |
| 257.4 | 348 | 62 | Fracture |
| 401.5 | 340 | 76 | Fracture |
| 405.7 | 323 | 58 | Fracture |
| 440.0 | 295 | 26 | Fracture |
| 464.1 | 352 | 81 | Fracture |
| 533.2 | 349 | 64 | Fracture |
| 542.7 | 310 | 40 | Fracture |
| 549.8 | 324 | 46 | Fracture |
| 550.1 | 289 | 23 | Fracture |
| | **Possible fractures (code 3)** | | |
| 39.6 | 299 | 23 | Possible fracture |
| 53.9 | 285 | 11 | Possible fracture |
| 187.6 | 347 | 64 | Possible fracture |
| 200.9 | 325 | 38 | Possible fracture |
| 288.1 | 288 | 7 | Possible fracture |
| 511.9 | 289 | 19 | Possible fracture |
| 550.6 | 284 | 16 | Possible fracture at bottom of hole |

**W-4**

| Midpoint depth, (in feet) | Strike (degrees) | Dip (degrees) | Comments |
|---|---|---|---|
| | **Major fractures (code 1)** | | |
| 55.1 | 305 | 4 | Bottom of wide fracture |
| 55.8 | 28 | 7 | Bottom of wide fracture |
| 73.8 | 316 | 10 | Bottom of wide fracture |
| 85.6 | 274 | 14 | Bottom of wide fracture |
| 96.5 | 274 | 25 | Top of wide fracture zone |
| 97.3 | 294 | 3 | Bottom of wide fracture zone |
| 110.2 | 330 | 12 | Bottom of wide fracture zone |
| 140.9 | 321 | 17 | Bottom of wide fracture zone |
| 227.4 | 300 | 24 | Wide fracture |
| 240.9 | 136 | 61 | Top of wide fracture zone |
| 251.0 | 162 | 64 | Top of wide fracture zone |
| 252.1 | 164 | 64 | Bottom of wide fracture zone |
| 288.9 | 73 | 32 | Top of wide fracture |

**Table 1.** Midpoint depth, strike, and dip of fractures identified in wells TBR-1, TBR-2, TBR-3, W-3, W-4, and W-5, by acoustic televiewer in Rye, New Hampshire--Continued

**W-4—Continued**

| Midpoint depth, (in feet) | Strike (degrees) | Dip (degrees) | Comments |
|---|---|---|---|
| | | **Fractures (code 2)** | |
| 38.8 | 304 | 13 | Fracture |
| 61.0 | 4 | 66 | Fracture |
| 79.9 | 329 | 23 | Fracture |
| 82.8 | 97 | 85 | Partial, vertical fracture |
| 114.3 | 322 | 13 | Fracture |
| 115.2 | 158 | 67 | Fracture |
| 117.6 | 201 | 47 | Fracture |
| 129.4 | 5 | 58 | Fracture |
| 168.6 | 218 | 18 | Fracture |
| 195.8 | 343 | 38 | Fracture |
| 196.4 | 337 | 40 | Fracture |
| 235.5 | 234 | 57 | Fracture |
| 245.4 | 172 | 56 | Fracture |
| 247.4 | 184 | 58 | Fracture |
| 250.0 | 150 | 59 | Fracture |
| 270.7 | 248 | 78 | Faint fracture |
| 276.3 | 13 | 69 | Fracture |
| 284.6 | 281 | 78 | Fracture |
| | | **Possible fractures (code 3)** | |
| 150.6 | 325 | 42 | Possible fracture |
| 285.3 | 73 | 43 | Possible fracture |
| 222.3 | 340 | 16 | Fracture or lithologic contact |

**W-5**

| Midpoint depth, (in feet) | Strike (degrees) | Dip (degrees) | Comments |
|---|---|---|---|
| | | **Major fractures (code 1)** | |
| 160.4 | 242 | 43 | Wide fracture |
| 166.0 | 69 | 31 | Wide fracture |
| 213.9 | 208 | 58 | Wide fracture |
| 234.0 | 74 | 0 | Top of wide fracture |
| 235.4 | 74 | 0 | Bottom of wide fracture |
| 241.5 | 203 | 63 | Top of wide fracture |
| 243.8 | 153 | 15 | Bottom of wide fracture |
| 248.0 | 204 | 41 | Top of wide fracture |
| 248.1 | 204 | 39 | Bottom of wide fracture |
| 393.0 | -- | -- | Fracture zone |
| | | **Fractures (code 2)** | |
| 332.9 | 158 | 2 | Fracture here -approximate strike and dip |
| 154.8 | 341 | 64 | Fracture |

**W-5—Continued**

| Midpoint depth, (in feet) | Strike (degrees) | Dip (degrees) | Comments |
|---|---|---|---|
| | | **Fractures (code 2)--Continued** | |
| 175.6 | 47 | 45 | Fracture |
| 181.3 | 197 | 38 | Fracture |
| 198.8 | 18 | 33 | Fracture |
| 226.9 | 233 | 19 | Fracture |
| 232.8 | 335 | 17 | Fracture |
| 237.2 | 221 | 8 | Fracture |
| 238.7 | 128 | 55 | Fracture |
| 246.3 | 213 | 55 | Fracture |
| 252.3 | 338 | 8 | Fracture |
| 258.7 | 205 | 74 | Fracture |
| 259.3 | 224 | 73 | Fracture |
| 287.8 | 308 | 47 | Fracture |
| 316.5 | 132 | 71 | Fracture |
| 326.0 | 337 | 3 | Fracture |
| 336.2 | 332 | 14 | Fracture |
| 355.7 | 349 | 21 | Fracture |
| 361.7 | 176 | 74 | Fracture |
| 370.1 | 343 | 29 | Fracture |
| 375.9 | 200 | 40 | Fracture |
| 377.3 | 320 | 23 | Fracture |
| 377.7 | 348 | 19 | Fracture |
| 381.6 | 319 | 24 | Fracture |
| 383.1 | 351 | 24 | Fracture |
| 386.3 | 19 | 31 | Fracture |
| | | **Possible fractures (code 3)** | |
| 170.9 | 27 | 62 | Possible fracture |
| 242.5 | 201 | 46 | Possible fracture |
| 254.0 | 79 | 68 | Possible fracture |
| 279.2 | 156 | 49 | Possible fracture |
| 280.3 | 141 | 48 | Possible fracture |
| 284.8 | 169 | 8 | Possible fracture |
| 291.9 | 266 | 39 | Possible fracture |
| 322.1 | 244 | 15 | Possible fracture |
| 355.2 | 23 | 34 | Possible fracture |
| 363.0 | 123 | 63 | Possible fracture |
| 363.7 | 121 | 58 | Possible fracture |
| 365.2 | 251 | 59 | Possible fracture |
| 365.5 | 247 | 55 | Possible fracture |
| 376.9 | 183 | 7 | Possible fracture |
| 390.1 | 196 | 74 | Possible fracture |

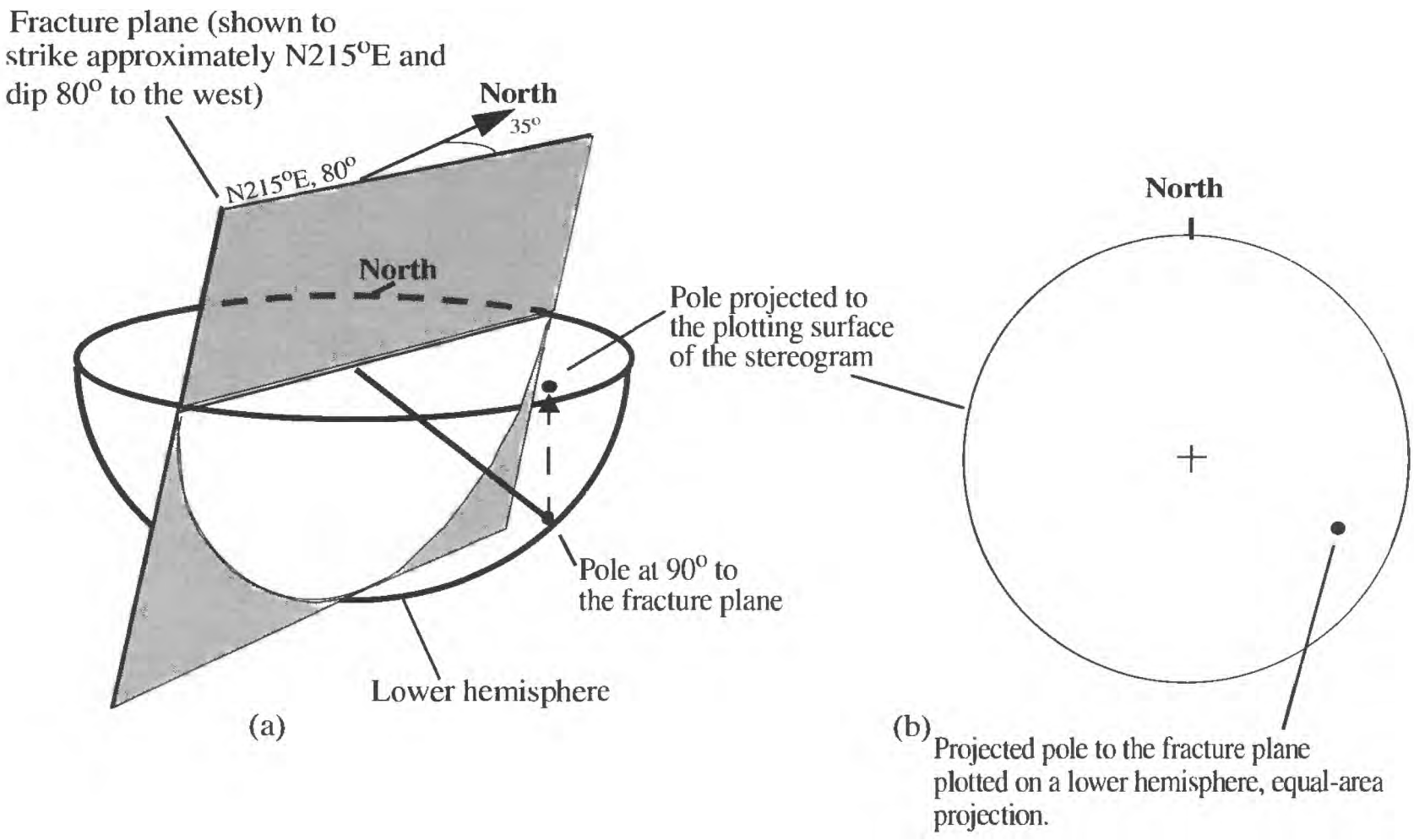


**Figure 11.** Schematic diagram of stereographic projections. The stereographic projection reduces the orientation of a fracture plane to a point on a stereogram by plotting the pole to the plane on a lower hemisphere and projecting it up to the plotting surface of the stereogram. The schematic (a) shows a three-dimensional representation of the fracture plane as it intersects the hemisphere and the projected pole to the plane, and (b) shows the stereogram that would correspond to example (a).

An eigenvalue that is close to one indicates a unimodal set of planes that is closely parallel to the eigenvector and could adequately be described by a mean vector. The magnitudes of the eigenvectors are used to determine if the fracture sets are statistically significant. An eigenvalue close to zero indicates an insignificant eigenvector with only a minimal amount of poles associated with it. For each well, the results of the analyses, including the mean vector, eigenvalue, and eigenvector are listed in table 2 for each fracture type and for all of the fracture types combined. The eigenvectors were generated using StereoNett software developed by Johannes Duyster at the Institute for Geology, Ruhr-University Borchum, Germany.

A comparison of the eigenvalues and eigenvectors for the wide fractures and fractures in TBR-1 and TBR-3 indicates there is a strong component of fractures that strike N171°E to N203°E and dip from 32 to 70° to the west. These features are similar in strike to the lineaments determined in the high- and low-aerial photography that are mapped to the west of the wells (fig. 1) and trend approximately N165°E and N169°E.

Well TBR-2 has a high proportion (eigenvalue = 0.556) of "wide fractures" (code = 1) that follows the same direction (N185°E, dipping 62°W). However, the "fractures" (code = 2) in TBR-2 have a dominant orientation of N320°E, dipping 74° (N-NE), which is parallel to the SLAR feature that is labeled N140°E (fig. 1). If these are coincident, it would imply that this SLAR feature dips northeast.

Well W-3 has a strongly clustered set of poles (eigenvalue = 0.910) about a plane oriented at N313°E, dipping 49°(N-NE) for the "wide fractures." and an eigenvalue of 0.850 at N307°E, 54°(NE) for "fractures." The dominant fracture planes in W-3 are nearly parallel to the fractures observed in TBR-2, as well as the SLAR feature that is trending N140°E.

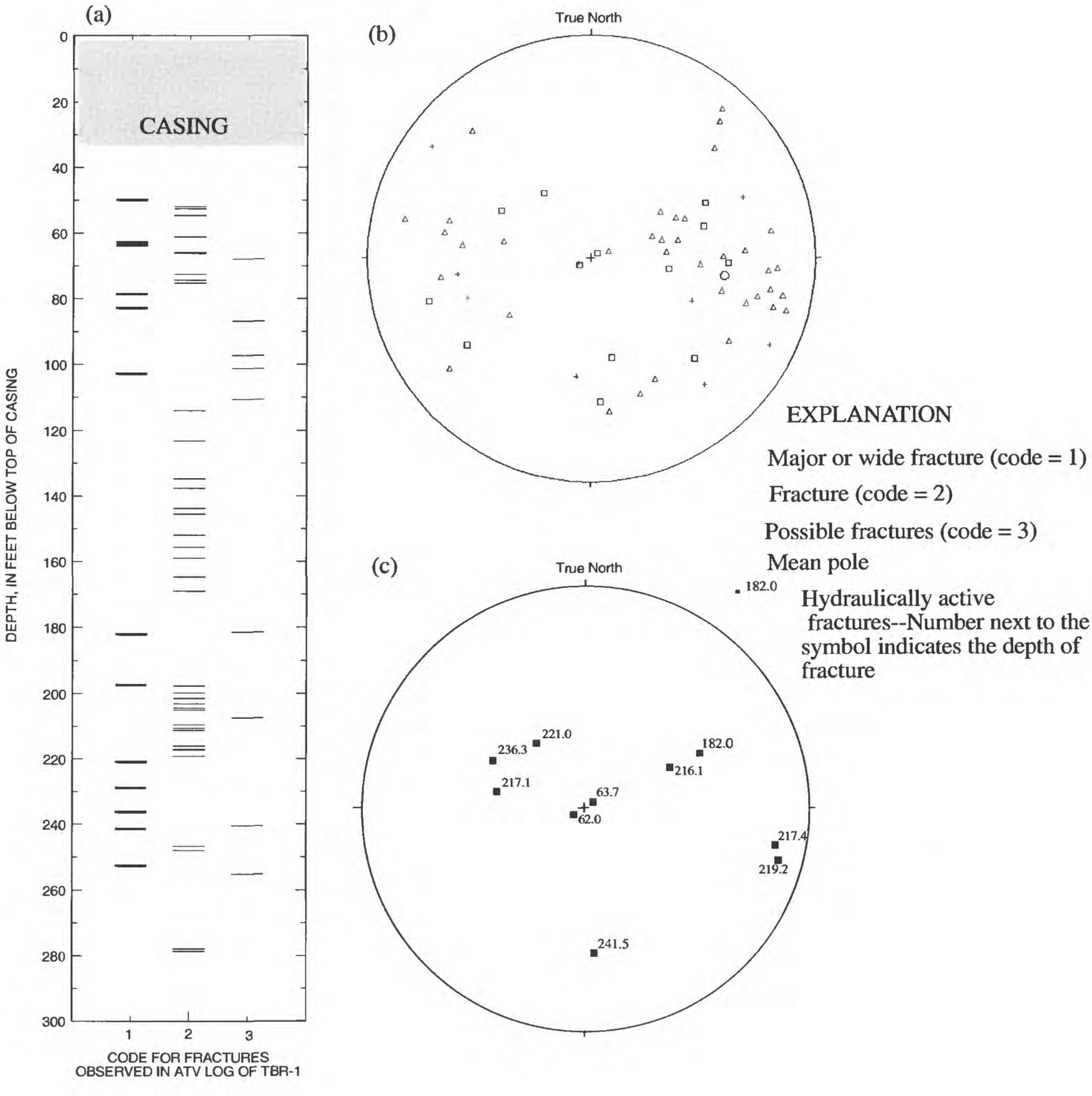


**Figure 12.** Location and orientation of fractures observed in acoustic televiewer (ATV) log of well TBR-1, in Rye, New Hampshire shows the (a) depths and fracture code, (b) lower-hemisphere equal-area projection (stereogram) of fracture poles for all fractures (the symbol indicates the fracture code), and (c) stereogram of hydraulically active fractures.

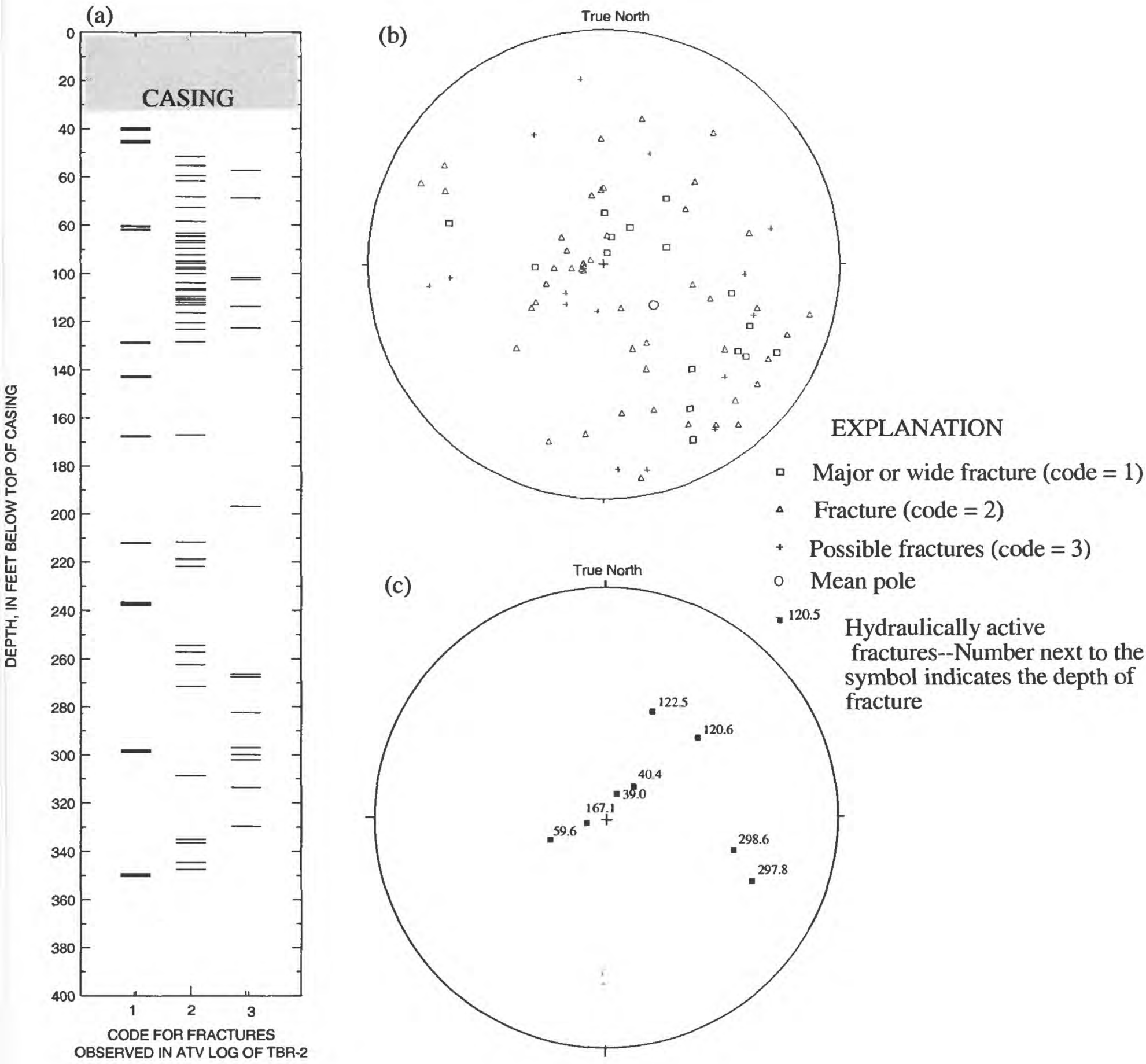


**Figure 13.** Location and orientation of fractures observed in acoustic televiewer (ATV) log of well TBR-2, in Rye, New Hampshire shows the (a) depths and fracture code, (b) lower-hemisphere equal-area projection (stereogram) of fracture poles for all fractures (the symbol indicates the fracture code), and (c) stereogram of hydraulically active fractures.

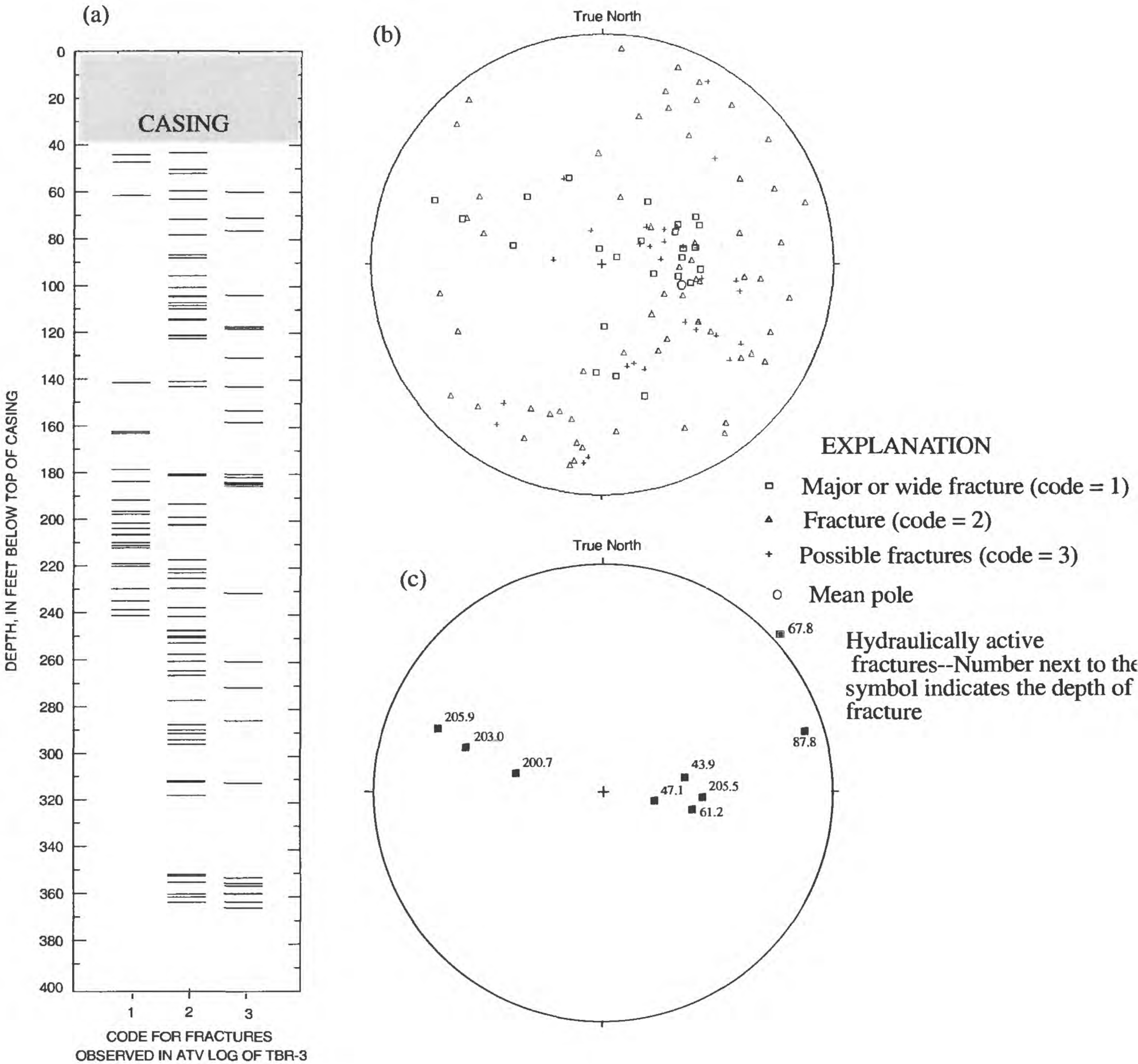


**Figure 14.** Location and orientation of fractures observed in acoustic televiewer (ATV) log of well TBR-3, in Rye, New Hampshire shows the (a) depths and fracture code, (b) lower-hemisphere equal-area projection (stereogram) of fracture poles for all fractures (the symbol indicates the fracture code), and (c) stereogram of hydraulically active fractures.

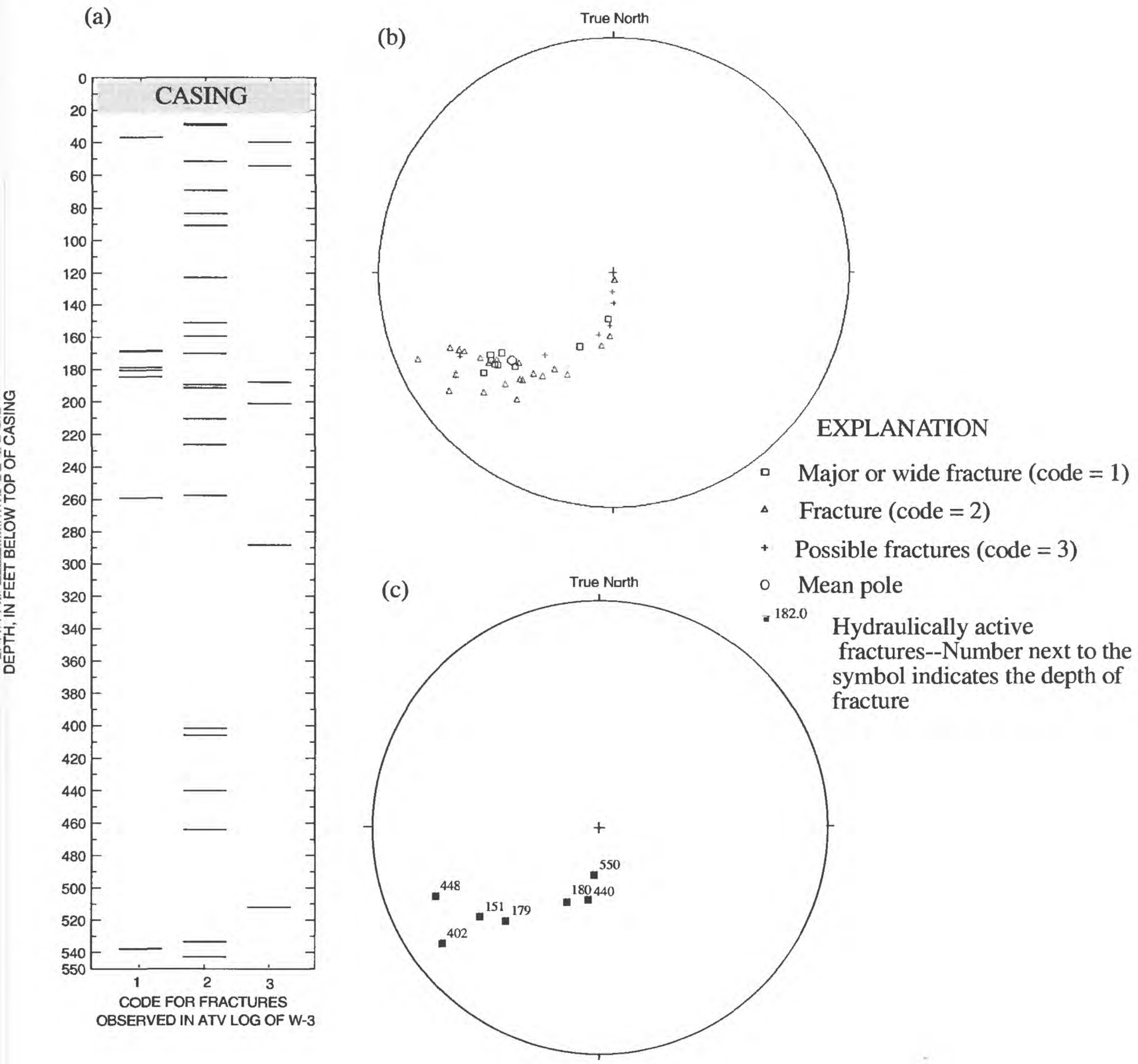


**Figure 15.** Location and orientation of fractures observed in acoustic televiewer (ATV) log of well W-3, in Rye, New Hampshire shows the (a) depths and fracture code, (b) lower-hemisphere equal-area projection (stereogram) of fracture poles for all fractures (the symbol indicates the fracture code), and (c) stereogram of hydraulically active fractures.

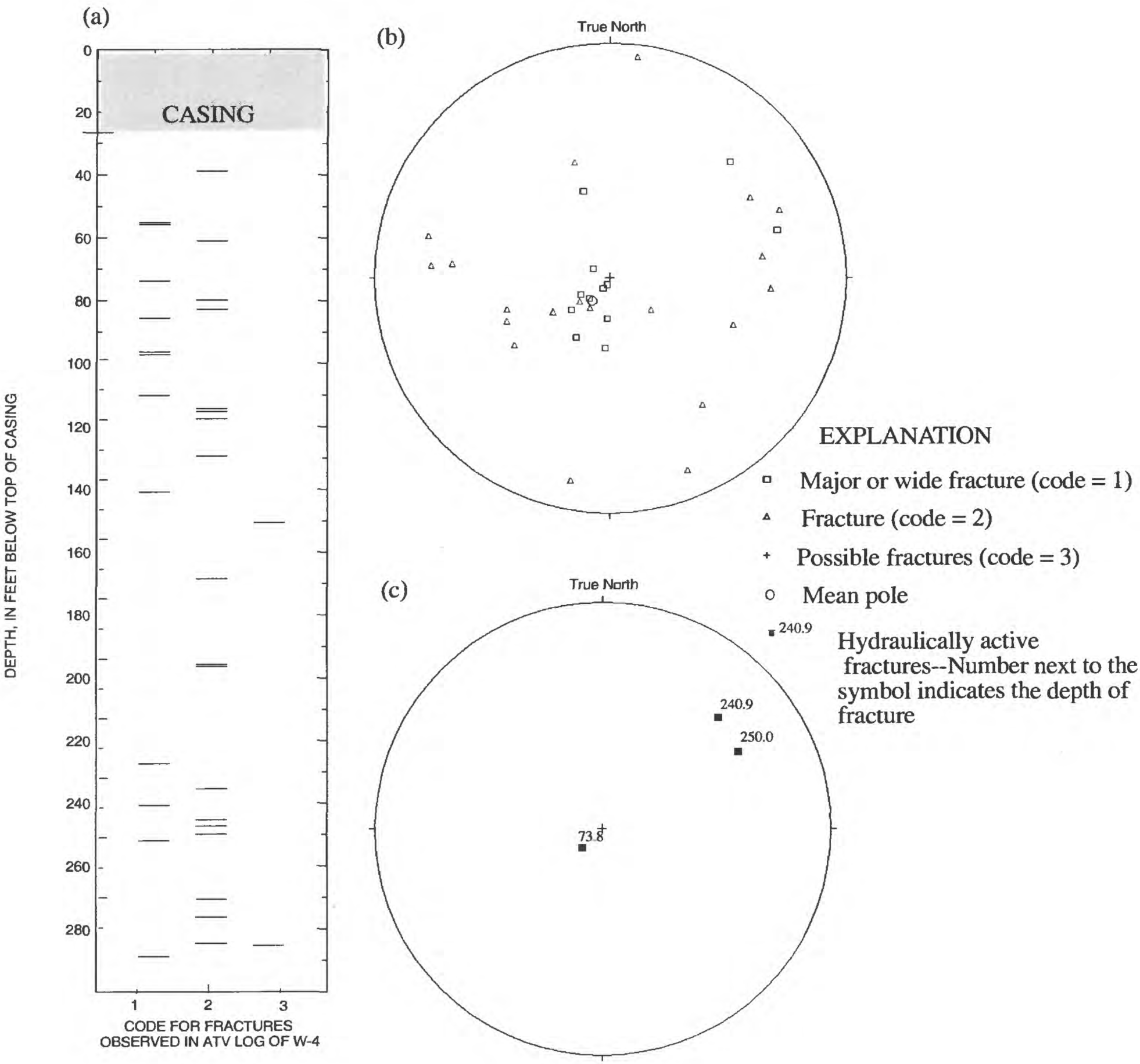


**Figure 16.** Location and orientation of fractures observed in acoustic televiewer (ATV) log of well W-4, in Rye, New Hampshire shows the (a) depths and fracture code, (b) lower-hemisphere equal-area projection (stereogram) of fracture poles for all fractures (the symbol indicates the fracture code), and (c) stereogram of hydraulically active fractures.

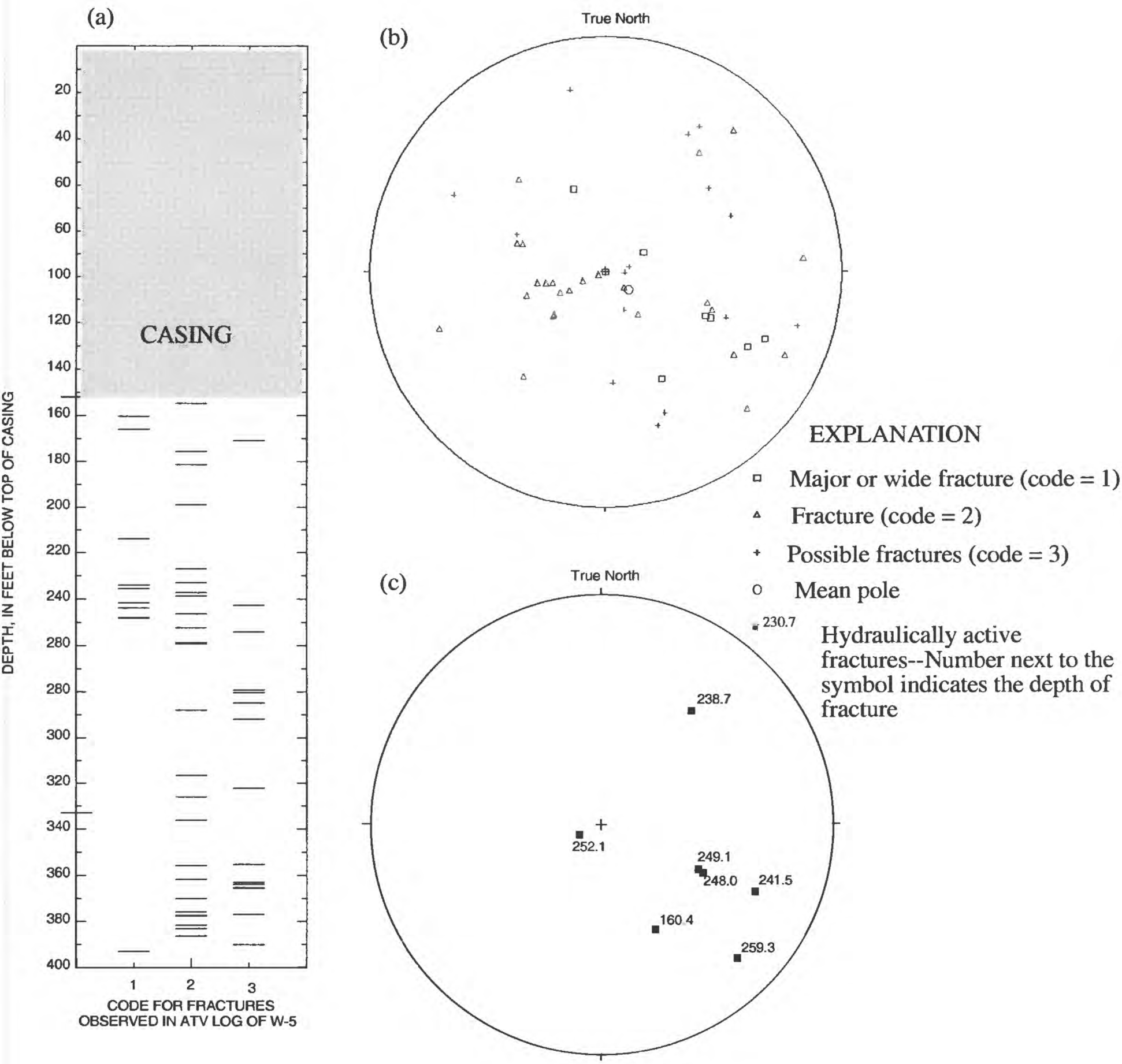


**Figure 17.** Location and orientation of fractures observed in acoustic televiewer (ATV) log of well W-5, in Rye, New Hampshire shows the (a) depths and fracture code, (b) lower-hemisphere equal-area projection (stereogram) of fracture poles for all fractures (the symbol indicates the fracture code), and (c) stereogram of hydraulically active fractures.

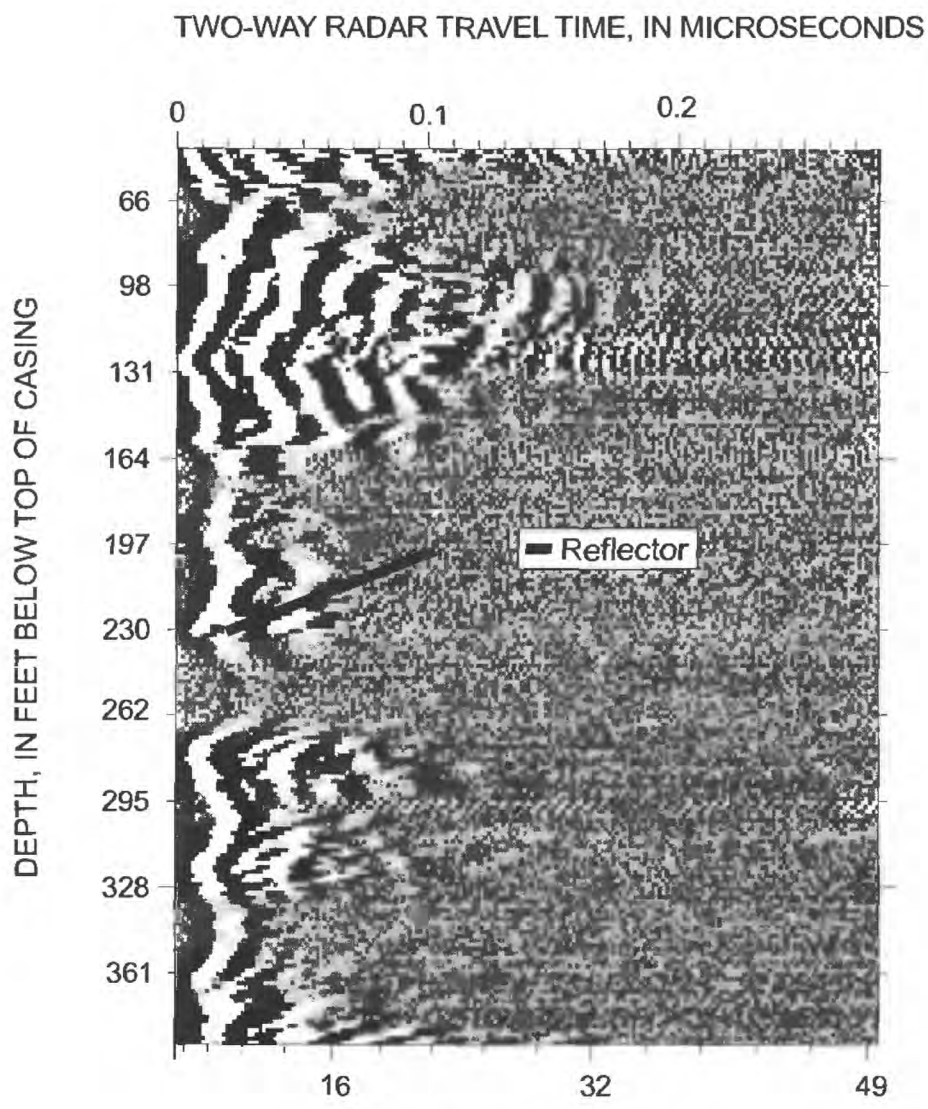


**Figure 18.** Unprocessed borehole-radar log of well TBR-2 in Rye, New Hampshire.

Well W-4 exhibits an eigenvector that strikes N301°E, for "wide fractures". However, the dip of the eigenvector is shallow, 8°(NE). A shallow dipping feature would not be expected to correlate with the lineaments. The "fractures" in well W-4 are clustered about a plane with an eigenvalue of 0.607 and an orientation of N282°E, dipping 81°(N). This plane is parallel to the SLAR feature that strikes N100°E (or N280°E). The interpretation of the ATV data implies that this SLAR feature is dipping North.

A pattern also emerges from the eigenvector analysis of well W-5. The "wide fractures" identified in W-5 were found to have two significant fracture sets. The dominant set had an eigenvalue of 0.622 for a plane oriented at N221°E, dipping 38°(NW), which coincides with the low altitude feature (N40°E). The second set had an eigenvalue of 0.30 for a plane at N100°E, dipping 33°(S), which is parallel to the SLAR feature trending N100°E that passes south of the well and with the orientation of Bailey Brook (fig. 1). The code-2 fractures had two significant fracture sets. The dominant set had an eigenvector of N347°E, dipping 29°(E) and an eigenvalue of 0.520, which is parallel to the high and low-altitude features trending N165°E and N169°E. A feature with a shallow dip, however, would not likely be visible from aerial photos. The second set has an eigenvalue of 0.348 at a vector of N195°E, dipping 58°(W), which is

**Table 2.** Statistical summary of fracture type and orientations for wells TBR-1, TBR-2, TBR-3, W-3, W-4, and W-5 in Rye, New Hampshire

[Fracture code 1 refers to a wide fracture; code 2 is a fracture; and code 3 is a possible fracture; All refers to all fractures (codes 1, 2, and 3)]

| Well | Fracture type code | Number of fractures | Mean vector | | Eigenvector | | Eigen value |
|---|---|---|---|---|---|---|---|
| | | | Strike | Dip | Strike | Dip | |
| TBR-1 | 1 | 13 | 173 | 69 | 199 | 64 | 0.486 |
| | | | | | 340 | 21 | 0.340 |
| | | | | | 76 | 15 | 0.175 |
| | 2 | 37 | 176 | 73 | 178 | 70 | 0.697 |
| | | | | | 348 | 20 | 0.249 |
| | | | | | 79 | 3 | 0.001 |
| | 3 | 9 | 226 | 78 | 278 | 78 | 0.652 |
| | | | | | 171 | 4 | 0.277 |
| | | | | | 80 | 11 | 0.007 |
| | all | 59 | 180 | 73 | 188 | 72 | 0.633 |
| | | | | | 346 | 17 | 0.281 |
| | | | | | 80 | 6 | 0.009 |
| TBR-2 | 1 | 16 | 158 | 54 | 185 | 62 | 0.556 |
| | | | | | 291 | 9 | 0.303 |
| | | | | | 26 | 27 | 0.141 |
| | 2 | 47 | 321 | 78 | 320 | 74 | 0.494 |
| | | | | | 2 | 13 | 0.297 |
| | | | | | 94 | 8 | 0.208 |
| | 3 | 15 | 282 | 81 | 232 | 85 | 0.633 |
| | | | | | 132 | 1 | 0.241 |
| | | | | | 42 | 5 | 0.125 |
| | all | 79 | 173 | 59 | 205 | 75 | 0.525 |
| | | | | | 332 | 9 | 0.263 |
| | | | | | 64 | 12 | 0.211 |
| TBR-3 | 1 | 24 | 191 | 28 | 203 | 76 | 0.550 |
| | | | | | 2 | 13 | 0.239 |
| | | | | | 347 | 58 | 0.211 |
| | 2 | 62 | 199 | 75 | 203 | 76 | 0.713 |
| | | | | | 2 | 13 | 0.159 |
| | | | | | 93 | 50 | 0.127 |
| | 3 | 29 | 193 | 51 | 193 | 51 | 0.640 |
| | | | | | 312 | 27 | 0.221 |
| | | | | | 56 | 31 | 0.138 |
| | all | 115 | 194 | 61 | 192 | 65 | 0.618 |
| | | | | | 342 | 22 | 0.221 |
| | | | | | 77 | 11 | 0.001 |
| W-3 | 1 | 9 | 311 | 48 | 313 | 49 | 0.910 |
| | | | | | 74 | 24 | 0.009 |
| | | | | | 180 | 30 | 0.002 |
| | 2 | 23 | 303 | 52 | 307 | 54 | 0.850 |
| | | | | | 75 | 24 | 0.137 |
| | | | | | 177 | 25 | 0.001 |
| | 3 | 6 | 284 | 28 | 283 | 26 | 0.825 |
| | | | | | 45 | 50 | 0.167 |
| | | | | | 178 | 30 | 0.007 |
| | all | 38 | 301 | 48 | 304 | 50 | 0.830 |
| | | | | | 73 | 28 | 0.158 |
| | | | | | 178 | 27 | 0.001 |
| W-4 | 1 | 12 | 307 | 2 | 301 | 8 | 0.615 |
| | | | | | 60 | 75 | 0.200 |
| | | | | | 209 | 13 | 0.188 |
| | 2 | 18 | 289 | 74 | 282 | 81 | 0.607 |
| | | | | | 164 | 4 | 0.301 |
| | | | | | 13 | 8 | 0.009 |
| | 3 | 2 | -- | -- | -- | -- | -- |
| | all | 32 | 321 | 12 | 311 | 57 | 0.477 |
| | | | | | 140 | 32 | 0.340 |
| | | | | | 48 | 4 | 0.173 |
| W-5 | 1 | 9 | 225.5 | 30 | 221 | 38 | 0.622 |
| | | | | | 101 | 33 | 0.299 |
| | | | | | 344 | 35 | 0.001 |
| | 2 | 25 | 324 | 58 | 347 | 29 | 0.520 |
| | | | | | 195 | 58 | 0.348 |
| | | | | | 84 | 13 | 0.138 |
| | 3 | 15 | 186 | 68 | 181 | 68 | 0.583 |
| | | | | | 30 | 20 | 0.244 |
| | | | | | 297 | 10 | 0.172 |
| | all | 49 | 192 | 30 | 200 | 59 | 0.450 |
| | | | | | 354 | 29 | 0.350 |
| | | | | | 90 | 11 | 0.195 |

similar to the results in TBR-1 and TBR-3. Although the strike of this second set may coincide with the high-altitude lineament that could project through W-5, the dip is shallow and to the west. This dip is not consistent with the interpretation of east dipping features striking in the same direction in TBR-1 and TBR-3.

The hydraulically active fractures that were identified in the standard logs of wells TBR-1, TBR-2, and TBR-3 strike in all directions from N12° to N349°E and dip from 3 to 80° in all directions. There were 32 features included in the eigenvector analyses. The results of the eigenvector analyses for all of the hydraulically active fractures from these wells indicate a dominant fracture set with an eigenvalue of 0.551 and an orientation of N167°E, dipping 30°(W) and a secondary set with an orientation of N9°E, dipping 58°(E). In general, the dominant fracture set coincides with the strike of nearby photolinear features to the west of the wells (fig. 1). The strike and dip of individual fractures can be obtained from table 1.

Correlating the water-bearing zones that were identified at the time of drilling with individual fractures in the ATV logs was difficult. In TBR-3, the zone from 205 to 210 ft was reported to have a yield of about 100 gal/min (Gary Smith, D.L. Maher, written commun., 1996). This discrete zone was intersected by six fractures (table 1) striking N40°E, N183°E, and N352°E and dipping SE, W, and NE. Because of the variation in orientation of fractures, it is not possible to correlate these well-drillers' yields with individual fracture orientations.

In conclusion, the ATV logs and results of the eigenvector analyses indicate that the wells in the two well fields are highly fractured. In addition, there are statistically significant fracture sets that coincide with the remotely-sensed lineaments that are mapped in the two well fields (fig 1). Although the mean vector for the entire distribution coincides with some of the dominant eigenvectors, eigenvector analysis helped identify multiple fracture sets in the widely scattered data. The eigenvectors that were computed coincide with several of the lineaments identified by fracture-trace analysis. The correlation of fracture sets identified in wells and lineaments might not have been evident through mean vector analysis alone.

## Radar-Reflection Logs

The average velocity of the radar waves at the site was approximately 88 m/μs. An unprocessed radar record, from TBR-2, which is also called a radargram (fig. 19), shows the direct-arrival radar amplitude plotted as a function of depth. The x-axis represents the two-way travel time in nanoseconds, as well as the radial distance from the well, in meters. Depth of the borehole is plotted on the y-axis in meters. In the radargram of TBR-2, the low-velocity zones were identified at center depths of 30 to 50, 170, and 240 ft. In addition, minor low-velocity zones are present at center depths of 301 and 344 ft. Each of these zones coincides with enlarged zones on the caliper log, deflections in the fluid logs, and (or) fractures identified in ATV and video interpretations (fig. 4). The low velocities at 240 and 344 ft were also

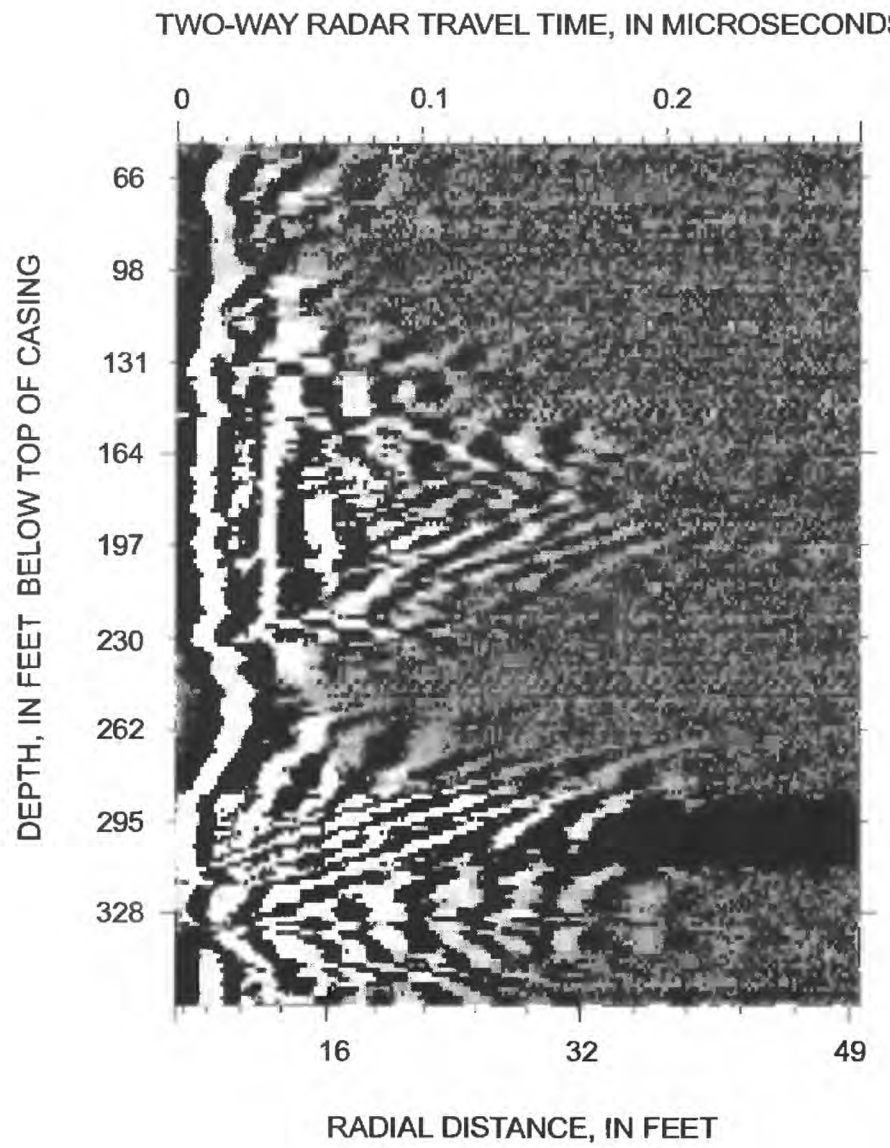


**Figure 19.** Unprocessed borehole-radar log of well TBR-3 in Rye, New Hampshire.

accompanied by high-attenuation signatures, which represent zones of minimal penetration of the radar signal. Radar responses that exhibit low velocity and high attenuation are indicative of saturated fractures that are potential-water-bearing zones (Chapman and Lane, 1996). Electromagnetic radiation penetration at the site extended approximately 50 ft from the well. In general, it was less than 30 ft. The low-signal propagation is probably caused by attenuation due to the highly fractured nature of this bedrock. The combination of many reflectors and high attenuation is indicative of a highly fractured water-bearing aquifer.

Interpreting the orientation of many of the individual radar reflectors was difficult. The trace of the reflector, which provided the location and the dip of the reflector, could be determined, however, because of the noise in the attenuation record, the strike could not always be resolved. Where the strike could be resolved, the accuracy of an interpreted strike of a reflector is about ±10 degrees. Midpoint depth (center depth between the high and low point of a dipping fracture), strike, and dip of the major planar reflectors interpreted in the bedrock surrounding the well are listed in table 3. The reflectors are projected to the borehole to determine the depth of intersection, but a reflector may not necessarily intersect the borehole wall. A negative depth of intersection indicates a reflector that is projected to intersect the well above the land surface or above the top of casing. A feature that has a depth of intersection that is below the bottom of the well is a reflector that was identified at some distance from the well and dips towards the well but does not intersect the well.

**Table 3.** Projected midpoint depth, strike and dip of reflectors identified by borehole radar for wells TBR-2, TBR-3, and W5, in Rye, New Hampshire

[Negative depths indicate a projected plane intersects above the well; -- indicates the strike cannot be determined. The strike is reported in RHR, "right-hand rule" where the direction of dip is to the right of the strike]

| Depth (feet) | Depth (meters) | Strike (degrees) | Dip (degrees) | Comments |
|---|---|---|---|---|
| **Reflectors from well TBR-2** | | | | |
| -551.9 | -168.2 | 44 | 87 | |
| -16.7 | -5.1 | 254 | 81 | Low confidence strike |
| -9.2 | -2.8 | 64 | 79 | |
| 35.4 | 10.8 | -- | 71 | |
| 122.4 | 37.3 | -- | 80 | |
| 129.3 | 39.4 | -- | 75 | |
| 136.8 | 41.7 | 264 | 83 | |
| 139.1 | 42.4 | 54 | 55 | |
| 156.8 | 47.8 | -- | 72 | |
| 161.8 | 49.3 | 144 | 77 | |
| 169.3 | 51.6 | 4 | 83 | |
| 177.5 | 54.1 | 134 | 58 | Low confidence strike |
| 195.9 | 59.7 | 184 | 66 | |
| 240.2 | 73.2 | 234 | 44 | |
| 252.6 | 77 | 254 | 64 | Low confidence strike |
| 284.5 | 86.7 | -- | 66 | |
| 288.7 | 88 | 314 | 49 | |
| 329.1 | 100.3 | 244 | 58 | Low confidence strike |
| 331.1 | 100.9 | 244 | 75 | |
| 344.5 | 105 | 294 | 46 | |
| 397.0 | 121 | | 59 | |
| 404.9 | 123.4 | | 51 | |
| **Reflectors from well TBR-3** | | | | |
| -645.4 | -196.7 | 24 | 88 | |
| -571.6 | -174.2 | 114 | 86 | |
| -394.4 | -120.2 | -- | 88 | |
| -387.5 | -118.1 | 294 | 82 | |
| -198.8 | -60.6 | 214 | 83 | |
| 18.0 | 5.5 | 74 | 86 | |
| 24.0 | 7.3 | 114 | 80 | |
| 35.1 | 10.7 | 304 | 82 | |
| 79.7 | 24.3 | 214 | 80 | |
| 93.8 | 28.6 | 304 | 68 | |
| 140.1 | 42.7 | 344 | 77 | |
| 159.5 | 48.6 | 24 | 53 | |
| 203.8 | 62.1 | 204 | 61 | |
| 210.6 | 64.2 | 14 | 75 | |
| 216.2 | 65.9 | 34 | 59 | |
| 251.0 | 76.5 | 234 | 56 | |
| 312.4 | 95.2 | 44 | 51 | |
| 423.9 | 129.2 | -- | 85 | |
| 552.2 | 168.3 | 294 | 84 | |
| **Reflectors from well W5** | | | | |
| -37.7 | -11.5 | -- | 85.3 | Faint feature |
| 18.0 | 5.5 | 194 | 82.2 | |
| 102.0 | 31.1 | 14 | 84.2 | |
| 167.3 | 51 | 344 | 70.3 | |
| 229.7 | 70 | 354 | 58.7 | Low velocity |
| 270.0 | 82.3 | 294 | 59.3 | |
| 304.1 | 92.7 | 334 | 78.2 | Low velocity |
| 412.4 | 125.7 | -- | 48.3 | |
| 418.0 | 127.4 | -- | 67.8 | |
| 458.7 | 139.8 | 214 | 81.5 | |

Many reflectors were observed in the directional radar logs of well TBR-3 (fig. 19). This unprocessed radar record, or radargram, from well TBR-3 indicates low velocity zones are at 20, 50, 215 to 260, and 340 ft. Reflectors with low velocity and high attenuation at center depths of 49 and 246 ft are interpreted as water-saturated fractures or fracture zones. These depths are close to major fractures that were identified in the standard logs.

The unprocessed radar record from well W-5 (fig. 20) indicates low-velocity zones at 245, 300, and 395 ft and high attenuation at 245 and 395 ft. These low-velocity and high-attenuation zones appear to correlate with major fracture intersections with the borehole and with the deflections in the fluid resistivity and temperature logs (fig. 9). The fracture at 395 ft is shown in figure 9. The individual radar traces are noted in table 3. In the highly attenuated zones, the strike of the reflector could not be determined because of high attenuation or because the strong reflectors produced apparent radar signals from all directions.

The radar surveys show the rock surrounding TBR-2 and TBR-3 is intensely fractured. In general, high-attenuation and low-velocity zones in the radargrams correlate with fractures and fracture zones observed in the standard and ATV logs. Many radar reflectors were identified in the aquifer surrounding the two wells. The reflectors identified in the radar surveys were steeply dipping and plot towards the outside of a stereogram. Interpreted orientations of reflectors of wells TBR-2 and TBR-3 are shown as a

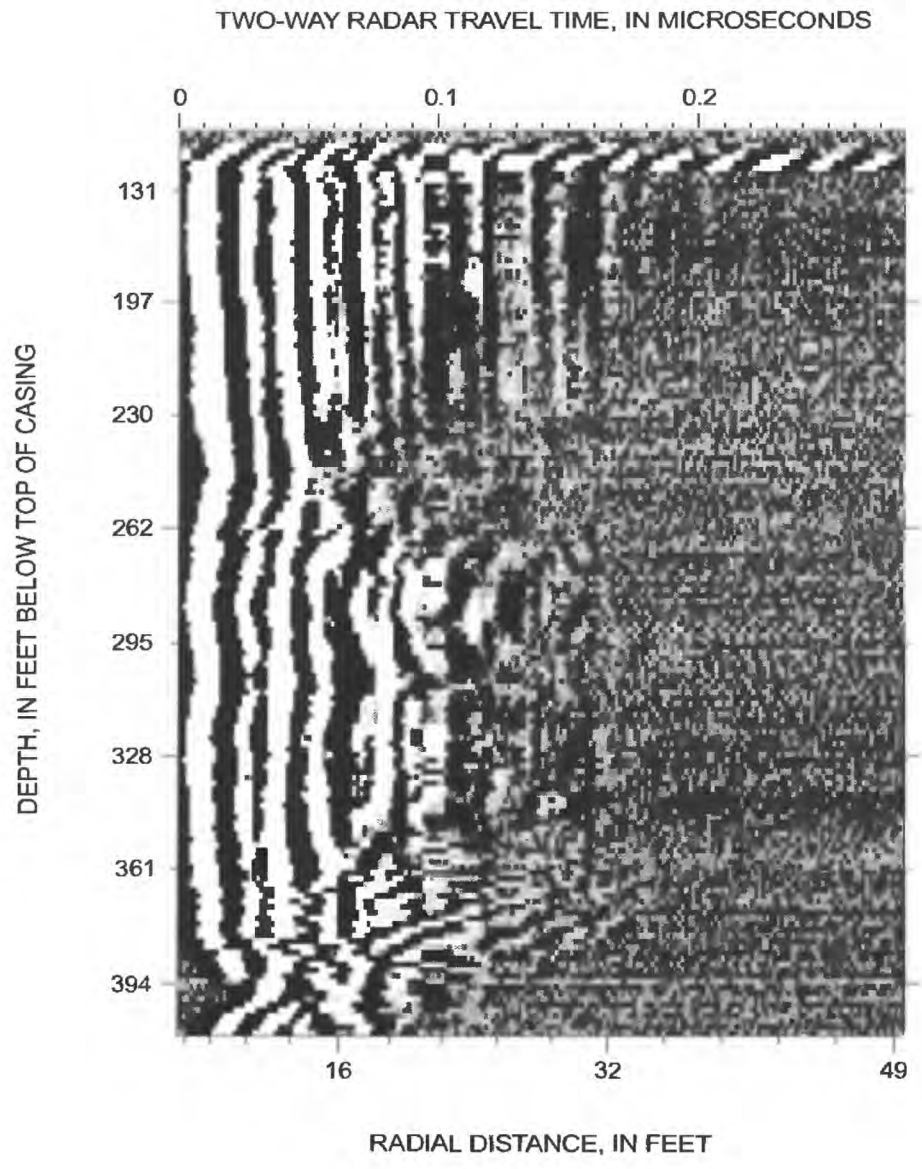


**Figure 20.** Unprocessed borehole radar log of well W-5 in Rye, New Hampshire.

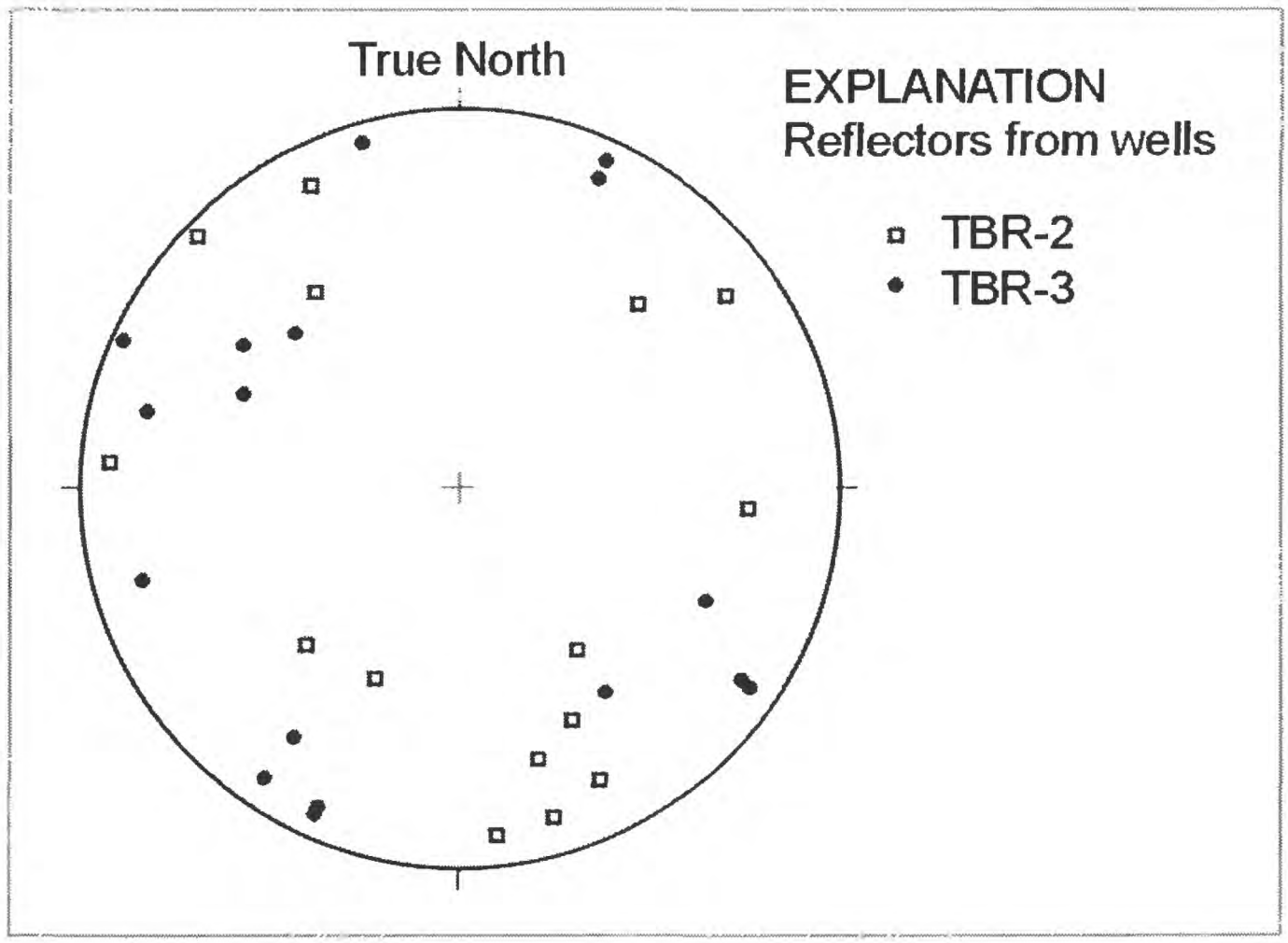


**Figure 21.** Stereogram of radar reflectors from wells TBR-2 and TBR-3 in Rye, New Hampshire.

stereogram in figure 21. A comparison of individual reflectors with fractures in the ATV logs (appendix 1) is difficult, as there is more variation in the fractures shown in the ATV logs. This difference is inherent in the two methods because different scales of observation are used. Borehole radar is primarily influenced by large-scale features, which can be several feet from the borehole, whereas the ATV log identifies relatively small-scale features that intersect the borehole. Aquifers that are intensely fractured, such as in the Cedar Run well field, produce different fracture patterns when different detection methods are used.

## SUMMARY AND CONCLUSIONS

Six wells were investigated in Rye, New Hampshire, to characterize a high-yield bedrock aquifer and to demonstrate how advanced geophysical techniques are applied and interpreted. The wells, which penetrate schists and gneiss of the Rye Complex, intersect a number of fractures. Borehole geophysical logs were collected to identify and determine orientation of the fractures and the water-bearing zones. Several of the wells had vertical flow between fractures under non-pumping, natural conditions. In well TBR-3, the vertical flow was measured by use of a heat-pulse flowmeter log. Under ambient conditions, flow was as much as 0.37 gal/min in the borehole.

The geophysical logs indicate that the bedrock aquifer is highly fractured with various fracture orientations. Statistical analyses of the orientations indicate that several fracture sets intersect the wells. The strikes of these fracture sets were found to be parallel to the trend of several of the lineaments that were identified on high- and low-aerial photography and SLAR platforms of the study area. The strike of the fracture sets and the trend of the lineaments were coincident at approximately N40°E, N100°E, N140°E, and N170°E. A prominent fracture set was identified in wells TBR-1, TBR-2, TBR-3, and W-5 that strikes N171° to N203°E and dips 32° to 70°W. Another set was identified in wells TBR-2 and W-3 that strikes N307° to N320°E and has a steep dip (49° to 74°) to

the northeast. These two sets also were identified by Brooks (1986).

Borehole-radar logs identified several reflectors in the aquifer surrounding three of the wells. The radargrams for these wells show zones of low velocity and high attenuation that coincide with fractures in the wells. The electromagnetic radiation had limited penetration (generally less than 30 ft) into the surrounding aquifer because the signal was attenuated in the intensely fractured aquifer. Fractured zones with low velocity and high attenuation are frequently indicative of water-bearing zones.

## SELECTED REFERENCES


Brooks, J.A., 1986, Geology of New Hampshire's inner continental shelf: University of New Hampshire, Durham, N.H., published Master's thesis, 109 p.

Brooks, J.A., and Rickerich, S., 1996, A field excursion to the coastal region of New Hampshire and the Isles of Shoals, 1996: Portsmouth, N.H., New Hampshire Geological Society, annual field outing, Guidebook to summer field trip and outing, 8 p.

Chapman, M.J., and Lane, J.W., Jr., 1996, Use of directional borehole radar and azimuthal square-array D.C. resistivity methods to characterize a crystalline-bedrock aquifer, *in* Symposium on the Application of Geophysics to Engineering and Environmental Problems, April 28-May 2, 1996: Keystone, Colo., p. 833-842.

Clark, S.F., Jr., Moore, R.B., Ferguson, E.W., and Picard, M.Z., 1996, Criteria and methods for fracture trace analysis of New Hampshire bedrock aquifer: U.S. Geological Survey Open-File Report 96-479, 12 p.

D.L. Maher Co., 1982, The evaluation of alternative groundwater supplies, Town of Rye, New Hampshire: North Reading, Mass., 20 p.

Ferguson, E.W., Clark, S.F., Jr., Moore, R.B., 1997, Lineament map of area 1, of the New Hampshire bedrock aquifer assessment, southeastern New Hampshire: U.S. Geological Survey Open-File Report 96-489, 1 pl., scale 1:48,000.

Hess, A.E., and Paillet, F.L., 1990, Applications of the thermal-pulse flowmeter in the hydraulic characterization of fractured rocks: American Society for Testing and Materials, Standard Technical Publications 1101, p. 99-112.

Hussey, A.M., and Bothner, W.A., 1993, Geology of the coastal lithotechtonic belt SW Maine and SE New Hampshire, *in* 1993 Geological Society of America annual meeting and 85th annual New England Intercollegiate Geological Conference, Boston, Mass., Oct. 25-28, 1993, Field trip guidebook for the northeastern United States: Geological Society of America, 20 p.

Johnson, C.D., 1996, Use of a borehole color video camera to identify lithologies, fractures, and borehole conditions in bedrock wells in the Mirror Lake area, Grafton County, New Hampshire, *in* Morganwalp, D.W., and Aronson, D.A., eds., U.S. Geological Survey Toxic Substance Hydrology—Proceedings of Technical Meeting, Colorado Springs, Colo., September 20-24, 1993: U.S. Geological Survey Water-Resources Investigations Report 94-4015, v. 1, p. 89-94.

Johnson, C.D., and Dunstan, A.H., 1998, Lithology and fracture characterization from drilling investigations in the Mirror Lake area, Grafton County, New Hampshire: U.S. Geological Survey Water-Resources Investigations Report 98-4183, 216 p.

Keyes, W.S., 1988, Borehole geophysics applied to ground-water investigations: U.S. Geological Survey Open-File Report 87-539, 305 p.

Lane, J.W., Jr., Haeni, F.P., and Williams, J.H., 1994, Detection of bedrock fractures and lithologic changes using borehole radar at selected sites, *in* Fifth International Conference on Ground-Penetrating Radar, Kitchner, Ontario, Canada, June 12-16, 1993, Proceedings: Kitchner, Ontario, Waterloo Center for Groundwater Research, p. 577-591.

Lyons, J.B., Bothner, W.A., Moench, R.H., and Thompson, J.B., Jr., 1997, Bedrock geologic map of New Hampshire: U.S. Geological Survey State Geologic Map, 2 sheets, scale 1:250,000 and 1:500,000.

Moore, R.B., and Clark, S.F., 1995, Assessment of groundwater supply potential of bedrock in New Hampshire: U.S. Geological Survey Fact Sheet FS 95-002, 2 p.

Novotny, R.F., 1969, The geology of the seacoast region New Hampshire: Concord, N.H., New Hampshire Department of Resources and Economic Development, 46 p., 1 pl., scale 1:62,5000.

Paillet, F.L., and Pedler, W.H., 1996, Integrated borehole logging methods for wellhead protection applications: Engineering Geology, v. 42, p. 155-165.

Paillet, F.L., and Williams, J.H., 1992, Proceedings of the U.S. Geological Survey workshop on the application of borehole geophysics to ground-water investigations, Albany, New York: U.S. Geological Survey Open-File Report 94-4103, 79 p.

Woodcock, N.H., 1977, Specification of fabric shapes using an eigenvalue method: Geological Society of America Bulletin, v. 88, p. 1231-1236.




-PAGE 37 FOLLOWS-

# APPENDIX

Acoustic Televiewer Logs of Wells:

**APPENDIX 1.** ACOUSTIC TELEVIEWER LOG OF WELL W-3, RYE, NEW HAMPSHIRE

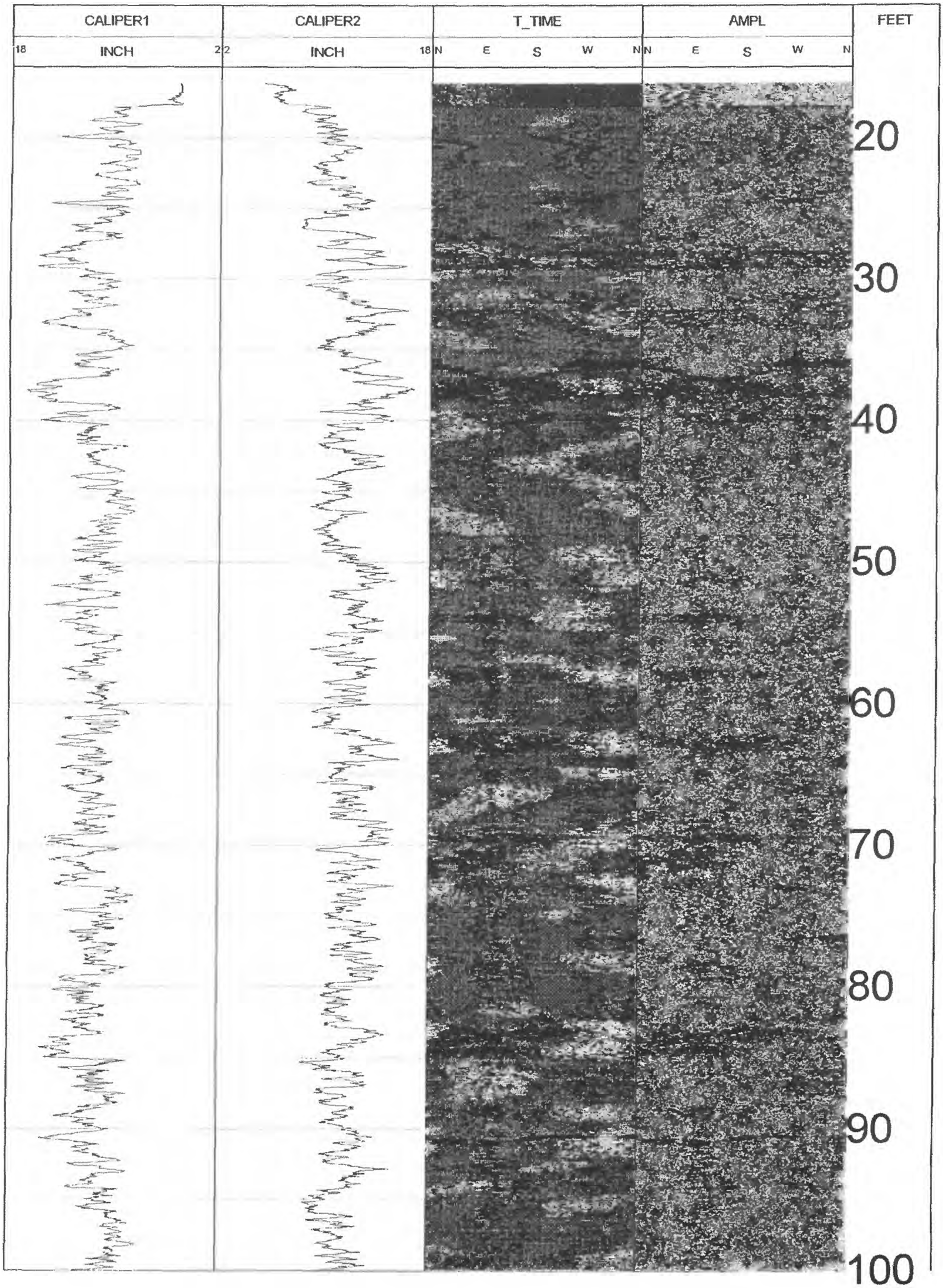

**APPENDIX 1.** ACOUSTIC TELEVIEWER LOG OF WELL W-3, RYE, NEW HAMPSHIRE--Continued

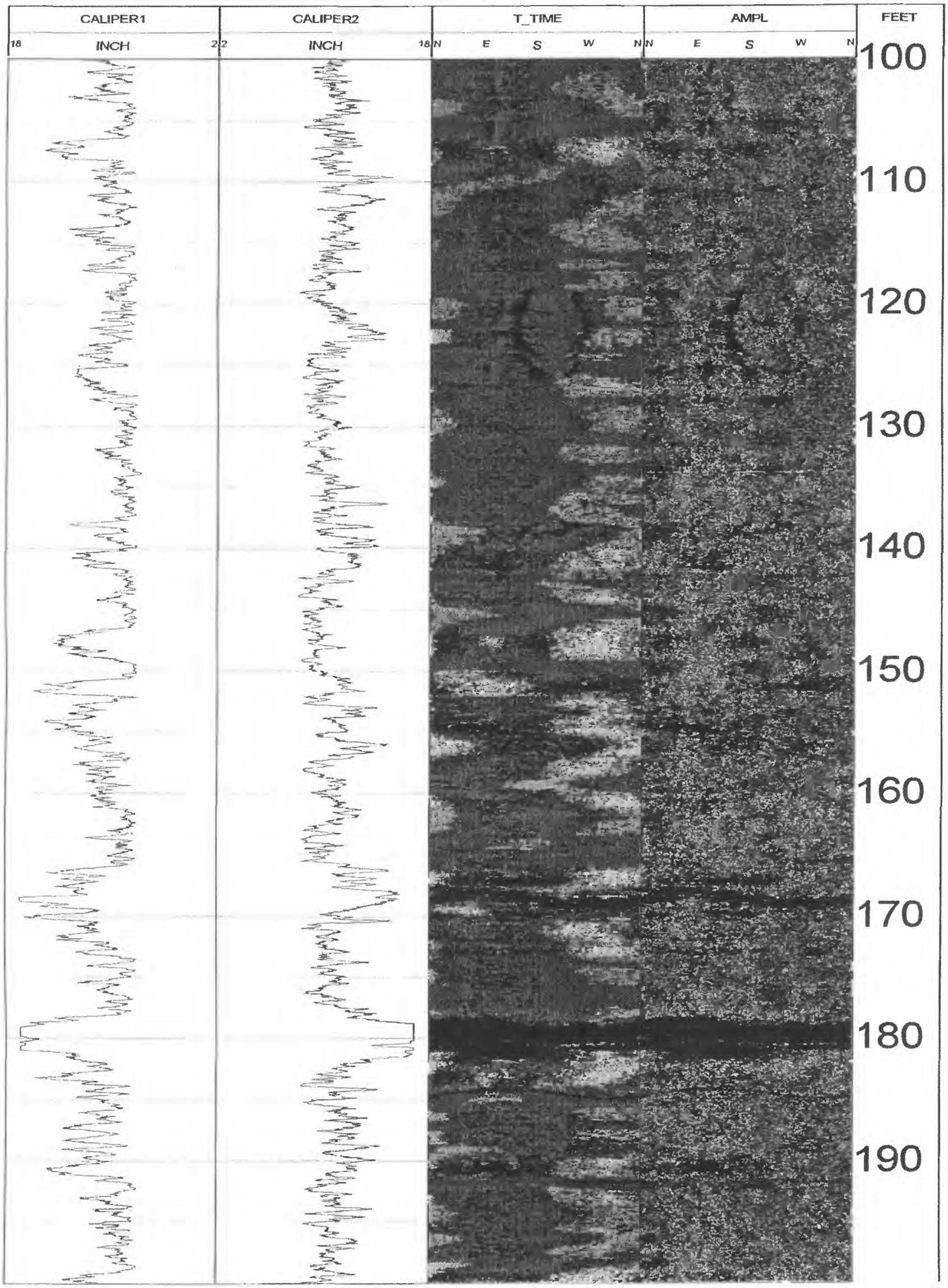

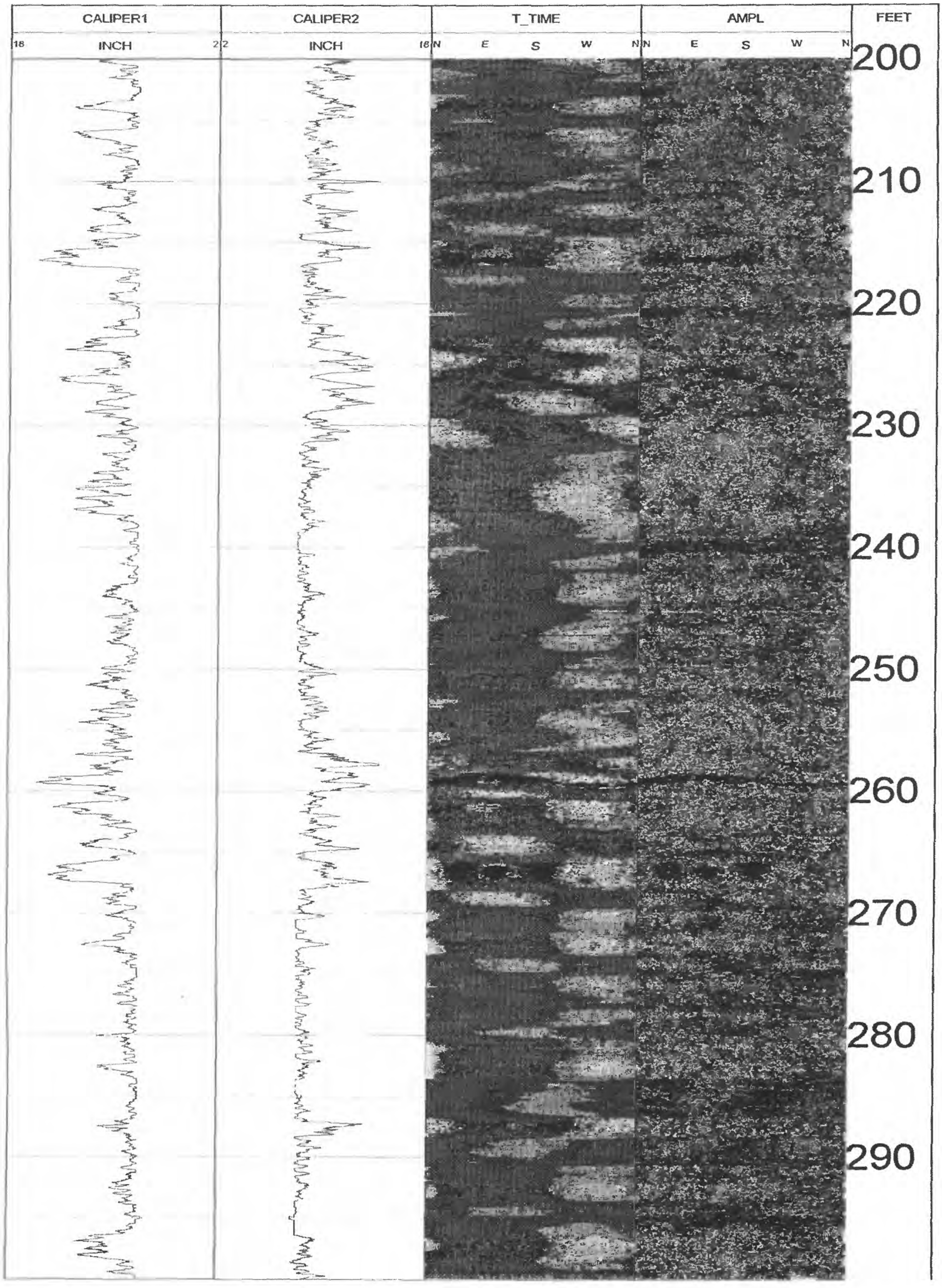
CALIPER1
18
INCH
22
CALIPER2
INCH
18
T_TIME
N E S W N
AMPL
N E S W N
FEET
200
210
220
230
240
250
260
270
280
290

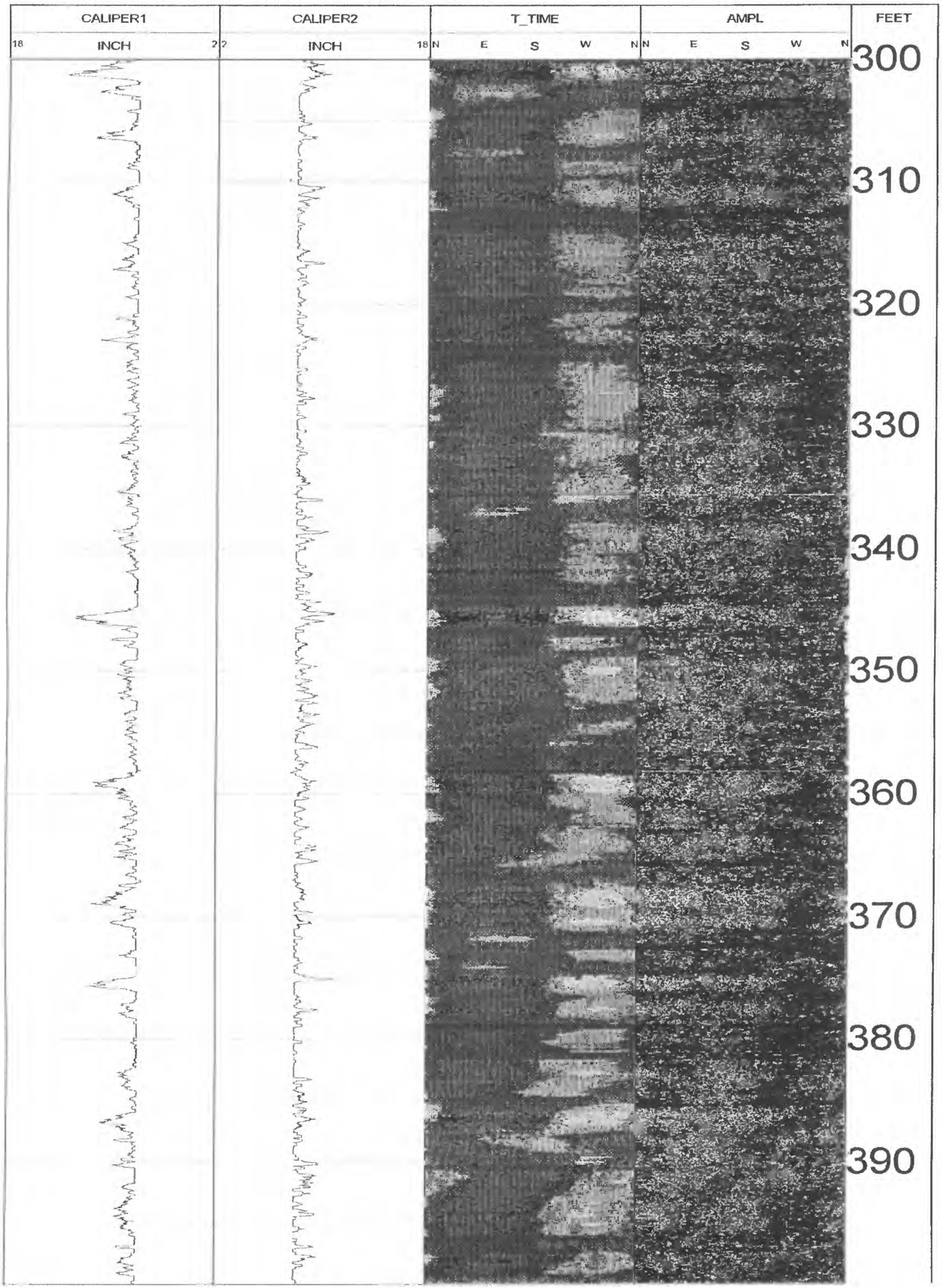
CALIPER1
18
INCH
22
CALIPER2
22
INCH
18
T_TIME
N E S W N
AMPL
N E S W N
FEET
300
310
320
330
340
350
360
370
380
390

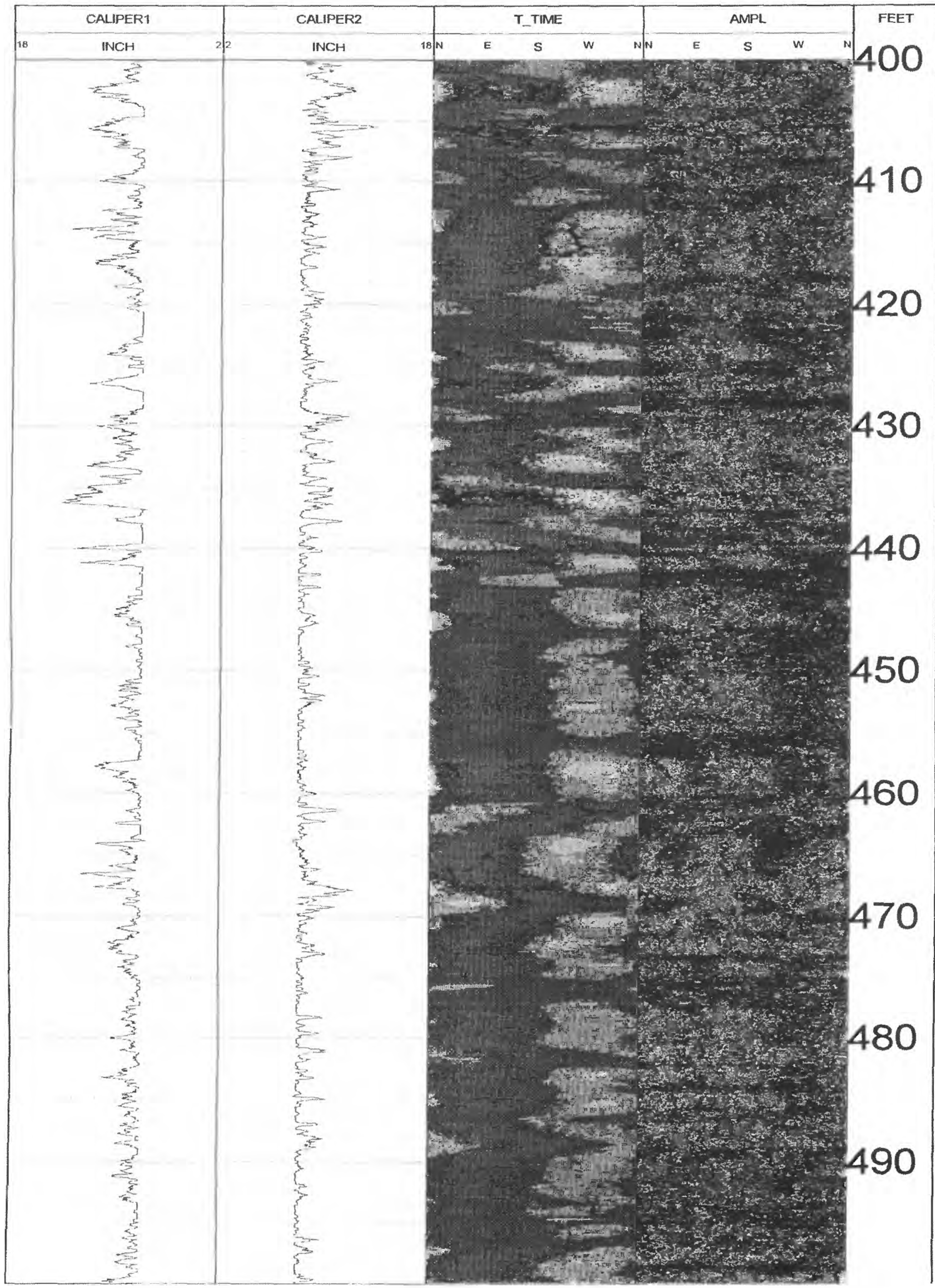
CALIPER1
18
INCH
22
CALIPER2
INCH
18
T_TIME
N E S W N
AMPL
N E S W N
FEET
400
410
420
430
440
450
460
470
480
490

**APPENDIX 1.** ACOUSTIC TELEVIEWER LOG OF WELL W-3, RYE, NEW HAMPSHIRE--Continued

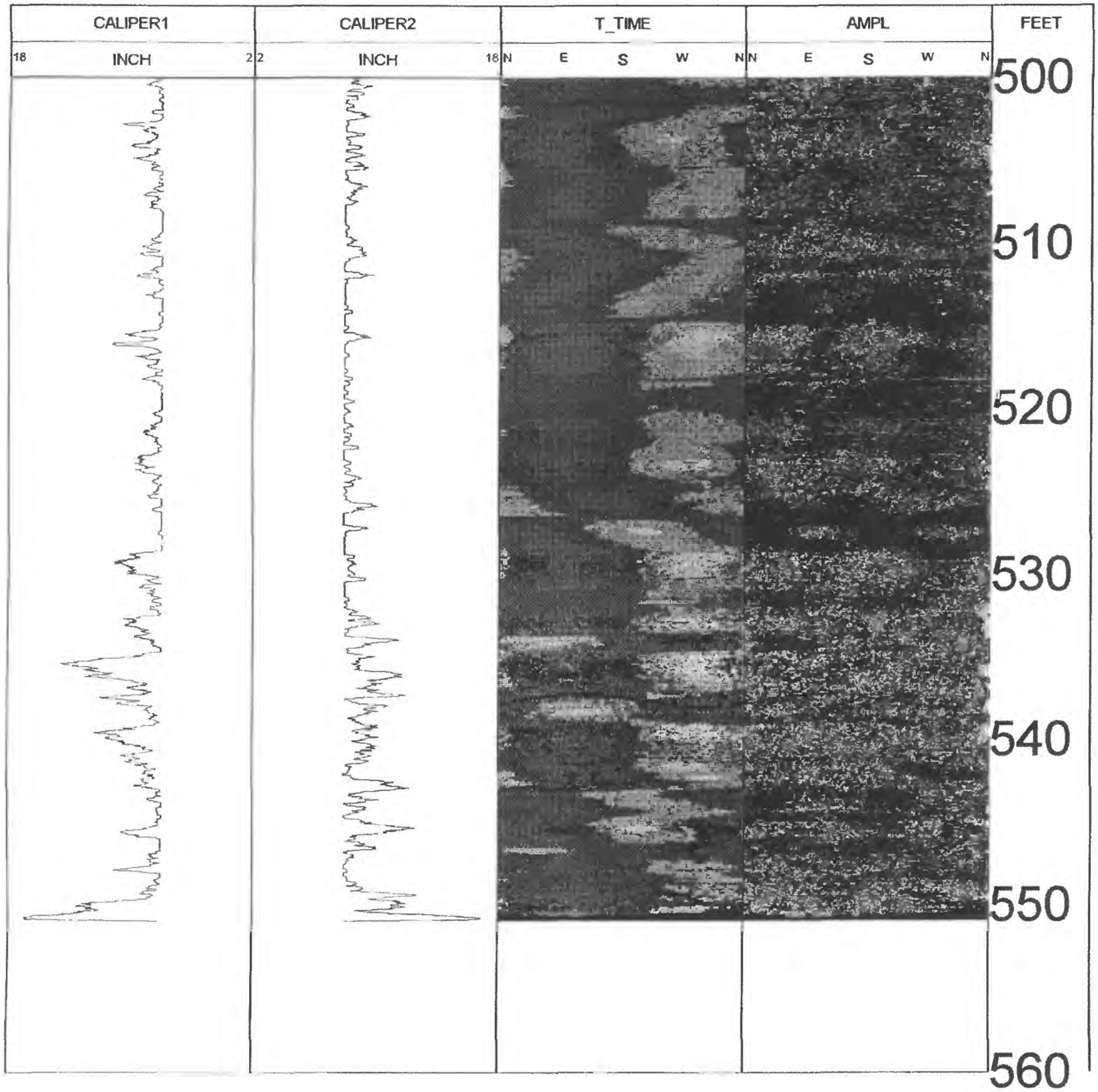

**APPENDIX 1.** ACOUSTIC TELEVIEWER LOG OF WELL W-4, RYE, NEW HAMPSHIRE

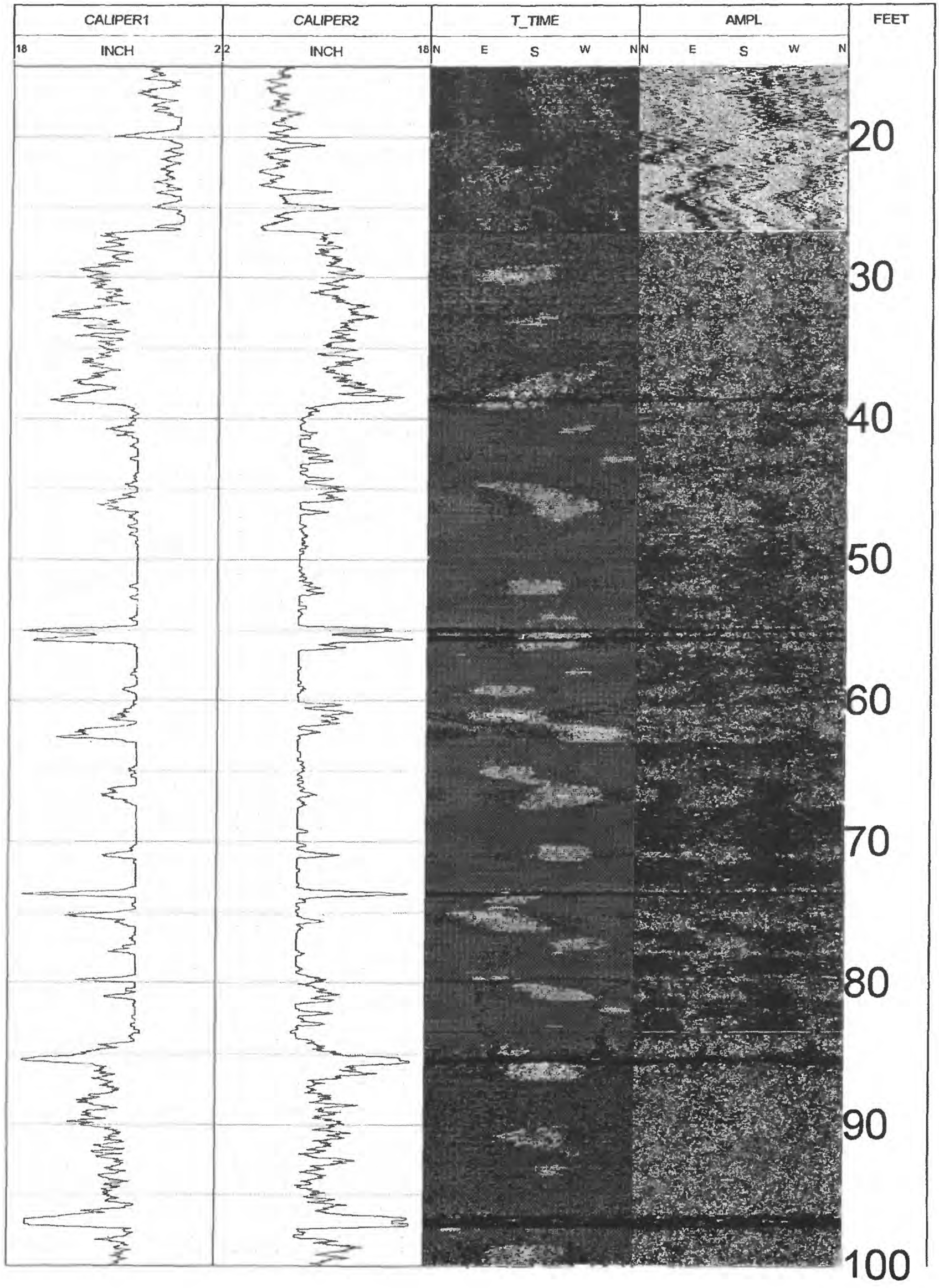

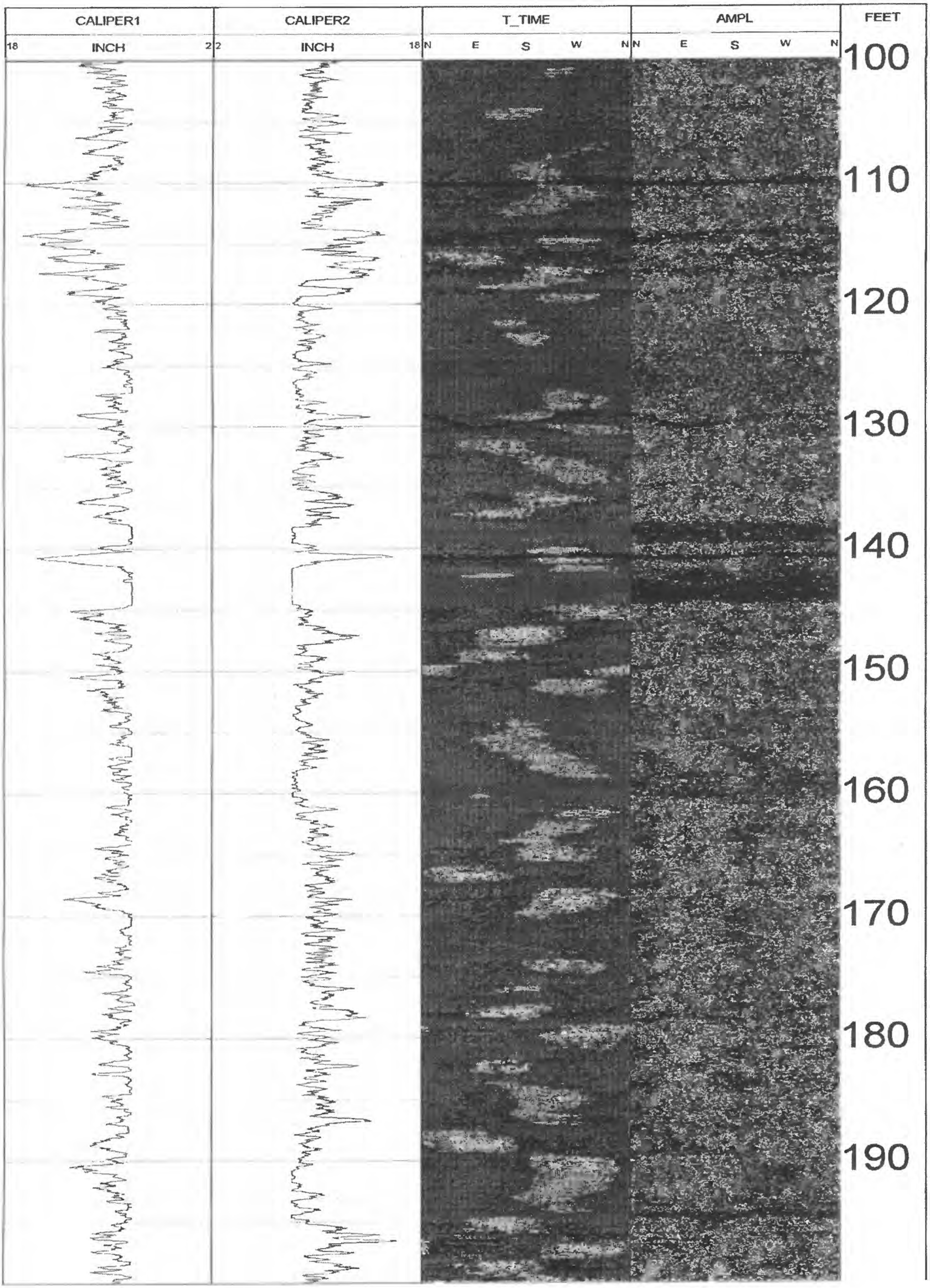
CALIPER1
18 INCH 2
CALIPER2
2 INCH 18
T_TIME
N E S W N
AMPL
N E S W N
FEET
100
110
120
130
140
150
160
170
180
190

**APPENDIX 1.** ACOUSTIC TELEVIEWER LOG OF WELL W-4, RYE, NEW HAMPSHIRE--Continued

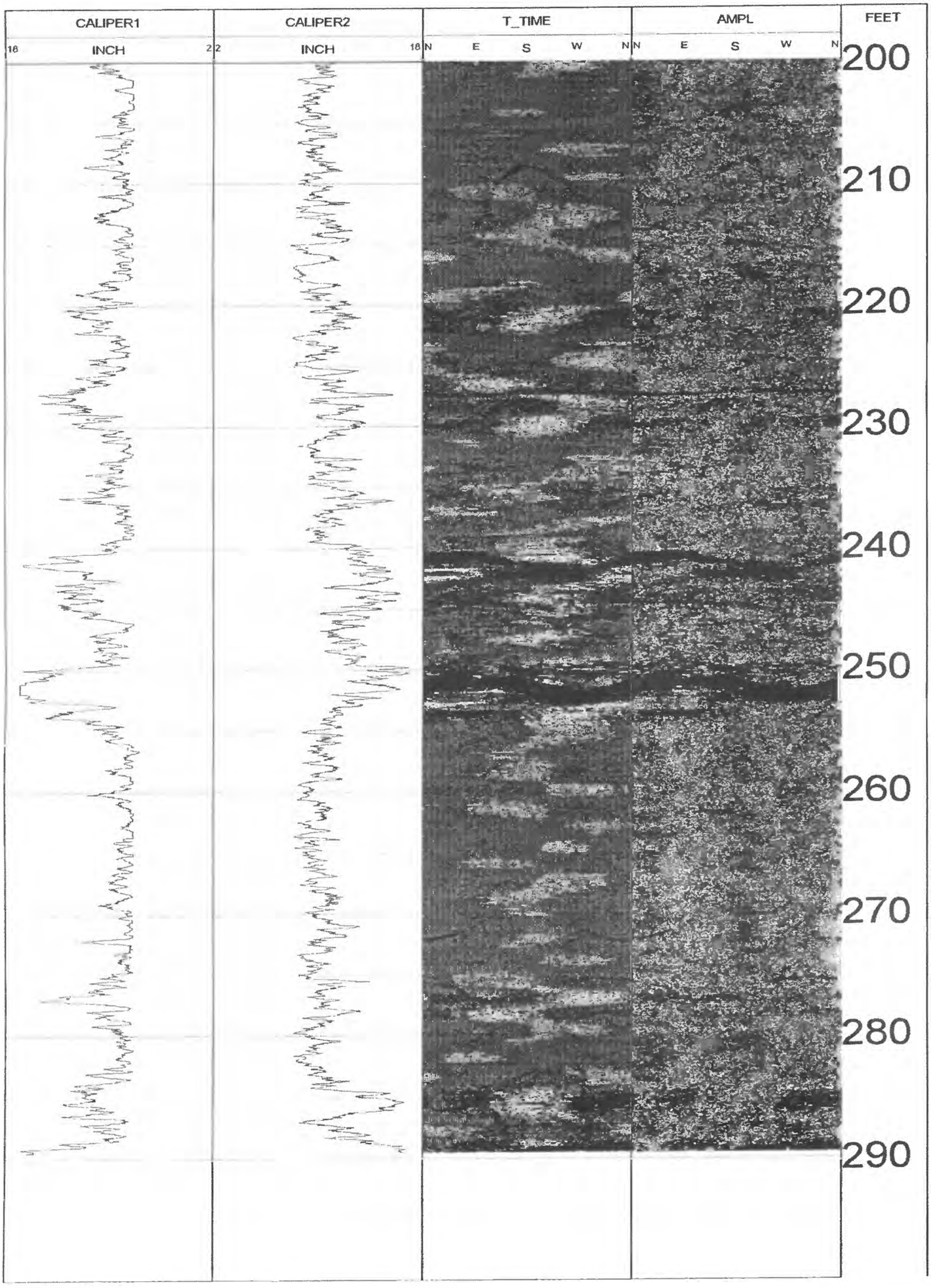

**APPENDIX 1.** ACOUSTIC TELEVIEWER LOG OF WELL W-5, RYE, NEW HAMPSHIRE

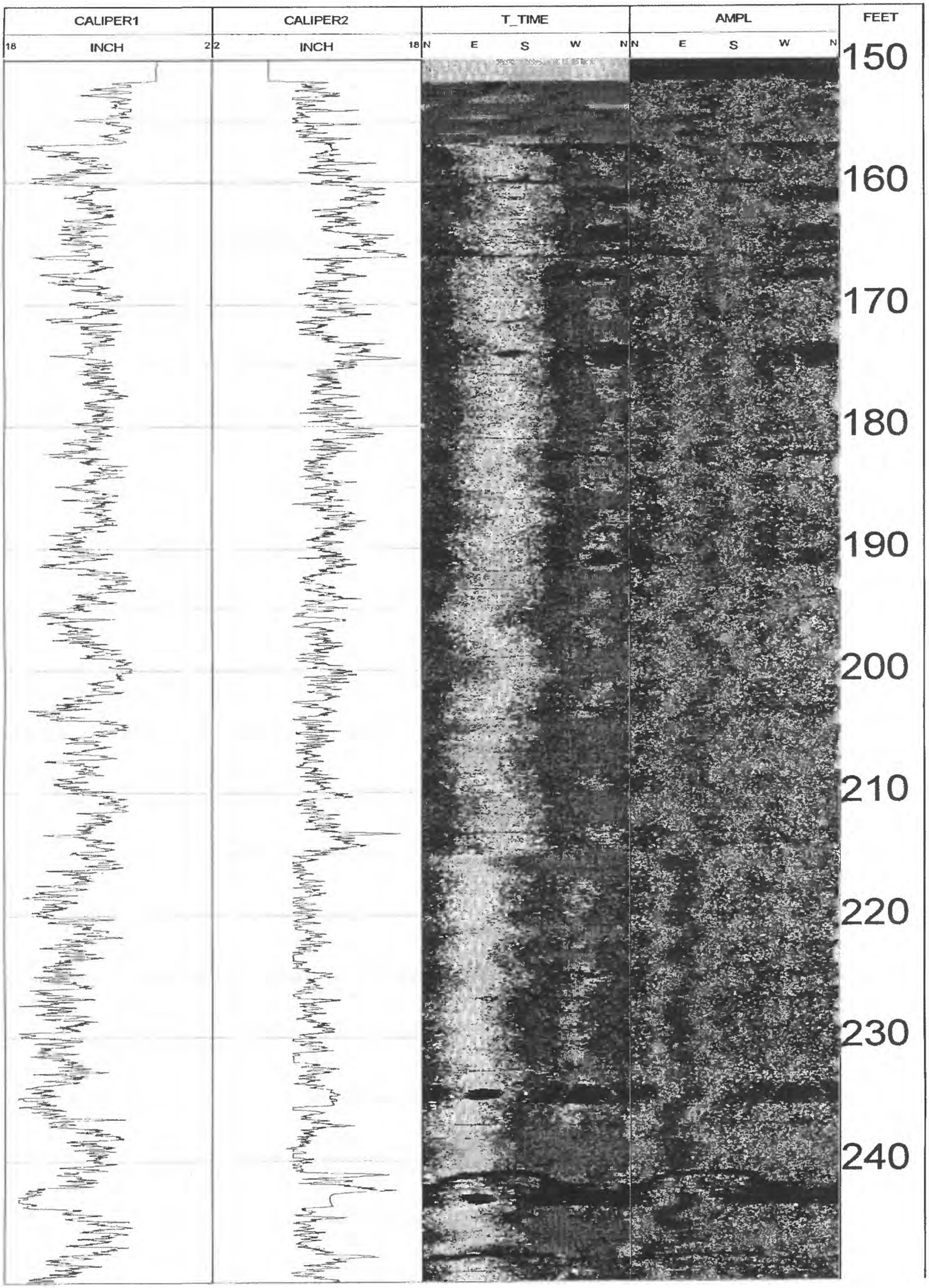

**APPENDIX 1.** ACOUSTIC TELEVIEWER LOG OF WELL W-5, RYE, NEW HAMPSHIRE--Continued

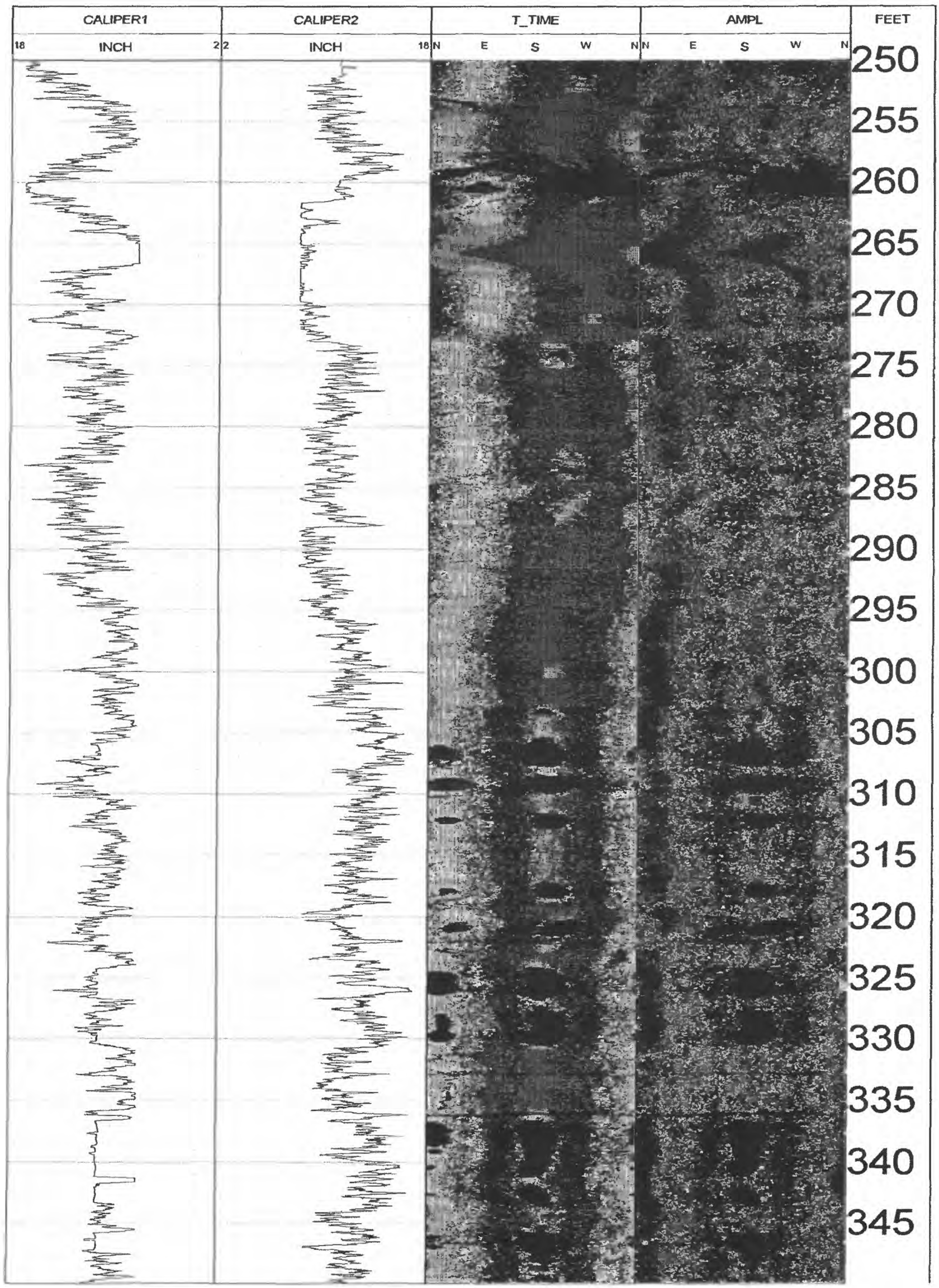

**APPENDIX 1.** ACOUSTIC TELEVIEWER LOG OF WELL W-5, RYE, NEW HAMPSHIRE--Continued

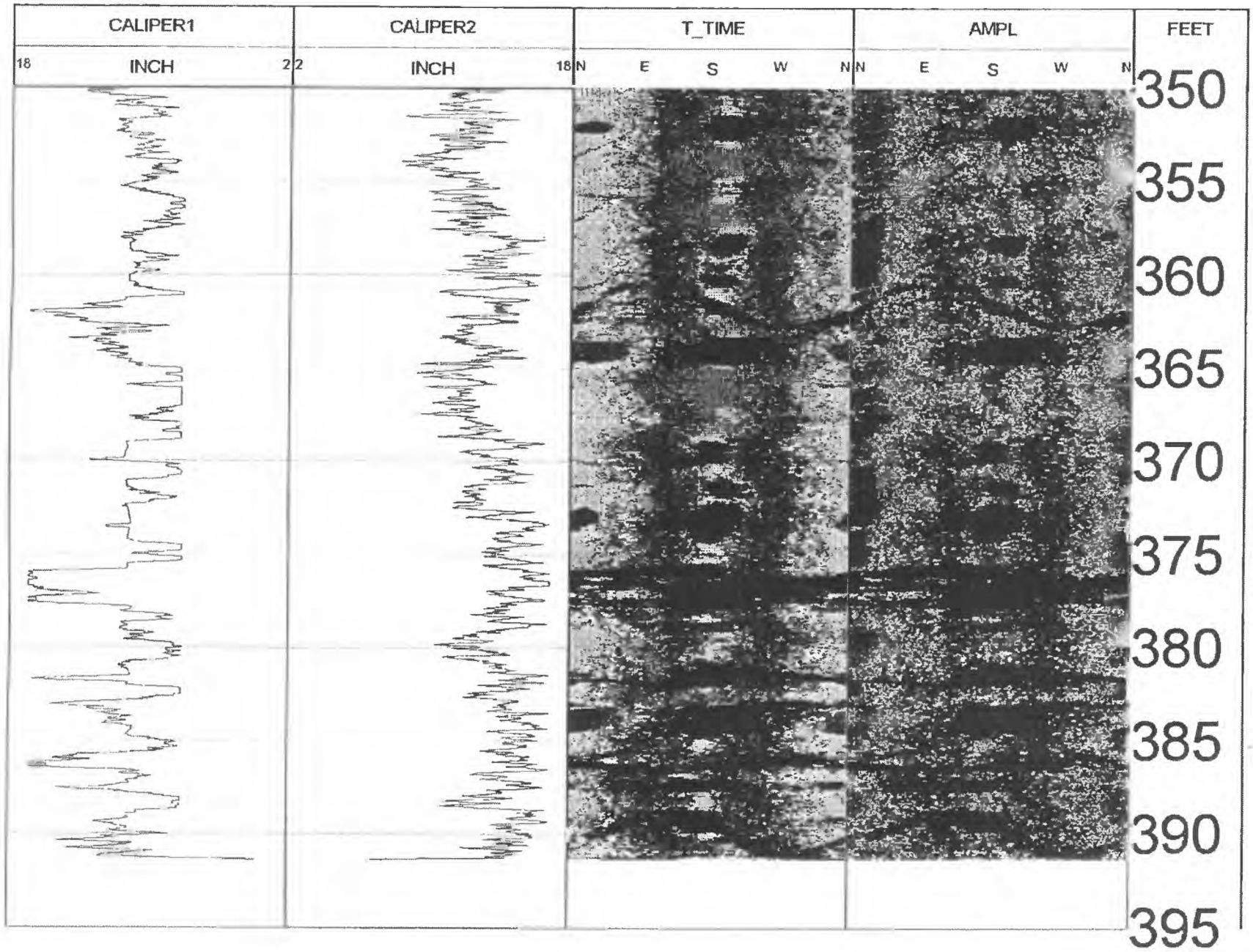

**APPENDIX 1.** ACOUSTIC TELEVIEWER LOG OF WELL TBR-1, RYE, NEW HAMPSHIRE

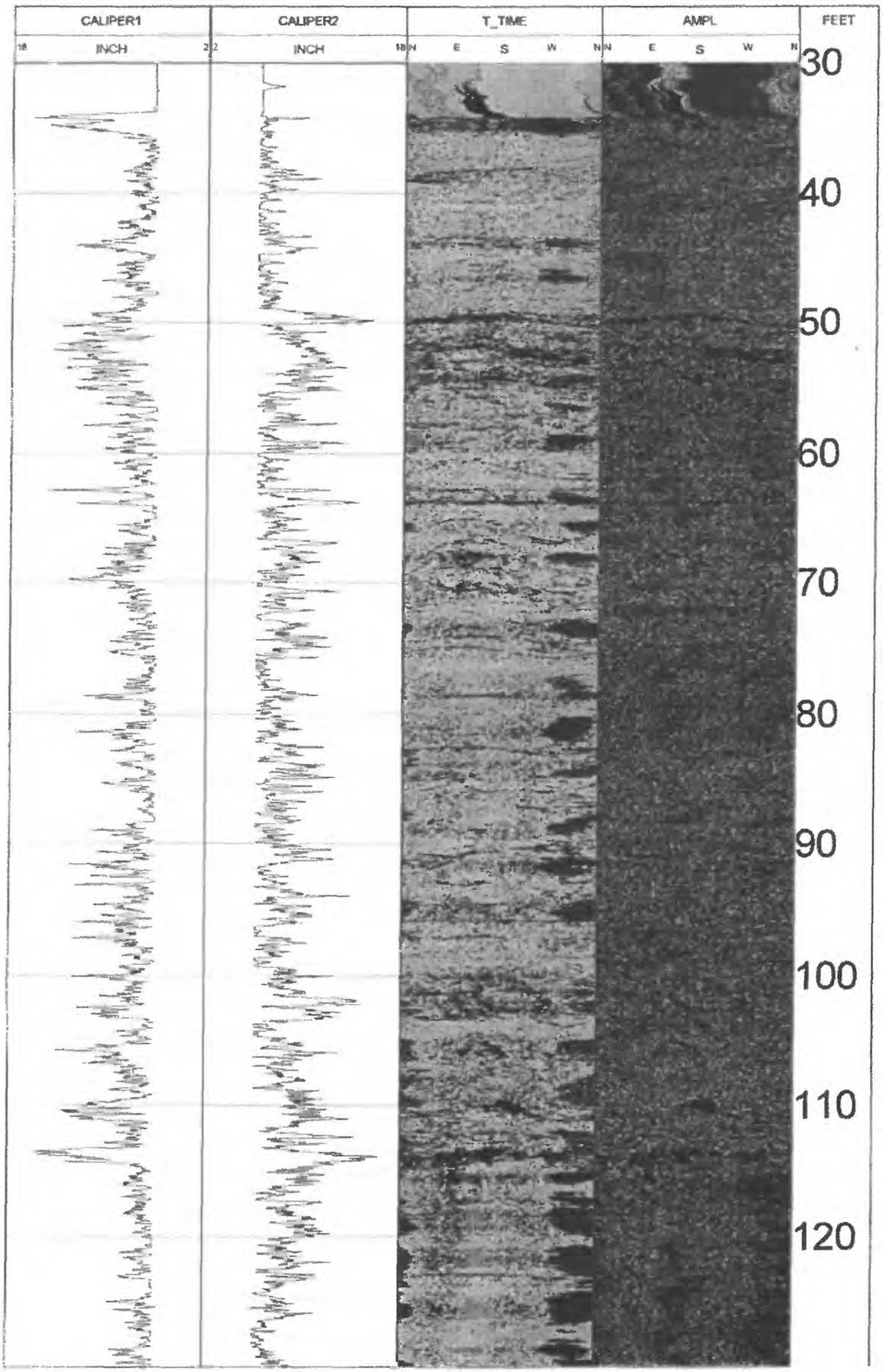

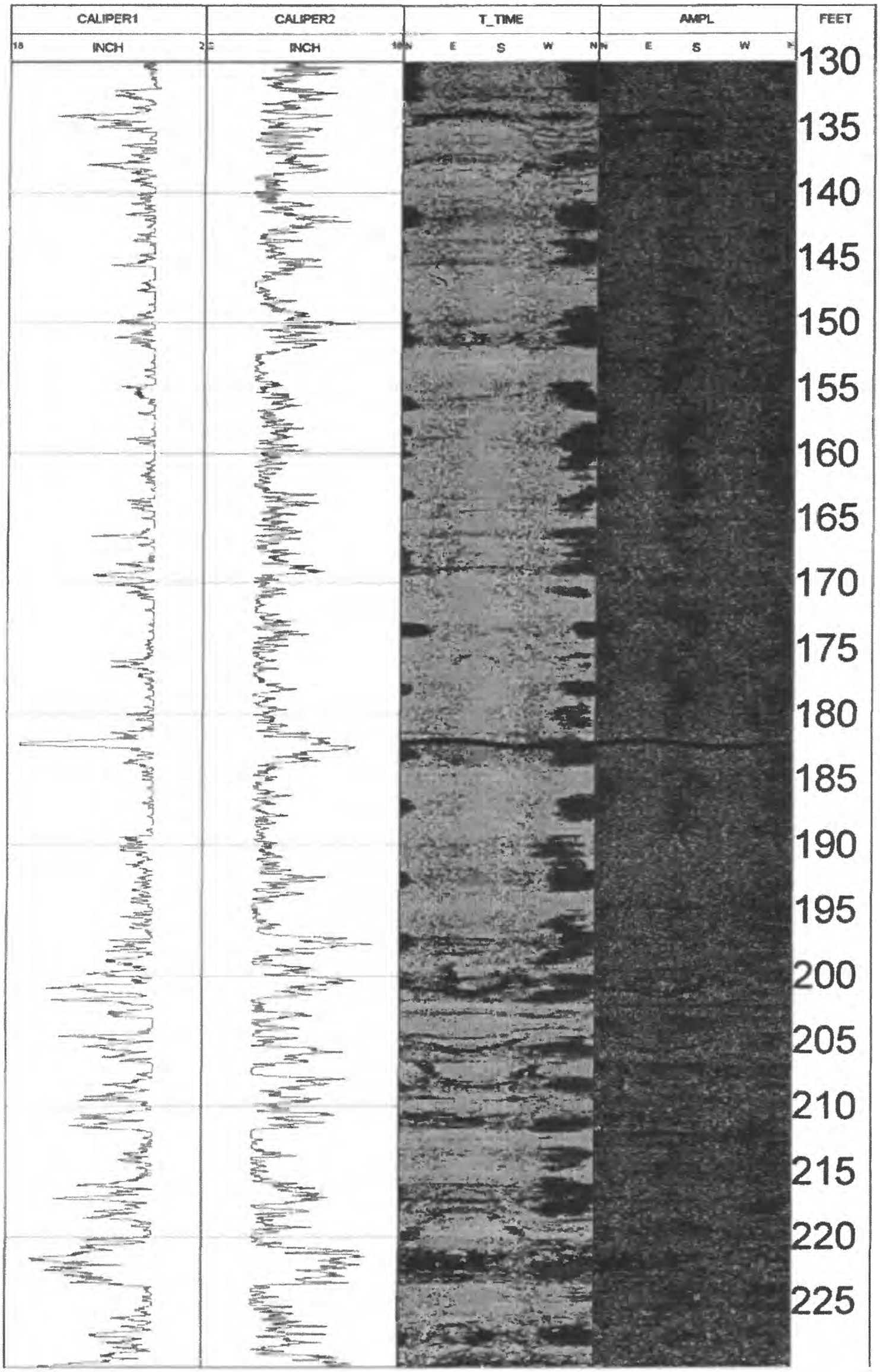
CALIPER1
18
INCH
CALIPER2
INCH
T_TIME
N E S W N
AMPL
N E S W
FEET
130
135
140
145
150
155
160
165
170
175
180
185
190
195
200
205
210
215
220
225

**APPENDIX 1.** ACOUSTIC TELEVIEWER LOG OF WELL TBR-1, RYE, NEW HAMPSHIRE--Continued

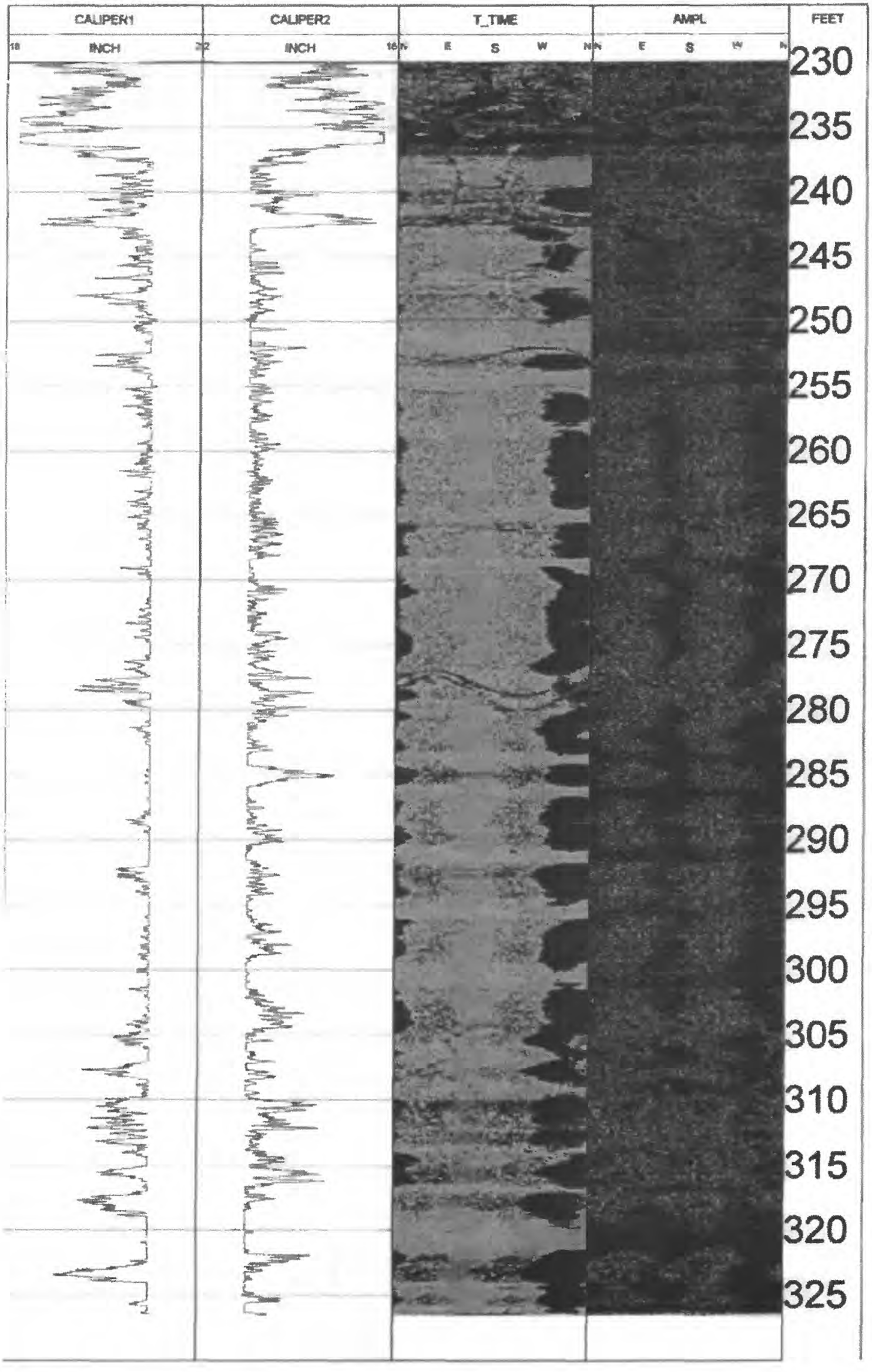

**APPENDIX 1.** ACOUSTIC TELEVIEWER LOG OF WELL TBR-2, RYE, NEW HAMPSHIRE

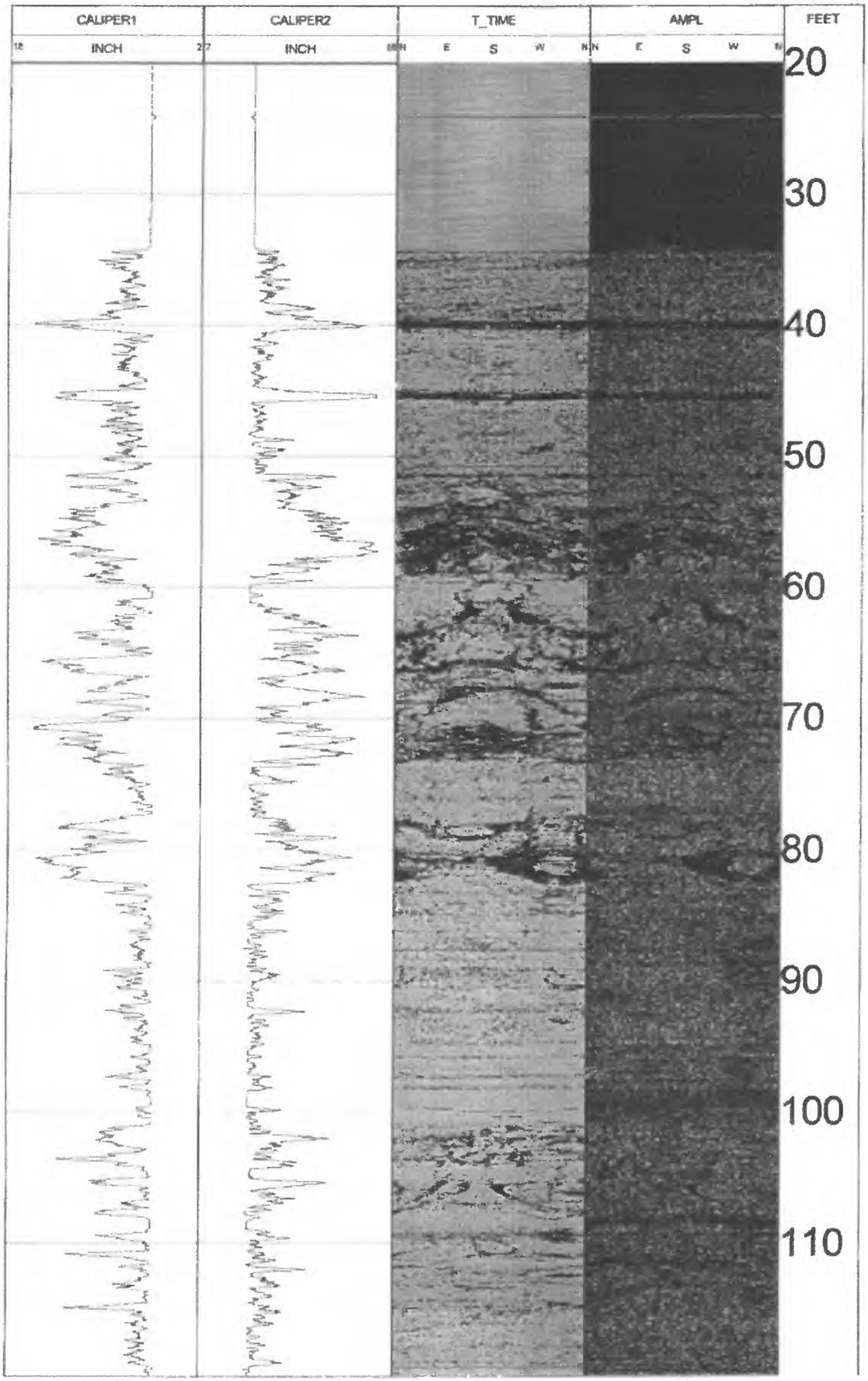

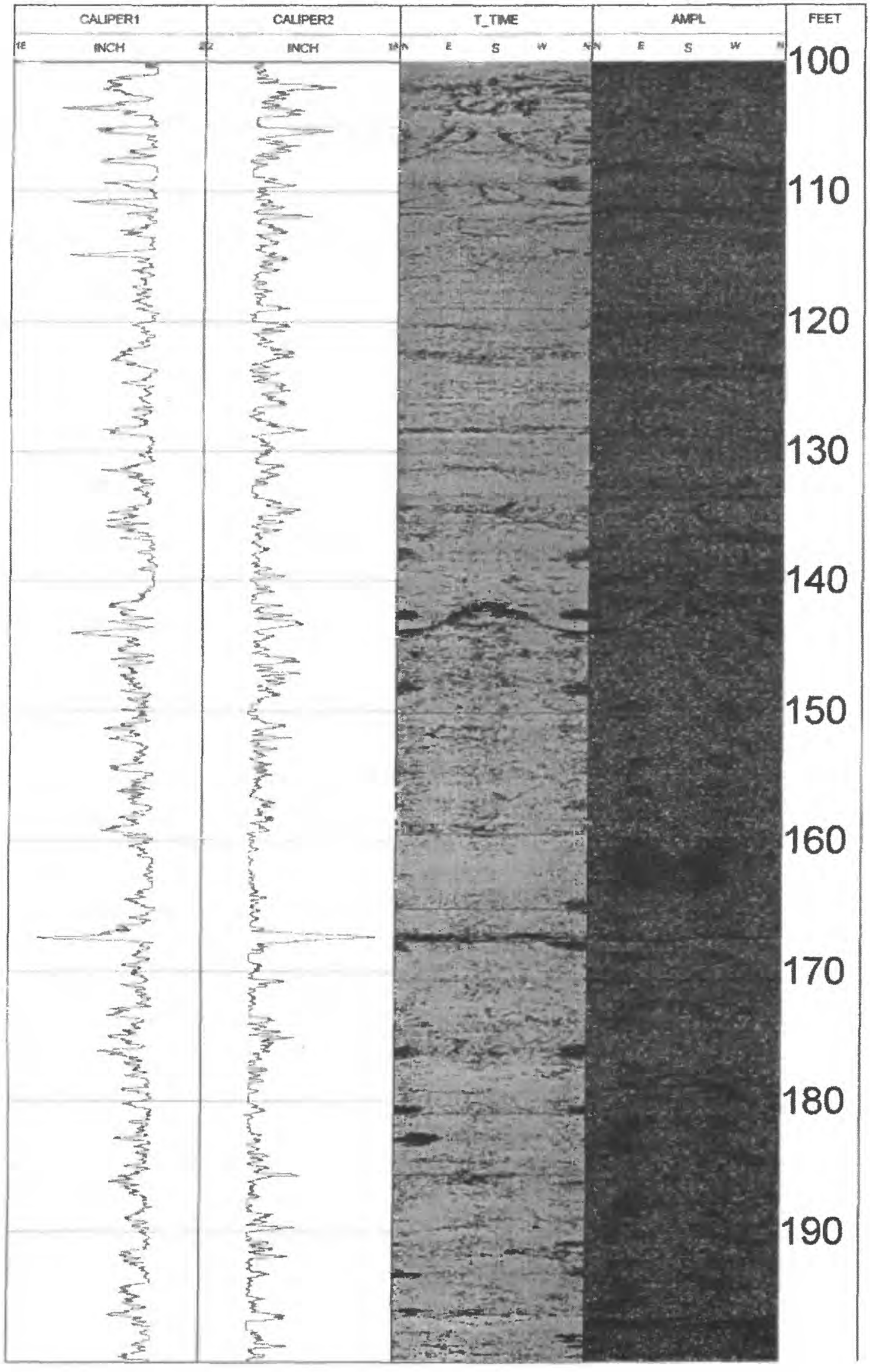
CALIPER1
INCH
CALIPER2
INCH
T_TIME
N E S W N
AMPL
N E S W N
FEET
100
110
120
130
140
150
160
170
180
190

**APPENDIX 1.** ACOUSTIC TELEVIEWER LOG OF WELL TBR-2, RYE, NEW HAMPSHIRE--Continued

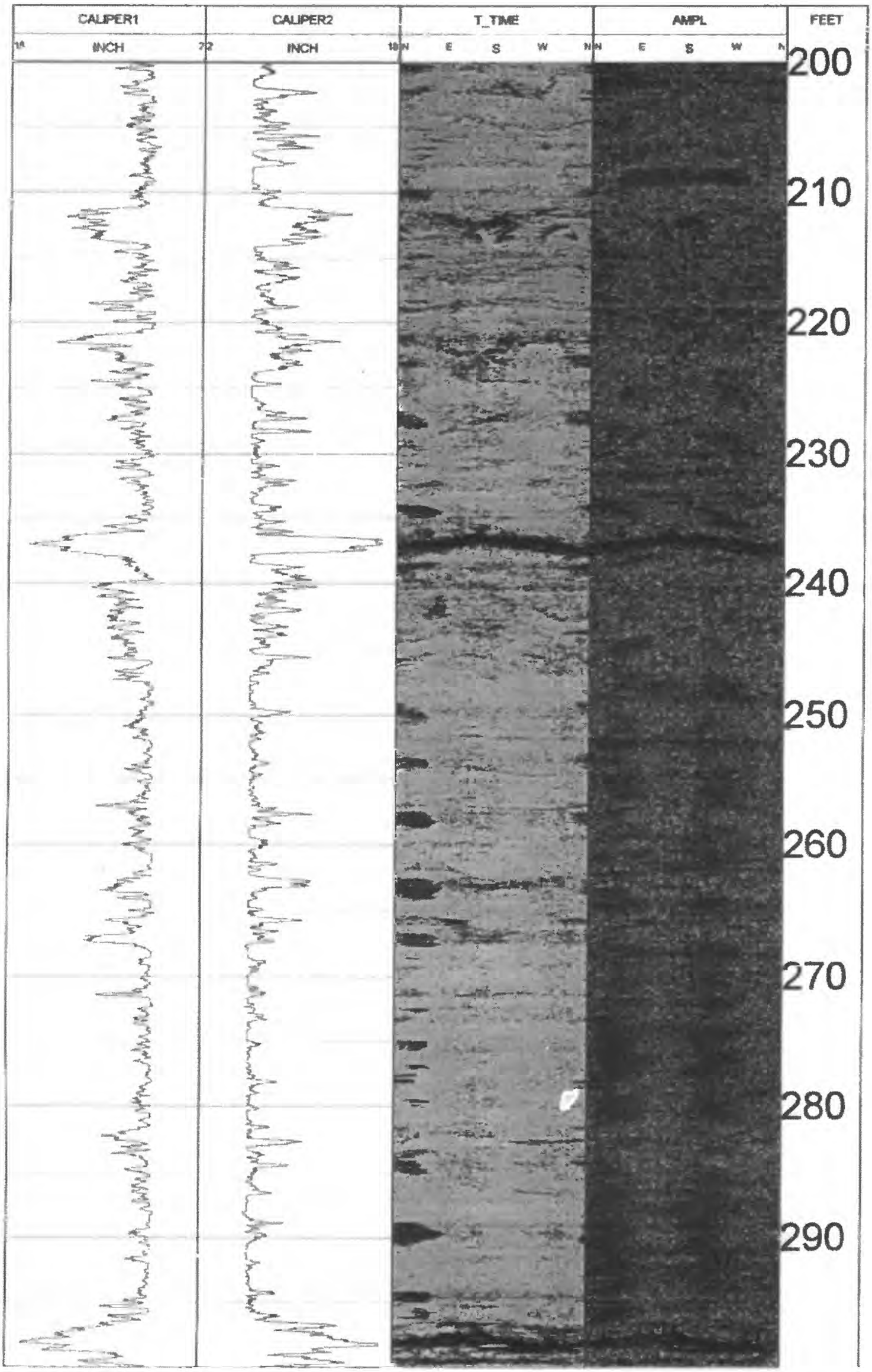

**APPENDIX 1.** ACOUSTIC TELEVIEWER LOG OF WELL TBR-2, RYE, NEW HAMPSHIRE--Continued

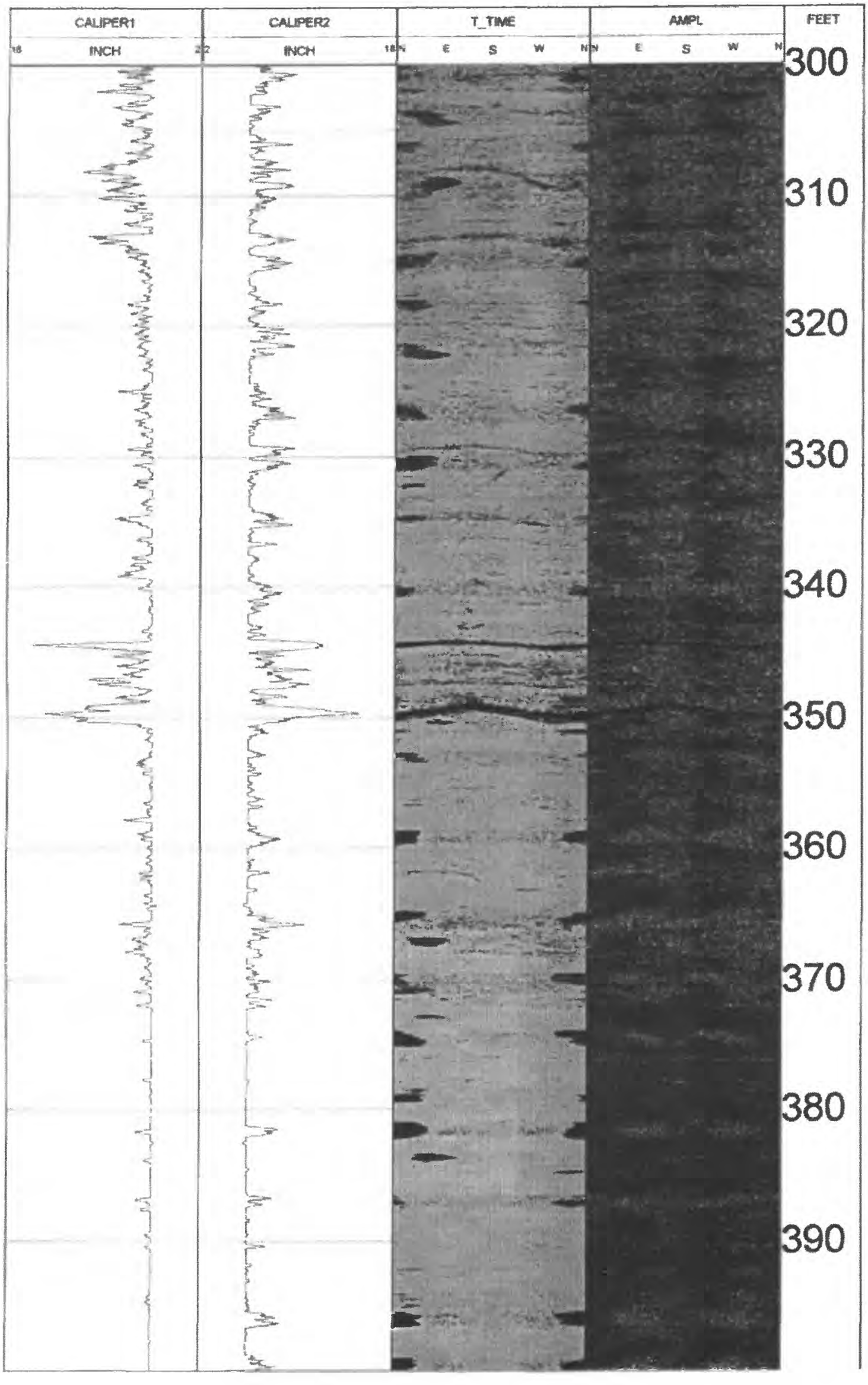

**APPENDIX 1.** ACOUSTIC TELEVIEWER LOG OF WELL TBR-3, RYE, NEW HAMPSHIRE

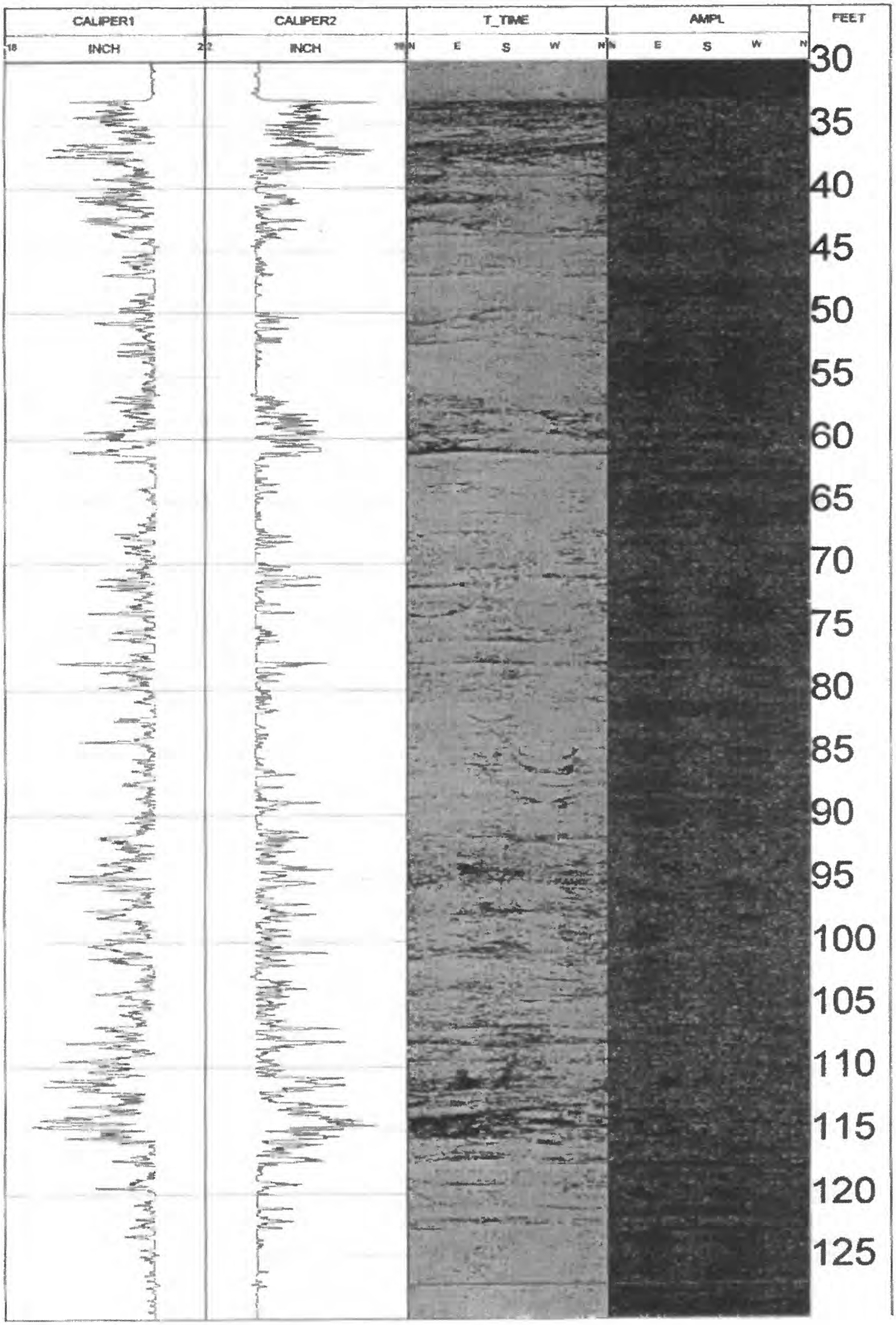

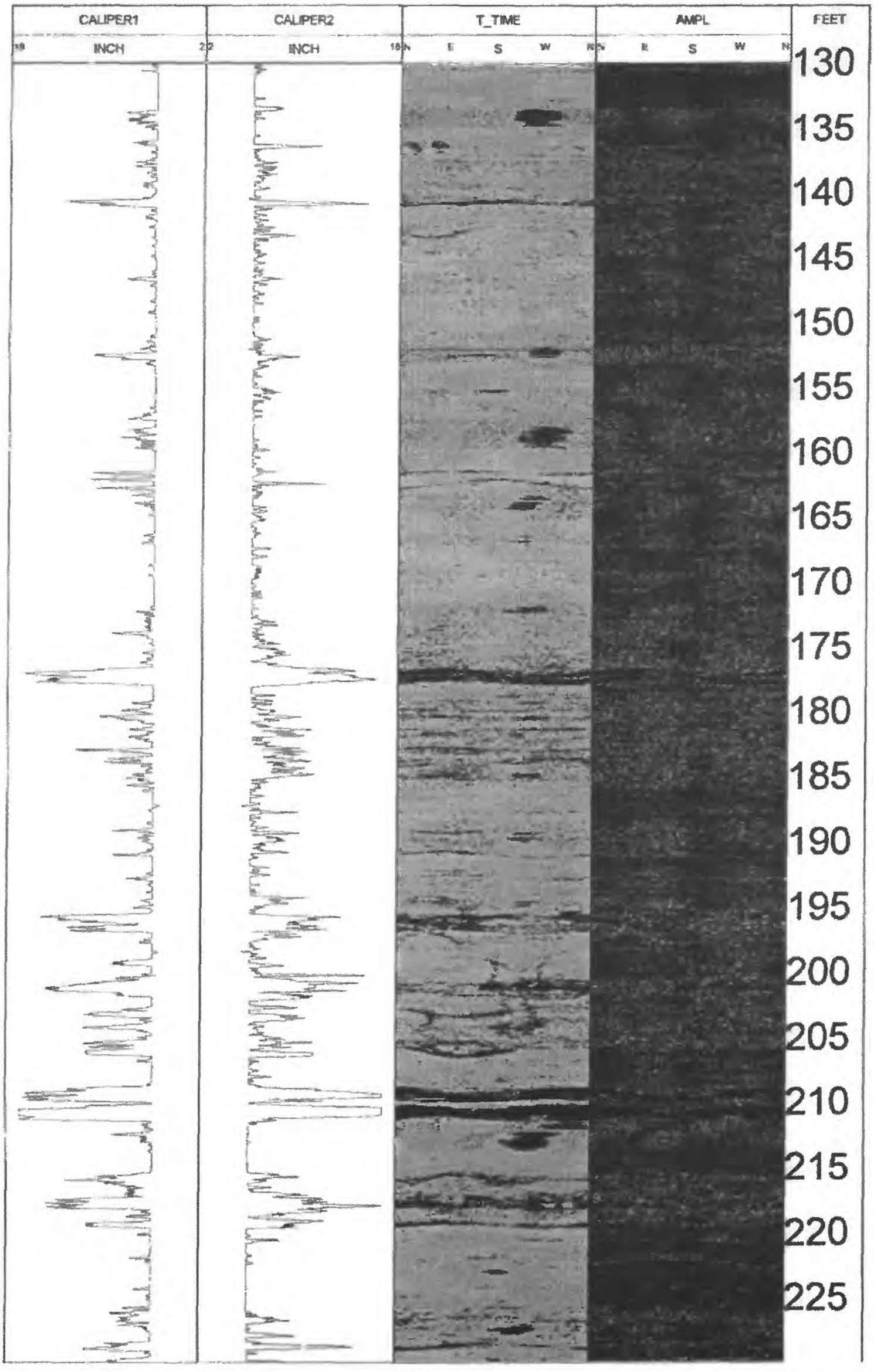
CALIPER1
INCH
CALIPER2
INCH
T_TIME
N E S W N
AMPL
N E S W N
FEET
130
135
140
145
150
155
160
165
170
175
180
185
190
195
200
205
210
215
220
225

**APPENDIX 1.** ACOUSTIC TELEVIEWER LOG OF WELL TBR-3, RYE, NEW HAMPSHIRE--Continued

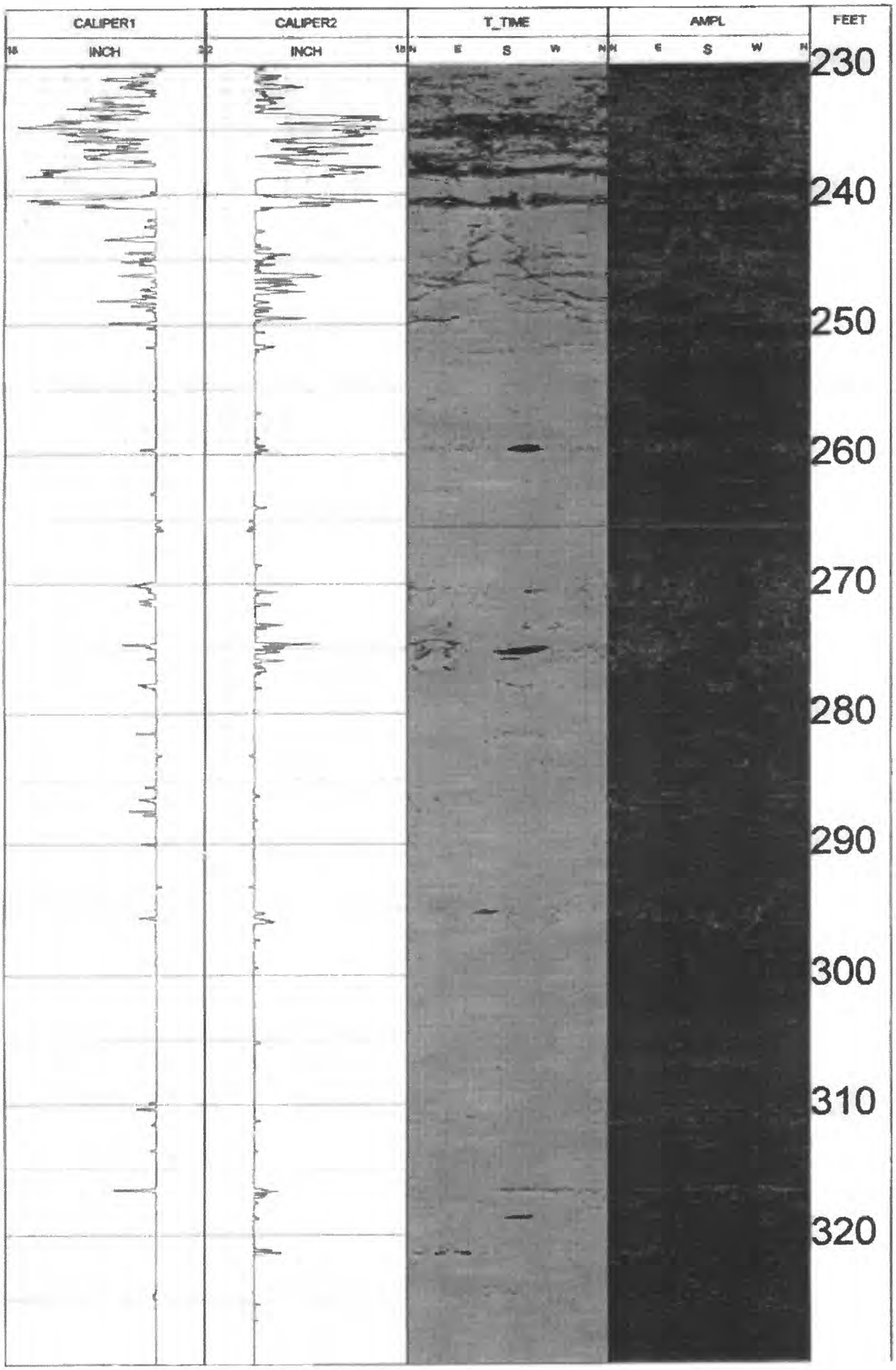

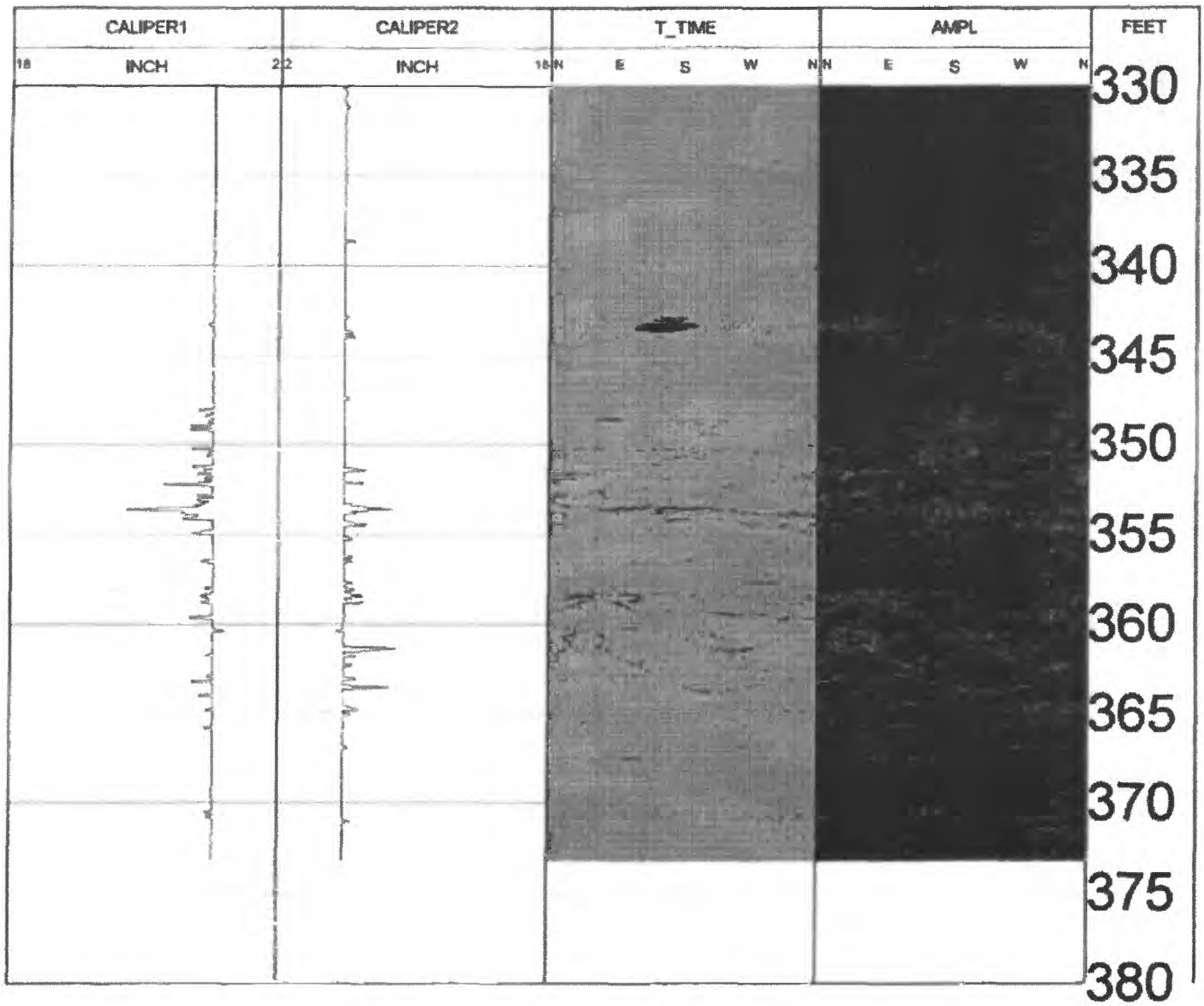
CALIPER1
18
INCH
22
CALIPER2
INCH
18
T_TIME
N E S W N
AMPL
N E S W N
FEET
330
335
340
345
350
355
360
365
370
375
380